UNIVERSITA' DEGLI STUDI DI VERONA

DIPARTIMENTO DI

Diagnostica e Sanità Pubblica

SCUOLA DI DOTTORATO DI

Scienze della Vita e della Salute

DOTTORATO DI RICERCA IN

Neuroscienze, Scienze psicologiche e psichiatriche

Con il contributo di Fondazione Cariverona

CICLO /ANNO XXIX° ciclo/2013

TITOLO DELLA TESI DI DOTTORATO

TOWARDS A COMBINATION THERAPY FOR SPINAL CORD INJURY: pRNA-3WJ NANOTHERAPEUTICS AND TRANSPLANTATION OF INDUCED-NEURAL STEM CELLS

S.S.D. BIO/14 FARMACOLOGIA

Coordinatore: Prof Leonardo Chelazzi

Firma _____

Tutor: Prof. Guido Francesco Fumagalli

Firma _____

Dottoranda: Dott.ssa Alice Braga

Firma _____

ABSTRACT

Spinal cord injury (SCI) is a debilitating pathology that has increased in prevalence over the last few decades. Despite improvements in modern medicine leading to a normal life expectancy, there are limited treatment options and still no fully restorative therapies. Several experimental therapies have been employed to ameliorate the hostile injured environment, amongst which stem cell transplantation is a standout. Neural stem cell (NSC) transplantation has shown promising results in promoting functional recovery in SCI models. However, major accessibility, ethical and immunocompatibility issues impede their clinical translation. These barriers can be overcome through the use of induced neural stem cells (iNSCs), obtained by direct reprogramming of autologous somatic cells, leading to the possibility of fully immunocompatible transplants. However, stem cell transplantations in pre-clinical models of SCI showed only limited CNS repair and protection, likely due to limited capacity of transplanted cells to robustly integrate *in vivo*. In this perspective, we envision that a combination of interventions aiming to first modulate the injured microenvironment will create a more hospitable context for the subsequent stem cell transplantation.

Expression of Lipocalin 2 (Lcn2), a siderophore-binding protein implicated in modulation of inflammatory response in CNS diseases, is upregulated in reactive astrocytes that play a major role in inhibiting regeneration in SCI. We aim to ameliorate the deleterious injured environment through the downregulation of Lcn2 expression by delivering packaging RNA (pRNA) nanostructures to create a more amenable niche for improving the engraftment and differentiation of transplanted iNSCs. To achieve this, we first established a reproducible and reliable *in vitro* protocol for NPC-derived astrocyte differentiation, a more homogeneous population compared to primary astrocyte cultures, subsequently employed for safety and efficacy screening of pRNA nanostructures. NPC-derived astrocytes showed mature astrocytic phenotype after 15 days *in vitro* culture and gene expression changes upon activation, as observed *in vivo*. To silence Lcn2 expression we employed pRNA nanostructures, a bio-inspired construct and promising candidates amongst different nanotechnologies. Remarkably, pRNA transfection did not show any cytotoxicity on cultured astrocytes and we

observed a specific and significant decrease in the expression of target mRNA upon pRNA transfection, i.e. reduction of classical hallmarks of activated astrocytes (GFAP and vimentin upregulation) here assayed as *a proof of concept,* and significant reduction in Lcn2 expression as a new therapeutic target. Finally, before combining pRNA transfection and iNSC transplantation *in vivo*, we first aimed to characterize and compare the therapeutic efficacy of transplanted iNSCs with the well-described NPCs in a murine contusion model of SCI. Preliminary data showed a similar survival rate after transplantation between iNSCs and NPCs and interestingly a similar trend in improvements of fine locomotor recovery 7 weeks after transplantation.

Therefore, transplantation of fully immunocompatible iNSCs represents an innovative and promising therapeutic approach for SCI and *in vitro* results obtained from Lcn2 silencing showed encouraging results for a future promising combinatorial approach that aims at healing the injured environment and promoting functional recovery in SCI.

INDEX

1) AIMS OF THE PROJECT

Trauma to the spinal cord triggers the activation of a cascade of molecular and cellular events that ultimately leads to different degrees of paralysis in correlation with the severity and location of the initial trauma. Although it has been observed that neural tissue repair may spontaneously occur in patients affected by acute and chronic inflammatory and degenerative disorders of the nervous system, this process is not robust enough to promote a functional and stable recovery of the nervous system architecture [1]. Furthermore, despite initial surgical approaches, such as surgical decompression and stabilization of the spinal cord, corticosteroid administration and physical therapy aiming to minimize the damage to the spinal cord and optimize the functionality of spared connections [2], there are still no fully restorative therapies for SCI [3].

From this perspective, promotion of tissue repair and regeneration represents one of the most intriguing although challenging therapeutic approaches [4], and different experimental regenerative therapies have been developed in the last decades aiming to diminish or modulate the devastating consequences of SCIs [5]. Amongst these experimental therapies, stem cell transplantation has shown promising results in ameliorating the damaged environment and promoting functional recovery. Pluripotent embryonic stem cells, the recently developed induced pluripotent stem cells (iPSCs) and somatic neural precursor cells (NPCs) are characterized *in vivo* by remarkable intrinsically differentiation potential and potential to adapt their fate and functions to the specific microenvironment requirements. However, clinical translation of stem cell transplantation is limited by major issues of accessibility, immunocompatibility of cell sources, and ethical concerns; moreover, the lesion site in SCI pathology is an hostile and inhospitable environment that limits the survival, differentiation and engraftment of transplanted cells. To address the first translational issues, the use of induced neural stem cells (iNSCs) [6] can overcome allogeneic limits arising from transplantation of foetal NPCs used in clinical trials. However, the inhibitory nature of the injured site still represents the major impediment for a successful engraftment of transplanted cells [7]. The major contributors to this hostile environment and inhibitory mechanisms are

represented by reactive astrocytes, thus combinations of strategies, such as stem cell transplantation augmented by modulation of secondary mechanisms, may lead to cumulative improvements in outcome after SCI [8]. Astrogliosis, as is called this phenomenon of reactivity observed in astrocytes, involves a broad range of mechanisms and its experimental modulation has yielded controversial outcomes. Indeed, it is now clear that complete ablation of reactive astrocytes leads to detrimental effects in SCI pathology [9] [10], but on the other hand chronic astrogliosis can limit and inhibit axonal regeneration. Most of the approaches aimed at modulating two of the hallmarks of reactive astrocytes, i.e. upregulation of the intermediate filaments glial fibrillary acidic protein (GFAP) and vimentin, yielded controversial outcomes. The targeted ablation of reactive astrocytes after CNS injury, by using the mouse GFAP promoter in transgenic mice, showed an exacerbation of tissue degeneration [9, 11] suggesting that loss of astrocytes in the acute phase after CNS injury may lead to secondary degeneration of other cell types (Liu and others 1999; Zhao and others 2003), on the other hand some studies showed increased axon regeneration by deletion of GFAP and vimentin genes [12, 13]. More intriguingly, the application of siRNA targeting GFAP and vimentin in *in vivo* SCI models showed functional recovery and improvements in urinary dysfunctions, by injecting siRNA soon after the injury [14, 15]. Contrary to the knockout technique, the RNAi systems achieves downregulation of dysregulated mRNA/proteins without the loss of genomic information of the targeted gene; moreover, they allow for the possibility of modulating the extent and timing of gene regulation [16]. Thus, based on the dual role of astrogliosis in SCI, but more generally in CNS diseases, we strongly believe that a time-specific modulation of this phenomenon may lead to remarkable beneficial outcomes: while the presence of reactive astrocytes in acute stage of the disease would restrict the spread of secondary damages, their modulation in sub-acute stage would avoid the consolidation of such phenomena that have been shown to become detrimental, especially in the chronic phase.

However, based on the fact that reactive astrocytes exert contradictory effects after CNS insults, beneficial or harmful depending o context and timing, it may be efficacious to look for new therapeutic targets that modulate these different activities in a controllable

fashion and test these mechanisms. Amongst potential candidates for modulation, Lipocalin 2 (Lcn2), a siderophore-binding protein implicated in the modulation of the inflammatory response in several CNS diseases, may represent a more promising target [17]. Indeed, silencing of Lcn2 in sub-acute phase may lead to a modulation of the inflammatory response and secondary damages upon SCI, creating a more favourable environment for iNSCs transplantation and engraftment.

Small interfering RNA (siRNA) represents a great promise for targeted gene silencing in therapeutic applications, and advances in knowledge about the molecular mechanisms of endogenous RNA interference (RNAi) has been used to develop innovative nucleic-acid medicines as treatment of diseases, most commonly cancers [18]. However, clinical translation of RNA-based therapeutics is impeded by difficulties in delivery; nevertheless, over the last couple of decades nanotechnology has advanced the development of drug-delivery platforms, including siRNA–based drugs [19]. Specific to the purposes of this study, packaging RNA (pRNA) nanostructures, bio-inspired constructs, are a promising example of this technology. Its advantageous size, thermodynamic stability,resistance to chemical denaturation, and modular nature make it a suitable candidate for translational approaches.

Therefore, the overall goal of this project is to conduct preliminary investigations into a combinatorial approach for SCI therapy, aiming to ameliorate the deleterious injury environment through the downregulation of Lcn2 expression by delivering pRNA nanostructures, to ultimately create a more amenable niche for the engraftment and differentiation of therapeutically-potent transplanted iNSCs.

Thus, the aims of this project have been:
- establishment of a reproducible and reliable protocol for *in vitro* reactive astrocyte culture that would allow for screening of the safety and efficacy of pRNA nanostructures;
- evaluation of the safety and efficacy of pRNA nanostructures in silencing *Gfap* and *Vim* genes as *a proof of concept,* and the evaluation of *Lcn2* silencing in the perspective of a translational approach; and

- evaluation of the potential for clinical application of iNSCs compared to the most commonly used and characterized NPCs, by analysing the effects of subacute iNSC transplantation-induced functional recovery in a mouse model of moderate contusive spinal cord injury.

2) MATERIALS AND METHODS

2.1 NEURAL PROGENITOR CELL (NPC) EXPANSION CULTURES

Neural progenitor cells (NPCs) were isolated from the sub-ventricular zone (SVZ) of adult C57BL/6 mice as previously described [20]. NPCs were cultured as neurospheres in NPC proliferation medium: Neurocult basal medium (mouse; Stem Cell Technologies) containing 10% Neurocult proliferation supplement (mouse; Stem Cell Technologies), 2 μg/ml heparin (Stem Cell Technologies), 20 ng/ml recombinant human EGF (PeproTech), 10 ng/ml recombinant human FGF-basic (PeproTech), and 100 U/ml penicillin-streptomycin (Gibco), and passaged every 3-5 days [21] in order to allow neurospheres to reach a diameter of 150-200 nm. To passage, NPC neurospheres were spun at 200 x g for 10 min and the pellet was enzymatically dissociated into single cells by resuspension in 200 μl Accumax (Sigma-Aldrich) and incubation for 10 min at 37°C. Accumax was then inactivated by adding 800 μl of NPC proliferation medium at 37°C. Cell densities were determined with a haemocytometer using Trypan Blue to stain for dead cells. NPCs were plated at a clonal density of 8,000 cells/cm², as described [22]: 200,000 in 5 mL for a T25 flask, 600,000 in 10 mL for a T75 flask, and 1,400,000 in 15 mL for a T175 flask. All cells were cultured at 37°C in a humidified atmosphere of 5% CO_2. All proliferating cell lines were routinely checked for Mycoplasma contamination.

2.2 INDUCED NEURAL STEM CELL (iNSC) EXPANSION CULTURES

Induced neural stem cell (iNSC) lines from MEFs (mouse embryonic fibroblasts) were obtained from Frank Edenhofer (Stem Cell Engineering Group, Institute of Reconstructive Neurobiology, University Bonn). Cultures were started from a frozen vial of iNSCs (stored in liquid nitrogen), using iNSC proliferation medium: 1X N-2 supplement, 100 U/ml penicillin-streptomycin, 10 ng/ml bFGF (PeproTech), and 10 ng/ml EGF (PeproTech) in DMEM/F12 (Gibco).

Every other day, half of the total volume of the medium was added to the iNSCs. Cells were passaged every 5 days allowing neurospheres to reach a diameter of 150-200 nm. To passage, neurospheres were spun at 325 x g for 10 min and the pellet was enzymatically dissociated as for NPCs, with the difference that before counting for the cell density cells were spun again in order to remove Accumax and cells were resuspended in 1 ml of iNSC proliferation medium. Cell density was counted as for NPCs. iNSCs were plated at a clonal density of 10,000 cells/cm²: 250,000 in 5 mL for a T25 flask, 750,000 in 10 mL for a T75 flask, and 1,750,000 in 15 mL for a T175 flask. All cells were cultured at 37°C in a humidified atmosphere of 5% CO_2. All proliferating cell lines were routinely checked for Mycoplasma contamination.

2.3 NPC-DERIVED ASTROCYTE DIFFERENTIATION PROTOCOLS

For adherent astrocyte differentiation, plastic plates or glass coverslips were coated with 20 μg/mL poly-D-lysine (PDL) in sterile water at 37 °C for 3 h, before being washed 3 times with sterile water and left to dry in sterile conditions. Single NPC-dissociated cells were plated at 80,000 cells/cm^2 prior to differentiation in astrocyte media, yielding approximately 70-90% astrocyte confluence at the later time of analysis.

NPCs were differentiated into astrocytes by using two different conditions: *high-FBS/FGF2-free condition* or *low-FBS/+FGF2 condition*. NPC-derived astrocytes were cultured in high-FBS/FGF2-free conditions for 15 days; medium was refreshed every 3 days by replacing half of the total medium volume. High-FBS/FGF2-free astrocyte differentiation medium was prepared by using low glucose Dulbecco's Modified Eagle Medium (DMEM, 1 g/l glucose; Gibco) with 10% fetal bovine serum (FBS; Gibco), 1 mM glutamine, and 100 U/ml penicillin-streptomycin. NPC-derived astrocytes cultured in low-FBS/+FGF2 conditions were first grown for 7 days in high-FBS medium: DMEM enriched with 10% FBS, supplemented with 50 ng/ml FGF2 (PeproTech); medium was refreshed every 3 days by replacing half of the total medium volume. After 7 days, medium was completely replaced by low-FBS/+FGF2 medium: DMEM, 1% FBS, supplemented with 1X N-2 Supplement (Life Technologies) and 50 ng/ml FGF2.

NPC-derived astrocytes, both high-FBS/FGF2-free and low-FBS/+FGF2, were activated at day 13 (*therapeutic activation*) or at day 15 (*preventative activation*) by adding to the corresponding medium 2 μg/ml LPS (Sigma-Aldrich) and 3 ng/ml murine IFNγ (PeproTech).

2.4 pRNA-3WJ NANOSTRUCTURE DESIGN AND ASSEMBLY

Packaging-RNA (pRNA)-based 3 way junction (3WJ)-siRNA were designed and assembled according to previously described methods[23], briefly elaborated as follows. pRNA 3WJs are characterized by three RNA strands: a 20-nucleotide ***B*** RNA strand common to each of the 3WJ structures and variable 41-nucleotide ***A*** and ***C*** RNA strands that contain the siRNA sequence distinct to each 3WJ. The siRNA sequences employed in the 3WJs described herein were derived from those used in the commercially-obtained anti-*Gfap*, anti-*Vim*, anti-*Lcn2*, and non-targeting siRNA pools used as positive/negative controls in these experiments (Table 2.1).

The common ***B*** RNA strand was purchased as a commercially-synthesised oligonucleotide stock (Sigma), whereas the ***A*** and ***C*** strands were generated by *in vitro* transcription of appropriate double-stranded (ds) DNA templates. These templates were purchased as individual, complementary DNA strands (Sigma), which were resuspended in Tris-EDTA (TE) buffer (10 mM Tris.HCl, 1 mM EDTA in nuclease-free water, pH 8.0) in order to obtain a stock concentration of 100 μM per strand. Equimolar amounts of each strand were annealed together in 1X Tris-Magnesium-Sodium (TMS) buffer (0.5 M Tris.HCl, 1 M NaCl, 100 mM $MgCl_2$ in nuclease-free water) using a thermal cycler (5 minutes at 80°C before cooling by 1°C every 30 s until reaching a minimum of 4°C) and stored at -20°C. Each dsDNA template was designed with a 5′ T7 RNA polymerase promoter sequence (**TAA TAC GAC TCA CTA TT**G G) to facilitate efficient transcription. Template concentrations were assayed using a NanoDrop 2000 spectrophotometer (Thermo Scientific).

Transcription of the ***A*** and ***C*** RNA strands was performed using a TranscriptAid T7 High Yield Transcription Kit (Thermo Scientific). RNA products were isolated and

purified by DNase treatment and subsequent denaturing polyacrylamide gel electrophoresis (PAGE; 10% polyacrylamide (w/v) gel with 8 M urea in 1X Tris-Borate-EDTA (TBE) buffer: 90 mM Tris base, 90 mM boric acid, and 2 mM EDTA in nuclease-free water, pH adjusted to 8.5). A 1:1 mixture of RNA transcript solution and 2X *denaturing loading buffer* was loaded into the gel and electrophoresed at 120 V for 1 h. The appropriate RNA bands were identified by UV shadowing, excised from the gel, and diced into small pieces that were transferred to 1.5 ml Eppendorf tubes. Subsequently, the gel pieces were eluted in a *denaturing* elution buffer (0.5 M ammonium acetate, 0.1 mM EDTA, 0.1% SDS) at 37°C for 2 h. The supernatant was collected and stored on ice while the gel pieces were subjected to a further hour of elution using a fresh aliquot of elution buffer. All fractions of each eluate were then combined into the same tube and the eluted RNA precipitated by the addition of 1/10 equivalent volumes of 3 M sodium acetate (pH 5.2) and 2.5 equivalent volumes of 100% ethanol. The solutions were mixed well and stored at -20°C overnight to allow them to precipitate. Samples were then centrifuged (16,500 *g* for 30 min at 4°C), supernatant was removed, and the pellet was washed in 500 µl of cold 75% ethanol with a further centrifugation (16,500 *g* for 15 min at 4°C). The supernatant was again discarded and the pellet briefly dried in a vacuum concentrator (SpeedVac, Thermo Scientific) prior to storage at -20°C until ready for 3WJ assembly.

Before assembly, the transcribed ***A*** and ***C*** RNA strands and the ***B*** strand oligonucleotide were re-dissolved in RNase-free water and the concentration of each solution quantified using a NanoDrop. Where desired, RNA strands were labelled with a fluorophore (i.e. Cy3) using a Label IT Nucleic Acid Labeling Kit (Mirus BioScience) according to the supplier's protocol, with subsequent ethanol precipitation (as above), re-dissolution and re-quantification. Transcription and labelling success was assayed using an additional denaturing PAGE gel, running approximately 500 ng of each RNA strand or complex in lanes alongside an Ultra Low Range DNA ladder (Thermo Scientific) to ensure the purity and the correct length of RNA strands. Fluorescently-labelled bands were identified by eye or using a ChemiDoc XRS+ system with the appropriate excitation wavelength, while non-labelled bands were identified by UV transillumination following staining with ethidium bromide or GelRed (Biotium).

Assembly of each 3WJ was achieved by combining equimolar amounts of the appropriate strands ***A*** and ***C*** with strand ***B*** in 1X TMS buffer, typically on a 50 µl scale in a 200 µl PCR tube. The solutions were then subjected to an annealing temperature profile in a thermal cycler, as follows: heating to 80°C, holding for 5 min before cooling 1°C every 30 s until reaching a minimum temperature of 4°C. Assembled 3WJs were purified of excess single RNA strands or misassembled byproducts using *native* PAGE (10% polyacrylamide in 1X Tris-Borate-Magnesium (TBM) buffer: 90 mM Tris base, 90 mM boric acid, and 5 mM $MgCl_2$ in nuclease-free water, pH adjusted to 8.5) the gel was run at 100V for 2 h at 4°C to inhibit thermal denaturation. The 3WJ bands were identified by using UV shadowing, then cut from the gel and eluted with a *non-denaturing* elution buffer: 0.5 M ammonium acetate, and 10 mM $MgCl_2$. The assembled 3WJs were ethanol precipitated from the collected eluate, re-dissolved in RNase-free water, and quantified using a NanoDrop. Success of assembly was assayed by running 500 ng of each 3WJ in an additional non-denaturing PAGE gel alongside the Ultra Low Range DNA Ladder, as well as samples of single ***A***, ***B*****,** and ***C*** strands and annealed two-strand constructs. Correctly assembled 3WJs showed lower gel mobility than did double- or single-stranded RNAs and were diluted to a stock concentration of 5 µM in 1X TMS buffer solution for subsequent use. The resultant nanostructures – G10, V10, and L12 – possessed anti-*Gfap*, *Vim* or *Lcn2* siRNA moieties, respectively, while the N03 negative control 3WJ possessed an siRNA sequence that does not match any known mammalian gene.

RNA	**Sequence**[*]	**Length**	**Reference**[†]
3WJ Strand a	5'- GGN NNN NNN NNN NNN NNN NNN AAG GGU CAU GUG UAU GU GGG -3'	41-nt	n.a.
3WJ Strand b	5'- CCC ACA UAC UUU GUU GAU CC -3'	20-nt	n.a.
3WJ Strand c	5'- GGA UCA AUC AUG GCC CAA NNN NNN NNN NNN NNN NN NNU UUU -3'	41-nt	n.a.
Anti-*GFAP* moiety	5'- AGC ACG AAG CUA ACG ACU A -3'	19-nt	J-043455-10
Anti-*Vimentin* moiety	5'- AGG AAG AGA UGG CUC GUC A -3'	19-nt	J-061596-10

Anti-*Lipocalin 2* moiety	5'- GCG CAG AGA CCC AAU GGU U -3'	19-nt	J-042638-12
Non-Targeting moiety	5'- UGG UUU ACA UGU UUU CUG A -3'	19-nt	D-001810-03

Table 2.1: Sequences of pRNA 3WJ strands.
* Red nucleotides depict variable siRNA moiety
† GE/Dharmacon catalogue number

2.5 Transfection of NPC-Derived Astrocytes with siRNA/3WJs

Intra-cellular delivery of RNAs was performed via transfection using the liposomal transfection agent Lipofectamine RNAiMAX (Life Technologies) on near-confluent astrocyte cultures.

To compare the knock-down efficiency of 3WJs to commercial siRNAs, transfection was performed at day 15 on astrocytes cultured under high-FBS/FGF2-free resting conditions using three different concentrations of siRNA/3WJ: 5, 0.5 and 0.05 nM. Silencing experiments were performed under both resting and activation conditions (*therapeutic* and *preventative*) by transfection at day 15 of 5 nM concentrations of siRNA/3WJ. Immediately prior to transfection the astrocyte differentiation medium was replaced with low glucose (1 g/l) DMEM serum-free medium. Transfections were performed according to the protocol accompanying the Lipofectamine agent. Briefly, 5 μM stock solutions of the siRNAs or 3WJs of interest were diluted in DMEM and combined with an equivalent volume of DMEM containing Lipofectamine RNAiMAX (1:1 ratio of siRNA/3WJ to Lipofectamine solutions). The solution was mixed well and allowed to incubate for 10 minutes before being added to cells such that the final concentration of siRNA/3WJ was 5, 0.5, or 0.05 nM, as desired, in a 3 ml final volume of serum-free medium. Each experiment included controls for the transfection, such as mock transfections (Lipofectamine only, no RNA) and untreated control wells (DMEM only, no RNA or Lipofectamine). 6 hours after transfection the serum-free transfection medium in each well was replaced with the corresponding serum-containing medium. RNA samples were collected 48 hours post-transfection and proteins collected at different timepoints post-transfection (24 h and 48 h after transfection for Lcn2 assessment, 120 h after transfection for GFAP and Vim assessment).

2.6 CYTOTOXICITY ASSAY

The toxicity of siRNA-3WJ treatments were assessed by using LDH-Cytotoxicity Assay Kit II (Abcam), following the instructions provided. Lactate dehydrogenase (LDH) is a stable enzyme present in all cell types that is rapidly released upon damage of the plasma membrane. This assay kit is based on an enzymatic coupling reaction that allows for direct correlation of the intensity of a generated colour to the number of lysed cell. Supernatant was collected from each sample and spun at 600 x g for 10 min to precipitate any debris, 20 µl of each sample were transferred into an optically clear 96-well plate as triplicates. The LDH reaction mix was reconstituted for 10 minutes and 100 µl were added to each well, well-mixed and incubated for 30 minutes at room temperature. The absorbance of all wells was measured with an Infinite 200 plate reader (Tecan) set with a 440-490nm filter, and 650nm as reference wavelength. Toxicity/viability was normalised to non-transfected controls (100% viability) and samples lysed with a 10% v/v solution of Triton X-100 (0% viability). Assays were performed on the supernatant of low-FBS/+FGF2 astrocytes grown in 6-well plates, at timepoints of 24 h, 48 h and 120 h post-transfection. The 48 h and 120 h timepoints included a medium change at 6 h post-transfection.

2.7 CONDITIONED MEDIUM EXPERIMENTS

Confluent astrocytes were used for conditioned medium experiments. Donor astrocytes were transfected as described herein. "Conditioning" astrocytes, activated with-or-without a concomitant transfection with 5 nM L12-3WJ, were washed 2 times with PBS and medium was exchanged with low-glucose DMEM (containing 100 U/ml penicillin-streptomycin) at 24 h post-transfection/activation. At 48 h post-transfection/activation this astrocyte conditioned medium (ACM) was collected and spun at 600 x g for 10 minutes before 300 µl of sample was set aside for enzyme-linked immunosorbent assay (ELISA) experiments and the remainder (2 ml) transferred to recipient *resting*

astrocytes. After a further 24 h, the RNA of the recipient astrocytes was collected for qPCR analysis

2.8 IMMUNOFLUORESCENCE

Cells grown on PDL-coated glass coverslips were fixed in 4% paraformaldehyde (PFA) for 10 min at room temperature at the appropriate timepoint post-differentiation or post-transfection. The coverslips were washed three times with 1X phosphate buffered saline (PBS) before being incubated in blocking solution (1X PBS containing 0.1% Triton X-100 (Sigma-Aldrich) and 5% normal goat serum (NGS; Sigma) for 60 minutes at room temperature. Fixed cells were subsequently incubated in 60 μl of the same blocking solution containing the desired primary antibodies (Table 2.2) overnight at 4°C. The following day cells were washed 3 times in 1X PBS and incubated in 60 μl of blocking solution containing the species-appropriate fluorochrome-conjugated secondary antibodies (1:1000 dilution) for 60 minutes at room temperature. Coverslips were subsequently washed 3 times with PBS 1X before cell nuclei were counterstained with a 1 μg/ml solution of 4′,6-diamidino-2-phenylindole (DAPI; Roche) in 1X PBS for 5 minutes at room temperature. After a final wash, coverslips were mounted onto slides with fluorescent mounting medium (Dako). Images were acquired at 40X and 20X magnification using a Leica DM6000 vertical epifluorescent microscope, and images processed using the Fiji software package [24]. Consistent settings were used to acquire all images, using the appropriate filter set for each fluorophore/antibody combination. At least two independent coverslips were imaged for each biological replicate, each comprising 10 independent fields-of-view randomly distributed across distinct regions of the coverslip: 4 in the centre and 3 respectively in the upper and lower side of the coverslips.

Antibody	**Supplier**	**Dilution**
Chicken anti-GFAP	Abcam	1:500
Rabbit anti-GFAP	Wako	1:500
Chicken anti-Vimentin	Abcam	1:500
Rat anti-Lipocalin2	R&D Systems	1:250
Mouse anti-S100B	BD Bioscience	1:500

Mouse anti-Nestin	Millipore	1:100
Rabbit anti-β-tubulin III	Covance	1:500
Rabbit anti-cleaved Caspase III	New England Biolabs	1:400
Rabbit anti-pSTAT3	Cell Signaling	1:100
Mouse anti-O4	R&D Systems	1:50
Mouse anti-MAP2	Abcam	1:500
AlexaFluor488 anti-chicken	Invitrogen	1:500
AlexaFluor488 anti-rabbit	Invitrogen	1:500
AlexaFluor546 anti-mouse	Invitrogen	1:500
AlexaFluor546 anti-rabbit	Invitrogen	1:500
AlexaFluor647 anti-rabbit	Invitrogen	1:500

Table 2.2: Antibodies used for ICC

2.9 ENZYME-LINKED IMMUNOSORBENT ASSAY (ELISA)

Levels of secreted murine Il6, Tnf and Lcn2 were quantified using sandwich ELISA development kits (Il6 and Tnf: BioLegend; Lcn2: R&D Systems). For Il6 and Tnf, $2x10^6$ NPCs were seeded in 10 ml of astrocyte medium on PDL-coated T25 plates. Medium was refreshed every 3 days, for which 3 mL was used for the assay. Before activation, medium was collected (i.e. 0 hours activation). Medium was collected at 6 h, 12 h, 24 h, and 48 h post-activation. Collected medium was spun for 15 minutes at 2,000 x g at 4°C and supernatant was collected and stored at -80°C. 96-well plates (Nunc-Thermo Scientific) were coated with 100 µL of Capture Antibody in PBS 1X overnight at room temperature. After 4 washes with washing buffer (PBS, 0,.05% Tween-20) wells were blocked with 200 µL of 1X Assay Diluent for 1 h at room temperature and subsequently washed 4 more times. Samples were diluted 9:10 with Assay Diluent and loaded in the plate in quadruplicate at 100 µL; astrocyte medium was loaded as blank. Antigen capturing took place for 2 h at room temperature, after which plates were washed 4 times, and incubated with 100 µL of Detection Antibody in for 1 h at room temperature. After 4 more washes, 100 µL of 1:1,000 avidin-HRP in 1X Assay Diluent was added for 30 min at room temperature, then washed again 4 times before adding TMB Substrate Solution for 15 minutes in the dark at room temperature. Finally, 100 µL of Stop Solution was added. Using a microplate reader, optical densities were measured at 450 nm and 570 nm.

For Lcn2, pre-coated 96-well microplates (R&D Systems) were brought to room temperature, and 50 µL of standard, control and samples as triplicate were loaded into the wells and incubated for 2 hours at room temperature. After 3 washes with 400 µL of Wash Buffer, 100 µL of Mouse Lipocalin-2 Conjugate was added to each well and incubated for 2 hours at room temperature. After 3 more washes with 400 µL of Wash Buffer, 100 µL of Substrate Solution was added to each well for 30 minutes in the dark at room temperature. Then, 100 µL of Stop Solution was added to each well. Using a microplate reader, optical densities at were measure at 490 nm with wavelength correction at 570 nm.

An eight point standard curve was generated using known concentrations of recombinant mouse Tnf (2 ng/ml, and a serial dilution of 1:2), recombinant mouse Il6 (4 ng/ml, serial dilution 1:2), and recombinant mouse Lcn2 (5 ng/ml, serial dilution 1:2). The standard was diluted with either the supplied diluent, or with astrocyte differentiation medium to assess any possible interference in the detection of the cytokines of interest. Data analysis was performed by interpolating unknown concentrations with the recombinant mouse Il6, Tnf or Lcn2 standard curves after nonlinear regression fit, using the sigmoidal four parameter logistic dose-response variable slope curve on log-transformed data (as described in the GraphPad Prism manual).

2.10 Quantitative Real-Time Polymerase Chain Reaction (qRT-PCR)

RNA extraction was performed using nuclease-free/diethyl pyrocarbonate (DEPC)-treated water and surfaces were cleaned with RNaseZap (Thermo Fisher Scientific) to prevent RNase contamination.

Astrocytes were grown adherent to 6-well plates. At day 17, cells were aspirated and washed with 1X PBS (Gibco) and subsequently lysed by incubation at room temperature with 1 ml TRI Reagent (Sigma) per 10 cm² well for 5-10 min. TRI Reagent cell lysates were mixed with 20% vol. chloroform, incubated for 2-3 min and spun at 12,000 x g for 15 min at 4 °C, allowing for phase separation. The RNA-containing upper aqueous phase was collected, added to an approximately equal volume of isopropanol, and incubated at room temperature for 10 minutes. To remove water-soluble contaminants such as sugars and salts, RNA was precipitated by spinning samples at 12,000 x g for 30 min at 4 °C. Pellets were washed twice with 1 mL 75% EtOH, spun at 12,000 x *g* for 15 min at 4 °C, and decanted before being allowed to air-dry under a fume hood and resuspended in 20 µL nuclease-free water. Samples were heated (55-60 °C) for 10 min, prior to quantification of concentration and purity using a NanoDrop spectrophotometer. RNA samples determined to have acceptable A_{260}/A_{280} and A_{260}/A_{230} purity ratios were stored at -80 °C until further use.

From 500 ng of total RNA, cDNA was generated using a High Capacity cDNA reverse transcription kit (Applied Biosciences) using random hexamer primers. Reverse transcription was performed using a T100 thermal cycler (Bio-Rad) and the following program: 10 min at 25 °C, 50 min at 50 °C, 5 min at 80 °C, and then held at 4 °C. qRT-PCR was subsequently performed using TaqMan reagents (TaqMan Fast Universal PCR Master Mix (2X) and FAM-labelled TaqMan Gene Expression Assays as listed in (Table 2.3) and an Applied Biosystems Quantstudio 7 real-time PCR system using the following program: 20 s at 95 °C, followed by 40 cycles of 3 s at 95°C – 30 s at 60°C. Where possible, exon-spanning TaqMan probes were used to control for possible genomic DNA contamination. Mouse *Gapd* (VIC-labelled, Life Technologies) was used as a reference gene for determining relative gene expression using the $2^{-\Delta\Delta Ct}$ method [25]. Each biological sample was measured in triplicate.

Target Gene	TaqMan Assay
Gfap	Mm01253033_m1
Vim	Mm01333430_m1
Lcn2	Mm01324470_m1
Nes	Mm00450205_m1
Il6	Mm00446190_m1

Tnf	Mm00443258_m1
Ifnb1	Mm00439552_s1
Nos2	Mm00440502_m1
Ciita	Mm00482914_m1
Il1b	Mm00434228_m1
Tlr4	Mm00445273_m1
Ifngr1	Mm00599890_m1
Ifngr2	Mm00492626_m1
Gapd	4352339E

Table 2.3: TaqMan probes for qPCR

2.11 WESTERN BLOTS

Cells were collected from 6-well plates at appropriate time points post-transfection. Astrocytes, grown in adherent conditions in 6-well plates, were washed with 1X PBS (4 °C). Cells were detached by scraping in 500 µl of 1X PBS (4°C) and transferred to a 2 mL Eppendorf tube, to ensure the collection of all cells, wells were further washed with additional 500 µl of 1X PBS. Samples were spun at 500 x g for 20 min at 4°C and the supernatant was discarded.

Proteins were extracted from the pellets by solubilisation in radioimmunoprecipitation assay (RIPA) buffer (Abcam) with the addition of Complete Protease Inhibitor Cocktail (Roche) and Halt Phosphatase Inhibitor Cocktail (Thermo Scientific), in addition to 1 mM phenylmethanesulfonyl fluoride (Sigma) to inhibit serine proteases. Protein quantification was performed using a Pierce BCA Protein Assay kit (Thermo Scientific): 25 µl of diluted samples, in triplicate, and 25 µl of Diluted Albumin Standards were incubated with 200 µl of Working Reagent for 30 minutes at 37°C, prior to reading the optical density of the samples at 562 nm with a microplate reader. Sample volumes equivalent to 20 µg total protein were mixed with NuPAGE LDS Sample Buffer (Life Technologies), NuPAGE Sample Reducing Agent (Life Technologies), and distilled water to a final volume of 30 µl prior to being heated at 95°C for 5 min. Proteins were separated by SDS-PAGE in a 10% gel using a Novex Bolt Mini Gel system and running buffer (Tris 25 mM, glycine 192 mM, SDS 10%) before being transferred onto Immobilon-P polyvinylidene fluoride membranes (Millipore, 0.45 µm pore size, methanol equilibrated) in transfer buffer (Tris 25 mM, glycine 192 mM, methanol 20%) for 1 h 45 min at 4°C using a Novex Bolt Mini Blot

Module. A SeeBlue Plus2 standard (Life Technologies) was used to estimate protein sizes, and transfer was confirmed by Ponceau S (Sigma) staining. For immunoblot analysis, membranes were blocked 1 hour at room temperature with 0.1% v/v Tween 20 in a 5% w/v solution of dried skimmed milk powder (Marvel) in PBS (pH 7.4), and then incubated with primary antibodies overnight at 4°C (Table 2.4) diluted in antibody solution (0.1% Tween 20, 5% dried skimmed milk powder in PBS) to the appropriate concentration. After washing with PBS/0.1% Tween 20, the membranes were incubated at room temperature with the species-appropriate horseradish peroxidase-conjugated secondary antibodies (Thermo Scientific) for 1 hour at a 1:10,000 dilution in antibody solution. Immunoreactivity was revealed using Western Lightning Plus-ECL (PerkinElmer) and imaged using a Bio-Rad ChemiDoc XRS+ system with Image Lab 5.1 software (Bio-Rad). Densitometry measurements were performed using Fiji (http://fiji.sc/Fiji) each protein band being normalised to the β-actin loading controls.

Antibody	**Supplier**	**Dilution**
Rabbit anti-GFAP	Dako	1:10,000
Mouse anti-VIM	Abcam	1:500
Rat anti-LCN2	R&D Systems	1:1,000
Rabbit anti-pSTAT3 (Tyr705)	New England Biolabs	1:1,000
Mouse anti-NOS2	BD Biosciences	1:2,000
Mouse anti-ACTB	Sigma	1:10,000
Mouse anti-GAPDH	Sigma	1:2,000

Table 2.4: Antibodies for Western blot

2.12 CONTUSION MODEL OF SPINAL CORD INJURY IN MICE

Adult 6-to-8 week-old (20-22 g) male C57Bl/6 mice were obtained from Charles River (UK) and housed in specific pathogen-free conditions. Mice were deeply anesthetized with 2% isoflurane in oxygen (1.5 l/min). Buprenorphine (Temgesic, RB Pharmaceuticals) was provived pre- and post-operatively, in addition to enrofloxacin (Baytril, Bayer). The hair on the back of the mice was shaved and swabbed with a germicide prior to surgery. Under a surgery microscope, a midline incision was made over the thoracic vertebrae using a sterile scalpel, the muscles were separated from either side of the vertebral column using a spring scissor (Fine Science Tools), and

laminectomy was performed at T12 using Dumont #2 laminectomy forceps (Fine Science Tools) and spring forceps (Fine Science Tools). The lateral part of the vertebra at the site of laminectomy was not removed in order to maintain vertebral column stability. The extension of the laminectomy (approximately 1.5 mm in diameter and 2 mm in length) was consistent between animals to allow room for the impactor tip. Small incisions were performed in the muscles correspondending to T11 and T13 vertebrae for stabilization of the vertebral column using forceps attached to the infinite horizon (IH) impactor clamping platform.

Contusion cord injury was then induced on the exposed cord at T12 on a total of n = 55 mice using the Infinite Horizon (IH) impactor device (Precision Systems and Instrumentation, Lexington, KY), as previously described [26].
The mouse-impacting tip (⌀ 1.25 mm) was aligned over the exposed cord, avoiding any impact on the lateral bones, and centred using the central vein as reference. A moderate contusion injury (70 kdyne) was then performed by using IH impactor. The IH device is computer-controlled that enables the application of standard-force injuries to the spinal cords of small rodents. It also allows the recording and monitoring of different parameters, such as the desired force (70 kdyne), the actual impact force, the cord displacement, velocity that are display for each subject concomitant with graphs showing force and displacement curves versus time (Fig. 2.1). The skin was subsequently closed with 7-mm wound clips. Mice received enrofloxacin (Baytril, Bayer) for two weeks to prevent infections. Urine was expelled by manual abdominal pressure twice a day for one week and then once a day for the duration of the experiment.

All experimental procedures were performed in accordance with the UK Animals (Surgical Procedures) Act 1996.

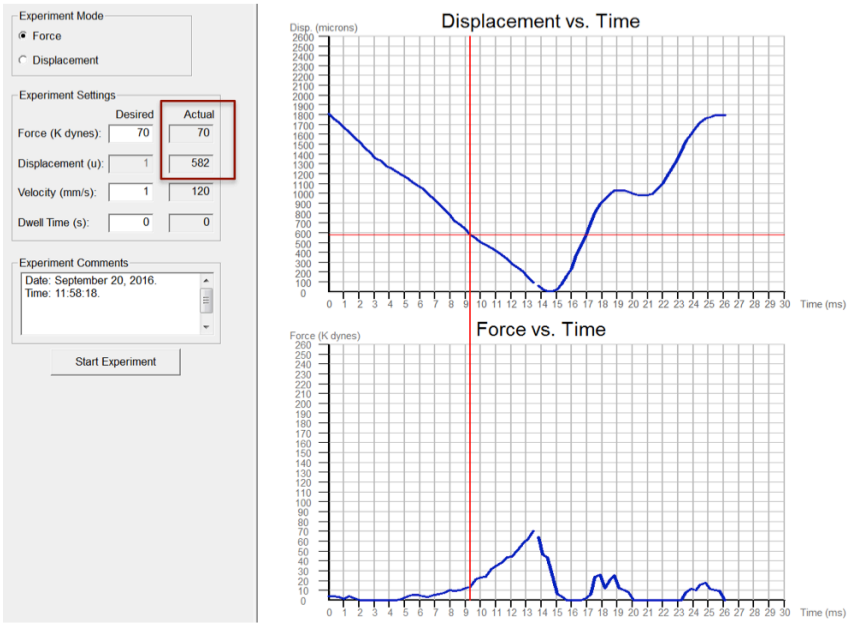

Position	Force	Time	Position	Force	Time
0	4	0.00	101	64	13.86
3	4	0.35	103	46	14.12
5	3	0.69	104	43	14.44
8	1	1.04	104	24	14.75
11	4	1.39	103	6	15.07
14	2	1.73	100	4	15.38
17	0	2.08	95	0	15.70
20	0	2.43	91	0	16.02
23	0	2.78	84	0	16.33
26	0	3.13	78	0	16.65
28	0	3.47	71	2	16.96
31	0	3.82	64	6	17.28
32	0	4.17	58	24	17.59
34	0	4.51	53	26	17.91
36	1	4.86	50	12	18.22
38	4	5.20	47	21	18.54
40	5	5.55	45	25	18.85
42	5	5.90	45	12	19.17
44	4	6.24	45	10	19.48
47	3	6.59	46	8	19.80
50	5	6.94	47	0	20.11
53	6	7.28	48	0	20.43
56	7	7.63	48	0	20.74
59	10	7.97	48	0	21.06
63	9	8.32	47	0	21.37
65	10	8.67	44	0	21.69
68	12	9.01	41	0	22.00
71	13	9.36	37	0	22.32
73	21	9.71	32	0	22.64
75	23	10.05	27	0	22.95
77	24	10.40	22	0	23.27
79	32	10.74	16	8	23.58
81	35	11.09	12	11	23.90
83	38	11.44	8	10	24.21
85	43	11.78	5	15	24.53
88	44	12.13	3	17	24.84
90	51	12.48	2	11	25.16
93	58	12.82	1	10	25.47
96	62	13.17	1	9	25.79
99	70	13.52	1	0	26.10

Figure 2.1: Representation of IH parameters. In the red box highlighted the actual force reached with the impact and the corresponding displacement. Red lines in the x-y graph represents the time of the initial impact on the spinal cord and the respective displacement. Panel on the right shows the temporal development of the contusion injury.

2.13 TRANSPLANTATION PROCEDURES

Farnesylated green fluorescent protein (fGFP) NPCs and iNSCs, having GFP localized into the plasma membranes, were freshly thawed and passaged as previously described for NPCs and iNSCs.

On the day of the transplantation 7 days after injury (subacute phase) cells were collected and spun as previously described, cells were resuspended in final a volume of ice-cold 1X PBS at a concentration of 150 x 10^3/µl and kept in ice prior to injection. Mice were anesthetized as mentioned above and the laminectomy site was re-exposed. Fibrotic tissue was remove by using Dumont #4 forceps (Fine Science Tools) and with the help of a sterile needle a small hole was created into the dura mater in order to allow the entrance of the injecting needle. The volume to inject (250 nl/injection site) was withdrawal and injected with a pump under a surgery microscope by using a 5 µl Hamilton syringe with a short 33G needle (Hamilton) placed onto a micromanipulator (World Precision Instrument). Each mouse received a total of four injection, of either iNSCs (150 x 10^3/µl), NPCs (150 x 10^3/µl) or an equal volume of vehicle, administered

bilaterally from midline at both the anterior aspect of T13 and the posterior aspect of T11. All cells used were at passage number ≤ 25.

2.14 BEHAVIOURAL ASSESSMENT

Hind-limb locomotor recovery was evaluated by the open-field Basso mouse scale (BMS), a 10-point scale [27] (Fig 2.2). All the evaluations were performed in blind conditions by 2 observers. Locomotor activity was monitored for 4 min in an open field at 1, 3, 5, 7,10, 14,18, 21, 24, 28, 31, 35, 38, 45, 49, 52 days post injury (dpi).

Score	
0	No ankle movement
1	Slight ankle movement
2	Extensive ankle movement
3	Plantar placing of the paw with or without weight support -OR- Occasional, frequent or consistent dorsal stepping but no plantar stepping
4	Occasional plantar stepping
5	Frequent or consistent plantar stepping, no coordination -OR- Frequent or consistent plantar stepping, *some* coordination, paws *rotated* at initial contact and lift off (R/R)
6	Frequent or consistent plantar stepping, *some* coordination, paws *parallel* at initial contact (P/R, P/P) -OR- Frequent or consistent plantar stepping, *mostly* coordinated, paws *rotated* at initial contact and lift off (R/R)
7	Frequent or consistent plantar stepping, *mostly* coordinated, paws *parallel* at initial contact and *rotated* at lift off (P/R) -OR- Frequent or consistent plantar stepping, *mostly* coordinated, paws *parallel* at initial contact and lift off (P/P), and *severe* trunk instability
8	Frequent or consistent plantar stepping, *mostly* coordinated, paws *parallel* at initial contact and lift off (P/P), and *mild* trunk instability -OR- Frequent or consistent plantar stepping, *mostly* coordinated, paws *parallel* at initial contact and lift off (P/P), and *normal* trunk stability and tail *down or up* & *down*
9	Frequent or consistent plantar stepping, *mostly* coordinated, paws *parallel* at initial contact and lift off (P/P), and *normal* trunk stability and tail *always* up.

Figure 2.2: Basso mouse scale (BMS) to evaluate locomotor functions. Modified from Basso et al. [27]

BMS subscore, assessed as previously described [27], was performed only on mice with a BMS score greater than or equal to 5. BMS subscore, compare to the more gross and generic evaluation performed by uding BMS score, allows the assessment of more fine locomotor capabilities, such as paw position or trunk stability (Fig. 2.3).

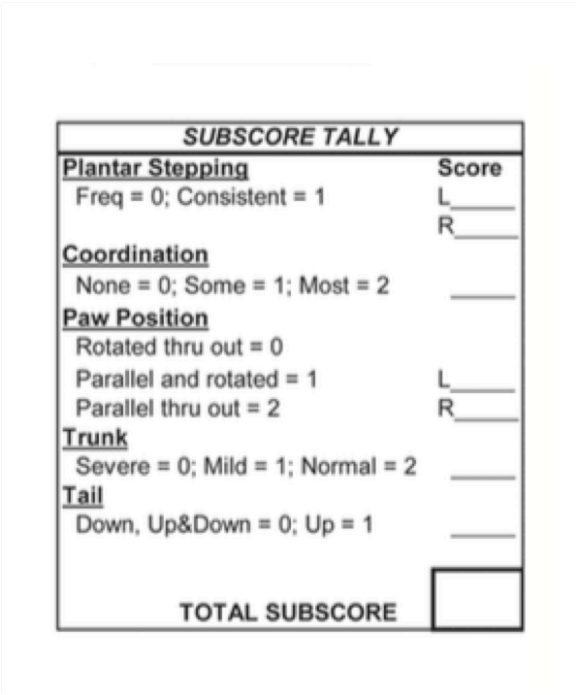

SUBSCORE TALLY	
Plantar Stepping	**Score**
Freq = 0; Consistent = 1	L_____
	R_____
Coordination	
None = 0; Some = 1; Most = 2	_____
Paw Position	
Rotated thru out = 0	
Parallel and rotated = 1	L_____
Parallel thru out = 2	R_____
Trunk	
Severe = 0; Mild = 1; Normal = 2	_____
Tail	
Down, Up&Down = 0; Up = 1	_____
TOTAL SUBSCORE	

Figure 2.3: Basso mouse scale (BMS) subscore to evaluate fine locomotor functions. Modified from Basso et al. [27]

Sensory functions were assessed by Von Frey Test. Different filaments, each with a corresponding force, were applied on the plantar surface of the hind paws of the mice in an attempt to elicit a response, following the up and down method as previously described [28]. Mice were placed onto an elevated grid and left to acclimatize for 15 min prior to the test. Testing was initiated with the 1.4 g filament. A positive response was defined as withdrawal, or licking or shaking in the stimulated hindpwas after 3 s. In case of a positive response, the next weaker stimulus was presented, in case of a negative response, the next stronger stimulus was applied. This procedure was repeated until 3 positive or negative responses were achieved, for a maximum of 6 times. The mice were tested prior to surgery and once a week for the entire duration of the experiment.

The Hargreaves apparatus (Ugo Basile) was employed to apply a thermal pain stimulation in order to measure hyperalgesia to thermal stimulation in unrestrained animals. Mice were placed onto a plexiglass surface and left to acclimatize for 15 min prior to testing. The Hargreaves' apparatus was set at 30% intensity and 20 sec were established as a cutoff time to avoid tissue damage. The mice were tested prior to surgery and once a week for the entire duration of the experiment. For each mouse, the

heat source was applied to the plantar surface of the hindpaws until the animal withdrew from the noxious thermal stimulus. 5 min was allowed between each session. Measurements were repeated 3 times for each paw.

2.15 HISTOPATHOLOGY ASSESSMENTS

Mice were anesthetized with ketamine/xylazine and transcardially perfused with saline (sodium chloride 0.9%) plus 0.5 M EDTA (Sigma) for 7 min to wash out blood, followed by cold 4% PFA in PBS pH 7.4 for other 7 min. The spinal cords were post-fixed in the same solution for 12 hours at 4°C and then washed with 1X PBS. The dissected spinal cords were cryoprotected for at least 24 hours in 30% sucrose (Sigma) in 1X PBS at 4°C, then the cords were embedded in Optimal Cutting Temperature (OCT) (VWR Chemicals) and frozen using dry ice. Frozen cord blocks were placed in a cryostat (Leica) and 30 μm-thick axial sections were cut and collected onto SuperfrostPlus slides (ThermoScientific). Immunofluorescence was performed as described above (Table 2.5).

Antibody	**Supplier**	**Dilution**
Chicken anti-GFP	Abcam	1:500
AlexaFluor488 anti-chicken	Invitrogen	1:500

Table 2.5: Antibodies for immunofluorescence staining

2.16 STATISTICAL ANALYSIS

Statistical analyses were performed using the GraphPad Prism 6 software package. For multiple comparisons of three experimental groups (NPC characterization and differentiation data) nonparametric test Kruskal-Wallis test was used, corrected with Dunn's post hoc test. One-Way analysis of variance (ANOVA) ,followed by Dunnet's multiple comparison test, was used for comparison of three or more experimental groups (qRT-PCR data), while two-way ANOVA with Bonferroni post tests was used for multi-group comparisons under multiple conditions. For comparison of two experimental groups, Student's t-test was applied. Results are expressed as mean ±

standard deviation (SD) unless otherwise stated, typically from the means of n = 3 technical replicates from N ≥ 3 biological replicates.

BMS, Von Frey and Hargreaves score was calculated as mean between scores attributed to the left and right paws, resulting in a unique score for each mouse. Data were analysed by using two-way ANOVA followed by Bonferroni post-hoc test correction. Results are expressed as mean ± standard deviation (SD) or standard error mean (SEM), as indicated. Statistical analysis was conducted at 95% confidence level. A *P* value less than 0.05 was considered as statistically significant.

3) INTRODUCTION

The role of astrocytes has been reconsidered in recent decades, initially thought to be passive support cells, they have been shown to have crucial roles in several functions within the CNS, such as controlling synapse formation[29] and function[30], controlling of the energy supply to neurons and the turnover of neurotransmitters [31], supporting the blood-brain barrier [32] and regulating the flow of blood within CNS tissue [33]. These changes in the astrocytic-point of view has led also to an increased interest in understanding the functional role of astrocytes in CNS disease, since growing evidences showed the capability of astrocytes to respond to CNS insults by changing their functions and gene expression [34-37].

3.1 ASTROCYTES IN NEUROGENESIS

Rudolf Virchow was the first to describe the central nervous system (CNS) as being composed of two main distinct cell populations, neurons and glial cells, where neurons were the real effector cells and glial cells served a simple supportive function [38]. As neuroscience progressed, so did our understanding of the role of glia beyond simply being the connective tissue of the brain. Glia were subsequently divided into two classes, microglia and macroglia, with the former representing the native immune system of the CNS and the latter including a variety of cell types, such as oligodendrocytes and astrocytes, that perform a multitude of integral CNS functions. The functional diversity and importance of astrocytes in particular has become increasingly prominent during recent years and, despite the common thought that neurons and astrocytes arise from different progenitors, more recent evidence suggesting that neurogenesis and gliogenesis are connected [39, 40] has highlighted the principal role of astrocytes in the CNS. Particularly noteworthy is the identification of radial glia, cells that retain similar characteristics to astrocytes while acting as progenitor cells able to generate cortical neurons in addition to macroglia [41, 42]. The name *radial* glia derives from the radial morphology of these cells which stretch from

the apical surface to the pial surface, while the adjective *glial* denote their shared characteristics with mature astrocytes [39, 43, 44], markers that distinguish them from their own progenitors, neuroepithelial cells. Through neurogenesis, neuroepithelial cells begin to acquire radial glial features at around embryonic day 9-10 (E9-E10) in the mouse; at this early stage radial glial still remain in contact with both pial and ventricular surfaces in the ventricular zone (VZ) [39] and they form adherent junctions to each other that help to maintain VZ integrity, similarly to neuroepithelial cells [45, 46] (Fig 3.1). Importantly, radial glial cells showed the expression of astrocytic marker such as the glutamate aspartate transporter GLAST, S100 calcium-binding protein B (S100B), glutamine synthetase (GS), the typical intermediate filaments vimentin (Vim) and glial fibrillar acidic protein (GFAP), the RC1 and RC2 epitopes, and tenascin-C (TN-C)[42, 47]. Furthermore, radial glia maintain their radial processes during cell division, functioning as a precursor and guide for neural precursors, and they undergo asymmetric cell division to either self-renew or to generate a daughter cell [39, 40].

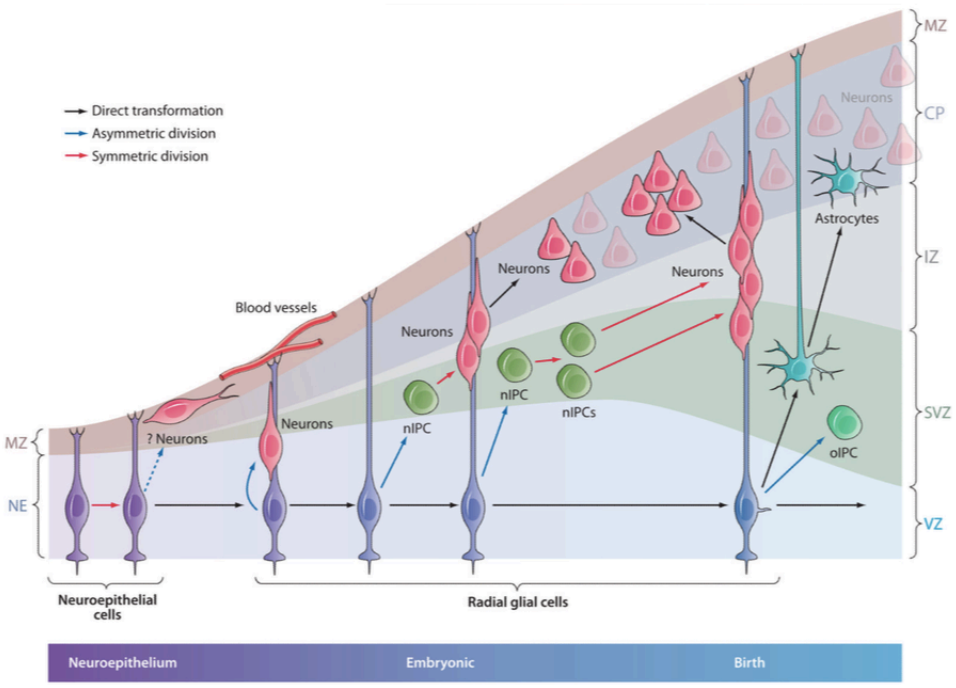

Figure 3.1: Representation of three different modes of neurogenesis during cortical development. Radial glia generate neurons through: - direct asymmetric division; - indirect generation of neurogenic progenitor cell and amplification; - indirect generation of neurogenic intermediate progenitor cell with two division rounds and amplification. CP, cortical plate; IZ, intermediate zone; MZ, marginal zone; nIPC, neurogenic intermediate progenitor cell; SVZ, subventricular zone; VZ, ventricular zone. Adapted from Kriegstein, et al.[39]

Another important accomplishment in the characterization of this particular astrocytic precursor population of radial glial is the identification of neurogenic zones in the adult CNS in which glial cells act as stem cells [48-51]. In the two principal neurogenic niches of the adult brain, the subventricular zone (SVZ) of the lateral ventricles and the subgranular zone (SGZ) in the dentate gyrus, radial glial cells are well characterized (Fig. 3.2).

In the SVZ, GFAP-expressing astrocytes represent the primary precursors of newly generated neurons [52]. SVZ astrocytes (type B cells) (Fig. 3.2 A) showed both self-renewal features and the capability to differentiate and generate transit-amplifying cells (type C cells), which subsequently generate migrating neuroblasts (type A cells) that, through the rostrary migratory stream, reach the olfactory bulb to differentiate into mature neurons [39, 50, 53]. The capability of dividing astrocytes to generate neurons in physiological conditions was assessed by using transgenic GFAP-TVA mice infected with an avian retrovirus carrying a reporter gene, showing that many labelled neurons migrated to the olfactory bulb [52]. Furthermore, SVZ astrocytes have been cultured as neurospheres *in vitro* to show their stem cell potential [54].

The second region that generates new neurons throughout adulthood is the SGZ of the hippocampus, at the interface of the granule cell layer (GCL) and the hilus of the dentate gyrus [50, 55]. The migration in this area is less extensive compared to the SVZ, nevertheless SGZ astrocytes (type B cells) (Fig. 3.2 B) show the same capability to generate mature neurons. The use of transgenic GFAP-TVA mice allowed for the tracing of the lineage of dividing SGZ astrocytes into granule neurons [55].

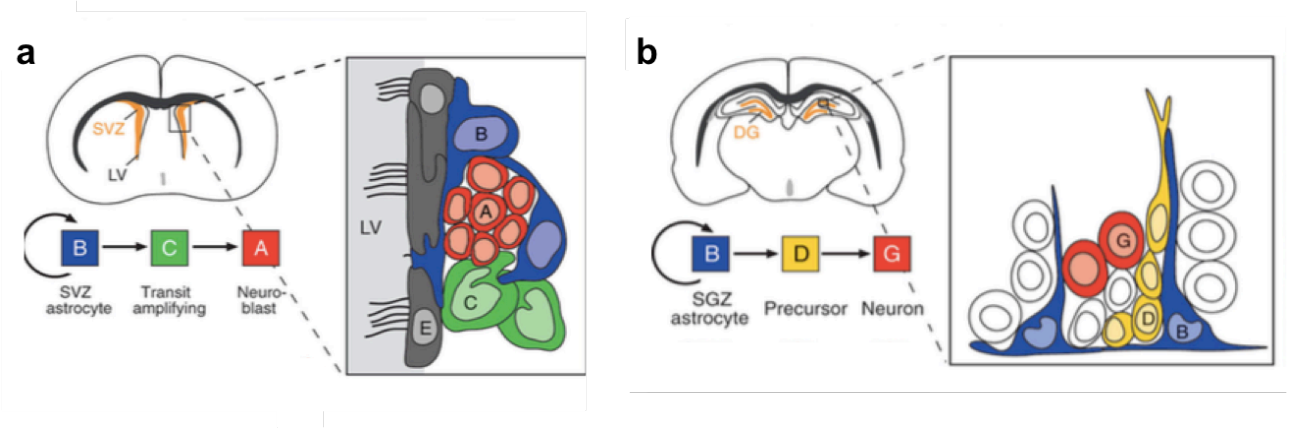

Figure 3.2: **A** Schematic representation of cell types in the SVZ (orange), adiacent the lateral ventricle (LV). Multicilated ependymal cells (E, grey) line the LV, chains of neuroblast (A, red) migrate guided by SVZ astrocytes (B, blue). Rapidly dividing transit-amplifying cells (C, green) are distributed along the network of chains. **B** Schematic representation of cell types in the SGZ (orange). SGZ astrocytes (B, blue) give rise to intermediate precursors (D, yellow) that generate granule neurons (G, red). Modified by Doetsch [56]

The affinity and the similarity observed between radial glial cells and astrocytes unravelled the vast heterogeneity and the different functions that astrocytes may exert in the CNS. Indeed, during recent years astrocytes have been distinguished based on different characteristics such as morphology and location. Astrocytes are therefore classified into two main categories: *protoplasmic* and *fibrous* astrocytes [36]. Protoplasmic astrocytes characterize the grey matter; the presence of this type of astrocyte was first demonstrated using classical silver impregnation techniques, showing that they exhibit an extensive branched morphology with many finely branching processes leading to a uniform globoid distribution [36]. Interestingly, by using more fine techniques such as the injection of fluorescent intracellular tracers and three-dimensional (3D) confocal analysis and electron microscopy, it has been demonstrated that protoplasmic astrocytes in the CA1 stratum radiatum are indeed characterized by a spongiform nature that allows them to infiltrate distinct volumes of the neuropil. Furthermore, protoplasmic astrocytes vary in size and overall shape, from spherical to elongated (Fig. 3.3); but, contrary to what was first speculated from silver impregnation results, the different morphologies allow astrocytes to avoid extensive interdigitation, defining specific domains by astrocytes [57].

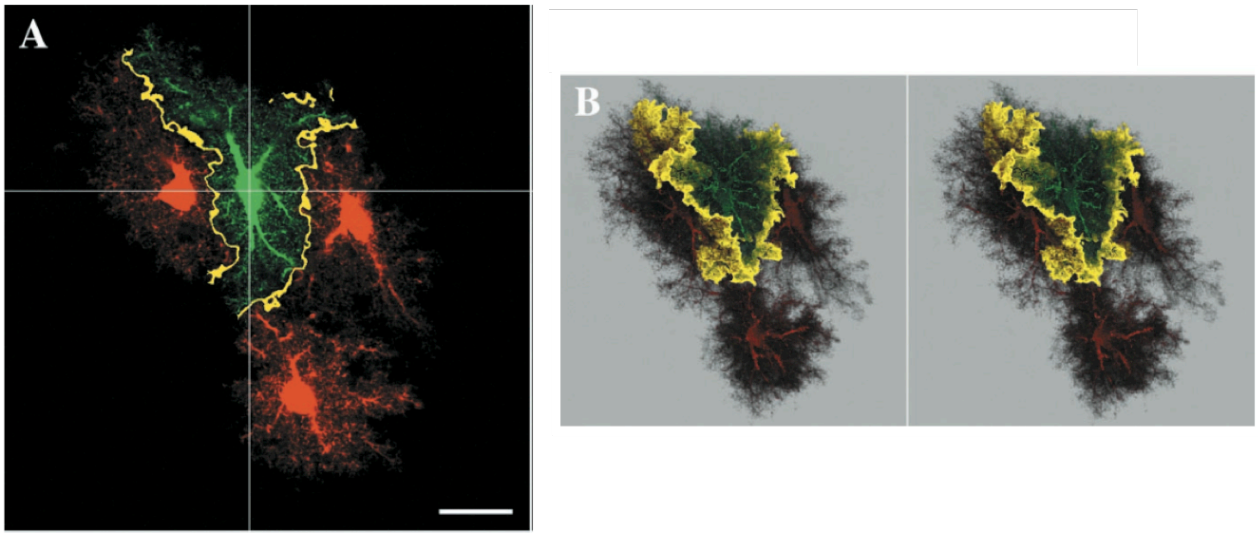

Figure 3.3: **A**, Colocalization between adjacent astrocytes is represented by the discrete yellow zone. **B**, 3D representation of colocalization of the same astrocytes reveal sheets in which neighbouring astrocytes interact with each other. Scale bar: 20 μm. Adapted from Bushong, et al.[57]

The second category of astrocytes, fibrous astrocytes, are found throughout the white matter and exhibit a morphology characterized by many long fiber-like processes. Mature astrocytes exert a wide range of functions in the CNS that are maintained between species, nevertheless there is a main evolutionary difference between species, namely the size, and thus complexity, of astrocytes [58]. GFAP labelling in rodent, rhesus monkey and human brain has shown an increasing complexity of astrocyte morphology correlated to the complexity of brain functions (Fig 3.4) [59].

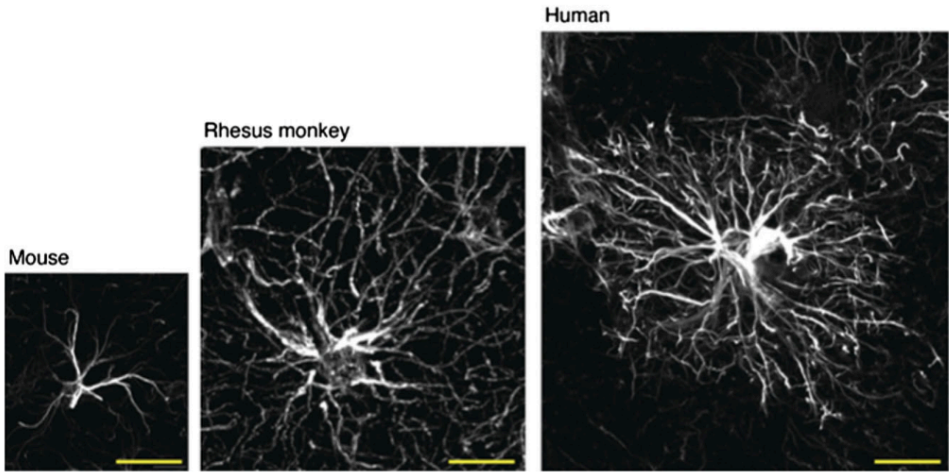

Figure 3.4: GFAP-labelled astrocytes in the cortex of mouse, rhesus monkey and human. Scale bar: 50 μm. Adapted from Kimelberg et al. [58]

Furthermore, two new subpopulations of astrocytes were described in human brains. A varicose projection astrocyte population, not observed in infraprimate species, is characterized by shorter, more spiny processes compared to typical protoplasmic astrocytes; interestingly, the domain organization is not present and their processes are spread in all directions crossing the domains of neighbouring protoplasmic astrocytes. These astrocytes may be involved in long-distance communication across cortical layers, or between grey and white matter. The second subpopulation is represented by interlaminar astrocytes; their functional role still remains unknown, but similarly to varicose projection astrocytes their long and tortuous processes suggest a role in long distance coordination of intracortical communication, and their close connection to vasculature suggest a role in coordinating blood flow [59].

3.2 ASTROCYTIC MARKERS

GFAP has been widely used as a specific marker to uniquely identify astrocytes, however GFAP-based identification presents a major limitation: not all astrocytes are immunohistochemically detectable in healthy CNS tissue since GFAP is not detectable in all astrocyte cell bodies, and it is absent in the finely branching astrocyte processes. As a consequence, GFAP-labelling can underestimate the quantity and extent of branching of astrocytes in the CNS [36, 60].

Alternative molecular markers has been used for the identification of astrocytes, such as GS and S100B [61, 62], or the glutamate transporters GLT1 or GLAST[63]; nevertheless these molecules are not entirely exclusive to astrocytes, since some other neural cells like neurons or oligodendrocytes can also be positive for these markers [64].

New and innovative techniques, such as genome-wide transcriptional profiling, have provided new information about the expression profiles of subpopulations present in the

CNS [65, 66]. From such studies a new and more reliable marker for astrocytes has been identified: aldehyde dehydrogenase family member L1 (Aldh1L1). Aldh1L1 is an enzyme that plays an important role in many reactions, such as the biosynthesis of nucleotides and the regeneration of methionine, thus playing a major role in cell division and growth. While GFAP remains the most commonly employed marker of astrocytes, Aldh1L1 provides a more representative alternative. Moreover, the generation of Aldh1L1- EGFP bacterial artificial chromosome (BAC) transgenic mice has facilitated the fluorescent labelling of the different astrocyte populations, providing a superior tool for visualization of astrocytes in the developing and adult mouse brain [65, 67].

3.3 PHYSIOLOGICAL ROLES

Contrary to the initial limited role ascribed to astrocytes as simple supportive cells for neurons, it is now clear that astrocytes enact a wide variety of complex and essential functions in the healthy CNS. Astrocytes play an important role in **CNS development**. Although the generation of astrocytes occurs after the initial generation of neurons in many CNS regions, astrocytes form molecular boundaries for guiding the migration of developing axons and certain neuroblasts [36]. In fact, astrocytes influence synapse formation and maturation; in the developing CNS astrocytes, concomitant with microglia, play a principal role in the elimination of excess synapses in a process called synaptic pruning [35]. For example, it has been shown that this process, governed by neuronal activity, requires expression of the phagocytic receptors multiple EGF-like domains 10 (MEGF10) and MER proto-oncogene, tyrosine kinase (MERTK) [68]; synaptic pruning, in the dorsal geniculate nucleus of the thalamus, is regulated by transforming growth factor (TGF)-β secreted by immature astrocytes in the retina that activate the expression of the complement protein C1q, with subsequent elimination of tagged synapses by microglia [35]. However, this process of remodelling is not limited to development, but also takes part in adulthood, particularly upon CNS damage where astrocytes contribute to axonal plasticity, leading to the compensation and recovery of function after injury [35]. In ischemic brain lesions, for example, astrocytes contribute

to the synaptogenesis by stimulating the formation of new blood vessels through the secretion of vascular endothelial growth factor (VEGF)[69]. Moreover, astrocyte-like radial glial cells contribute to the formation of new neurons until adulthood [50].

Astrocytes not only promote and modulate synapse formation, but emerging evidence has given rise to the so-called '**tripartite synapse**' hypothesis, describing the intimate involvement of astrocytes in neuronal synaptic communication [70]. Astrocytes are not merely passive actors in neuronal excitability, but rather it has been shown that bidirectional communication exists between astrocytes and neurons; astrocytes are characterized by a regulated release, into the synaptic environment, of a variety of signalling molecules including glutamate, purines (adenosine triphosphate), gamma-aminobutyric acid (GABA), and D-serine. These **gliotransmitters** are released upon an increase in Ca^{2+} in response to changes in neuronal synaptic activity and this release can ultimately alter neuronal excitability [31, 36, 71]. Furthermore, astrocytes express high levels of transporters for different **neurotransmitters** (such as glutamate, GABA, and glycine) with the aim of clearing these signalling molecules from the synaptic space through **reuptake**; the neurotransmitters are subsequently converted by enzymes, such as GS, into precursors, such as glutamine, and recycled back to synapses for reconversion into active transmitters after being reuptaken [36, 72].

Vasculature plays a major part in CNS development and function, and thus it is important to underline that astrocytes are characterized by extensive contacts with **blood vessels** [36]. As mentioned above, astrocytes create contacts with neurons, and with this tight connection between synapses and blood vessels, astrocytes participate in the control of local metabolic demands [33]. Blood flow is regulated according to neuronal requirements, and recent evidences have shown that astrocytes can produce and release different molecular mediators, such prostaglandins (PGE), nitric oxide (NO), and arachidonic acid (AA), in order to modify CNS blood vessel diameter and blood flow in a coordinated manner [33]. It is therefore clear that astrocyte processes, closely related to synapses and blood vessels, exert essential functions in maintaining the **homeostasis** of the synaptic interstitial fluid. In particular, aquaporin 4 (AQP4)

water channels in the endfeet of astrocyte processes are responsible for creating contacts with the blood vessels and for regulating fluid homeostasis [73].

The strategic position of astrocytes that sees them creating contacts with both blood vessels and neurons, axons (at nodes of Ranvier), and synapses, make them, therefore, an integral **source for neuronal energy**; glucose taken up from blood vessels by astrocytes is metabolised for energy by neurons in grey and white matter [36]. It is well-established that astrocytes can store glycogen, and recent evidences have demonstrated that the use of glycogen, as sustenance for neuronal activity, is modulated by neurotransmitters. In particular, during periods of high neuronal activity glycogen is degraded to lactate and transferred to neurons, ensuring the maintenance of appropriate function and protection of neurons [74]. Furthermore, astrocytes can exchange glucose and its metabolites in the complex astroglial networks through gap-junctions, such as connexins 43 and 30 [75].

As suggested above, astrocytes are characterized by their endfeet and the creation of tight junctions with brain vasculature and pericytes that contributes to the **maintenance** of the **blood brain barrier** (BBB) [32]. While the BBB appears to be fully intact before astrogenesis, different neural stem cell-derived mechanisms involved in the control of the barrier, such as Wnt signaling, are thought to be supplanted by astrocytes after embryogenesis, and astrocytes are known to play an important role in sealing the barrier after CNS injury [37, 65].

3.4 Reactive Astrocytes

Astrocytes not only play a major role in healthy tissue, but they also respond to CNS insults in a context/severity-dependent manner that leads to changes in gene expression, cellular structure, and functions [34, 35, 76, 77]. This heterogeneous phenomenon, exhibited by reactive astrocytes, is called astrogliosis and characterised by four main key features [34]:

1- *Astrogliosis refers to a broad range of molecular, cellular, and functional changes in astrocytes in response to all forms and severities of CNS injury and disease*

These phenomena manifest along a gradient of intensity correlating to the magnitude of the insult, with milder responses yielding ostensibly reversible changes in gene expression, morphological changes, and increased proliferation, while more severe injuries can result in scar formation and permanent tissue rearrangement. Two main hallmarks identifying reactive astrocytes are up-regulation of GFAP and cellular hypertrophy (Fig. 3.5) [10], with the expression of other typical astrocytic markers, such as S100B, Vim, nestin (Nes), and glutamate transporters, also altered in an effort to re-assert homeostasis [78].

Reactive astrocytes are common to all form of CNS injury and disease, including traumatic brain injury [79], spinal cord injury (SCI) [78], Alzheimer's disease [80], amyotrophic lateral sclerosis (ALS) [81], and many others, however the changes induced in astrocytes may vary depending on the stimulus [76]. In this regard, a recent study identified, through microarray gene profiling, several classes of genes differentially regulated upon different stimuli in cerebral astrocytes in models of transient ischemia (middle cerebral artery) and neuroinflammation (LPS injection). For example, gene ontology classification showed a prominent upregulation of categories such as metabolic activity, cell cycle-related genes and transcription factors in reactive astrocyte upon ischemia, while the antigen presentation pathway, complement pathway and response to inteferon classifications were more prominent in the LPS model [82].

A

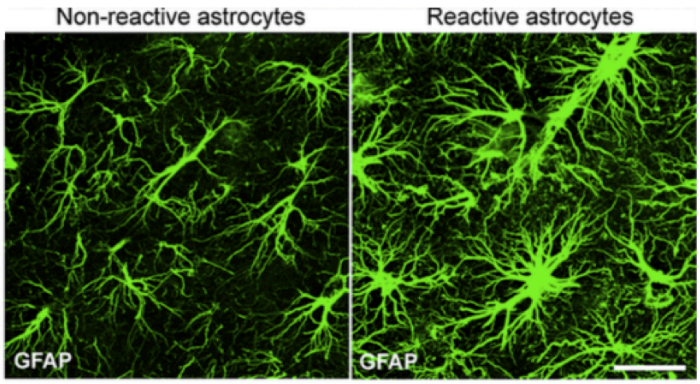

B

Specific aspect of astrogliosis	Signaling pathways and molecules
Structural molecules: GFAP ↑; vimentin ↑; nestin ↑	STAT3 NF-κB cAMP, Lipocalin-Rho-kinase
Astrocyte hypertrophy ↑	STAT3
Astrocyte proliferation ↑	Olig2 endothelin-1 JNK/c-Jun
Astrocyte migration ↑	CEPB1
Astrocyte scar formation ↑	STAT3 EphB2
Scar related axon growth inhibitors ↑	Egr-1 TGFβ SOX9 [84]
Pro-inflammatory	NF-κB P2X7 MAP-kinase [96]
Anti-inflammatory	STAT3 Nrf2 SOCS1 and 3 [97]
Limiting infection	gp130
Extracellular homeostasis and neuroprotection via glutamate transporters ↑	cAmp, PI-3K/Akt, EGF, FGF
Neuroprotection via glutathione ↑ and oxidative stress ↓	Nrf2
Bacteriocidal and cytotoxic molecules: NO ↑; NOS ↑	IFγ, Toll-like receptor ligands, TGFβ

Figure 3.5: **A**: The left panel depicts astrocytes in the healthy mouse hippocampus, the right panel shows upregulation of GFAP expression and hypertrophy upon entorhinal cortex lesion . Modified from Pekny et al. [10] **B**: Table shows pathways and molecules involved in specific aspects of astrocyte reactivity. Modified from Sofroniew et al. [77]

2 - *Changes observed in reactive astrocytes depend on the severity of the insult in a gradient manner*

Mild or moderate insults of the CNS are caused by mild non-invasive trauma and diffuse innate immune activation, such as viral infections and systemic bacterial infections, and occur in areas that are some distance from focal CNS lesions [36]. Upon such insults, reactive astrocytes show an upregulation in expression of GFAP and hypertrophy without substantial overlapping of the processes (Fig. 3.6A) There is little or no astrocyte proliferation in mild or moderate reactive astrogliosis, but the upregulation of GFAP in astrocytes can lead to the detection of astrocytes that would be otherwise unlabelled and invisible in healthy tissue, leading to the overestimation of proliferation [34, 36].

Severe insults result in more pronounced changes in astrocytes, including more substantial up-regulation of GFAP and cellular hypertrophy, resulting in the loss of individual astrocyte domains due to the overlapping of astrocyte processes (Fig. 3.6 A), as well as significant increases in proliferation [76]. These changes result in the reorganization of tissue to yield a dense and narrow barrier of overlapping, proliferative astrocytes, called a glial scar, which surrounds the lesion epicentre [36]. The nature of the glial scar is still under debate, yet it has appears to exert a dual role: to first delineate, in the acute phase of the CNS insult, the area of the damage in order to limit necrosis and the spreading of inflammation, and a more detrimental role during the chronic phase of injury as it represents an impediment to axonal regeneration, at both the physical and molecular levels (Fig. 3.6B)[83].

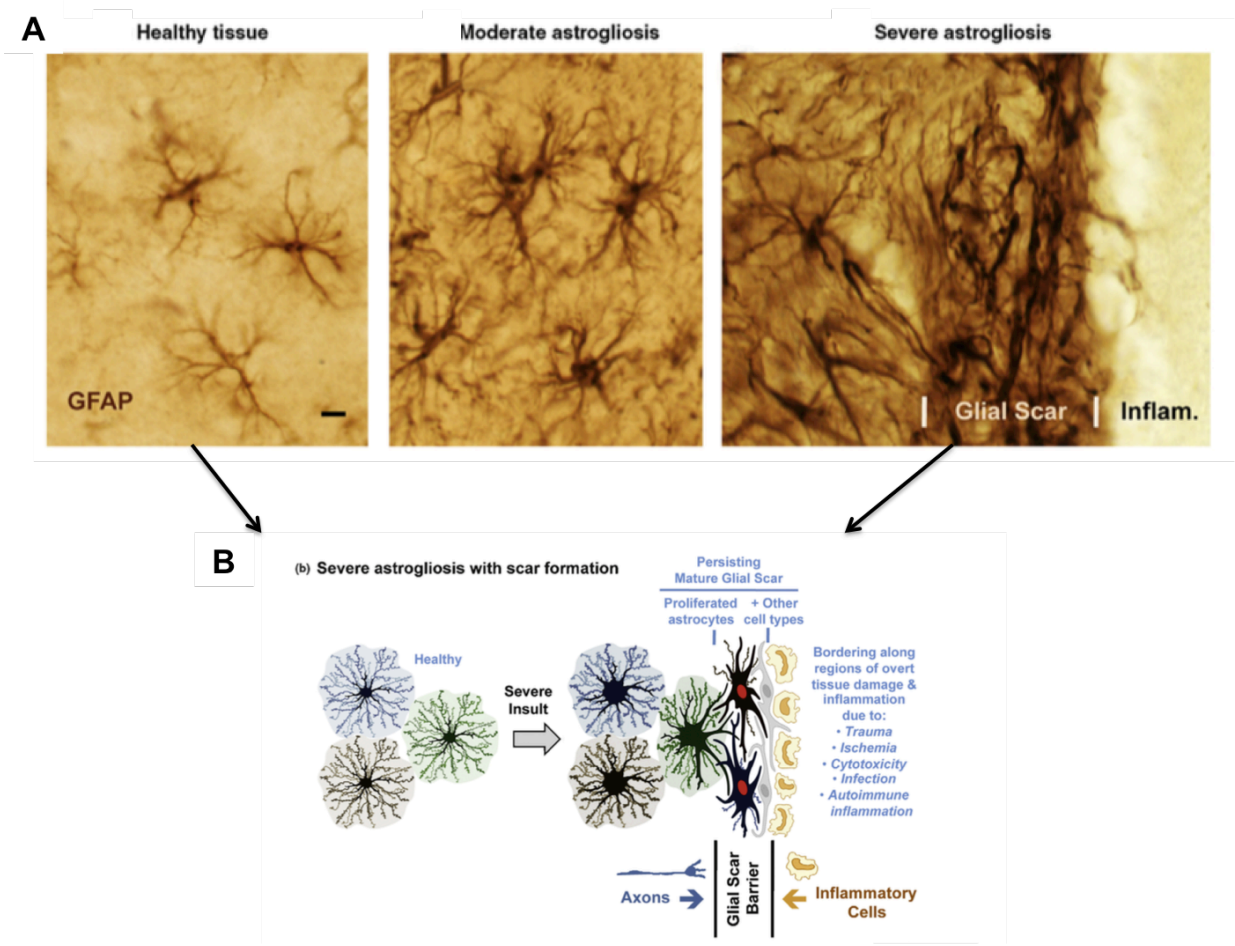

Figure 3.6: **A**: GFAP-immunohistochemically labelled astrocytes in the mouse cerebral cortex, in healthy tissue, moderate reactive astrocytes in response to intracerebral injection of the bacterial antigen lipopolysaccharide (LPS), and severe astrogliosis close to the lesion, respectively. **B**: Representation of glial scar formation: proliferative astrocytes (red nuclei), overlapping processes in astrocytes and other cell types such as fibromeningeal cells and other glia (gray nuclei). Modified from Sofroniew [77]

3- *Changes observed in reactive astrocytes are context-dependent and are regulated by inter and intracellular signals*

Astrocytes respond to all CNS insults, and while there are features common between reactive astrocytes across different diseases, reactive astrocytes are also characterized by a variety of pathology-dependent changes [81]. Interestingly, several lines of evidence have highlighted a new concept of astrocytopathies in which a disruption of normal astrocyte functions in healthy tissue is the primary cause of neurological dysfunction and disease [84]. For example, astrocytes in mutant SOD1 mice, a model of familial form of ALS, are characterized by a loss of GLT1 protein and consequently probably impaired glutamate transport and dysfunctional glutamate metabolism may drive the onset of the disease [85, 86]. In Alzheimer's pathology astrocytes accumulate amyloid material resulting from local neurodegeneration, with the subsequent formation of GFAP+ amyloid plaques that eventually lead to astrocyte death [87]. Astrocytes in the context of Huntington's disease exhibit, concomitant with an increase in GFAP expression, an altered expression of gap junctions, leading to a loss in their ability to maintain a neuronal-supportive environment [88].

Astrogliosis can be induced and regulated by a wide range of extracellular molecules that may initiate intracellular secondary messenger signaling cascades (Fig. 3.7). Transcriptome studies have demonstrated that upon different CNS insults, such as focal ischaemic stroke, LPS injection, or SCI, astrocytes show common changes in cell morphology, maintenance, growth, and proliferation [82, 89]. Signal transducer and activator of transcription 3 (STAT3) pathway stands out as one of the most well characterized instigators of astrocyte reactivity. STAT3 is phosphorylated by Janus kinases (Jaks) in response to extracellular binding of various cytokines, interferons and growth factors produced during CNS insult, and pSTAT3 subsequently translocates to the nucleus where it regulates the transcription of astrogliosis-related genes [90, 91]. This central role was demonstrated in experiments involving the deletion of STAT3, with a consequent marked downregulation in hypertrophy, GFAP overexpression, and scar formation during astrogliosis [92].

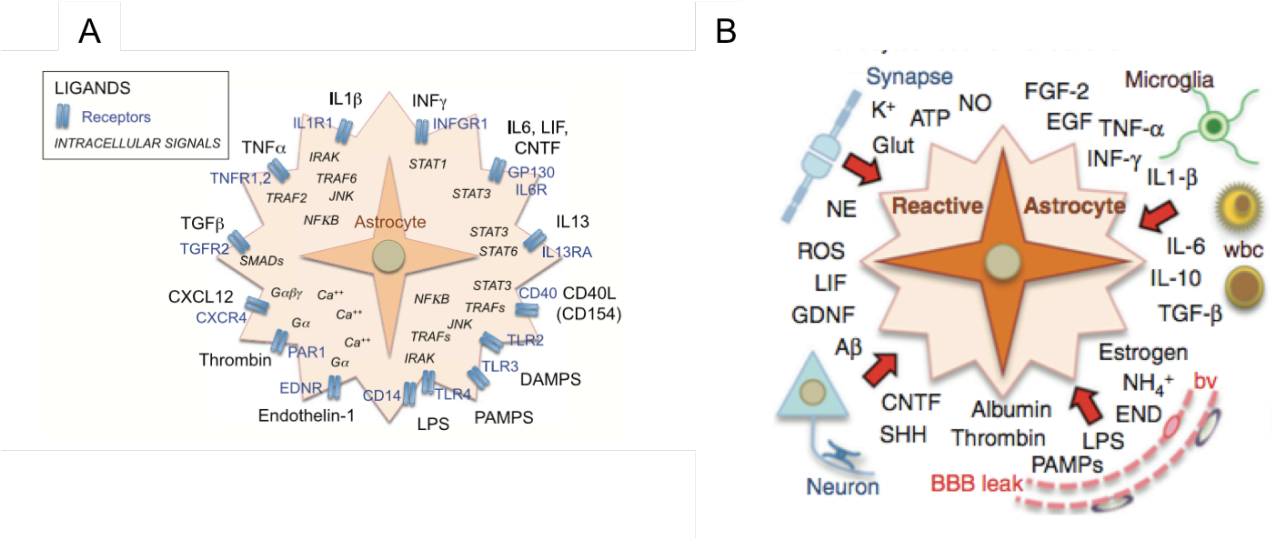

Figure 3.7: **A**,**B**: Representation of astrocyte receptors for different cytokines and other inflammatory molecules, and some of the associated intracellular signalling molecules. Modified from Sofroniew [93]

4- *Changes observed in reactive astrocytes can lead to a gain or loss of astrocyte functions*

Recent studies have shown that astrocytes exert important and beneficial roles not only in healthy tissue but also upon injuries; the dichotomous role of reactive astrocytes has become a topic of debate during recent years, particularly with the use of transgenic animal models [36]. In particular, these studies provided evidence that the loss of these functions associated with astrogliosis may lead to a worsening of the injury environment, since reactive astrocytes can limit the spread of inflammation and enact BBB repair and neural protection [9, 11, 92, 94]. Conversely, reactive astrocytes, especially during the chronic phase, elicit detrimental effects through inhibition of axon regeneration [95, 96]. Furthermore, reactive astrocytes can exacerbate the inflammatory response through the production of pro-inflammatory cytokines [36], or contribute to neurotoxicity by releasing reactive oxygen species [97], potentially excitotoxic glutamate [97], or by secretion of inhibitory molecules such as chondroitin sulfate proteoglycans (CSPGs) [83, 95].

Remarkably, recent transcriptome analyses have distinguished reactive astrocytes into two subpopulations termed A1 and A2. This nomenclature derives from analogy with the nomenclature conferred upon polarised macrophages: pro-inflammatory (classically activated) M1 and anti-inflammatory (alternatively activated) M2 macrophages [98]. As mentioned above, reactive astrocytes may be helpful or harmful upon context-specific CNS insults and their dual role is broadly reflected in the identification of these A1 and A2 astrocyte subtypes. A1 astrocytes are characterized by the significant upregulation of many genes that have been shown to be neurotoxic, promoting the destruction of synapses. For example, LPS activation was found to induce A1 reactive astrocytes to upregulate the initial part of the classical complement cascade (C1r, C1s, C3, and C4) involved in synapse pruning during development and synapse loss in neurodegenerative disease [82]. On the contrary, animal models of middle cerebral artery occlusion (MCAO) have shown that alternatively-reactive A2 astrocytes express high levels of neurotrophic factors and cytokines, such as cardiotrophin-like cytokine factor 1 (CLCF1), leukemia inhibitory factor (LIF), and interleukin-6 (Il6), that may aid in neuronal repair and protection [9, 82, 99].

Thus, extensive evidence exists showing that astrocytes in healthy CNS are highly heterogeneous in their gene expression profiles, and that is in turn reflected in functional diversity, not only across different CNS regions, but also locally within the same regions [60]. This heterogeneity is also reflected upon reactivity in astrocytes, and indeed astrogliosis is regulated by multiple specific signalling events, leading to heterogeneity in the gene expression, cell morphology, CNS regions, cell signalling and cell function of reactive astrocytes[100].

Nevertheless, heterogeneity is a crucial factor in studies aiming to screen the safety and efficacy of compounds *in vitro*, since variability between replicates may lead to misleading interpretation of results. For these reasons, we first aimed to establish a reproducible and reliable protocol for *in vitro* astrocytes cultures, with regards to expression of a canonical response of astrogliosis upon activation, to subsequently employ for nanotherapeutics screening

3.5 RESULTS

3.5.1 NPC-DERIVED ASTROCYTES EXHIBIT A MATURE ASTROCYTE-LIKE PHENOTYPE AND MORPHOLOGY

In order to evaluate the efficacy of pRNA-nanotherapeutics to modulate astrogliosis, we established a protocol for the *in vitro* differentiation of NPCs into mature astrocytes. Differentiation of NPCs into astrocytes was first induced by the use of a medium enriched with 10% fetal bovine serum (FBS), a well-established technique [101, 102]. NPCs were then cultured for 15 days in the differentiation medium and immunofluorescence staining was used to evaluate the maturation of the phenotype; during this time we observed an increase in cell size, acquisition of the typical astroglial morphology, high expression of the astrocytic intermediate filament (IF) proteins GFAP and Vim. S100B expression, another typical marker of mature astrocytes, increased during differentiation (Fig. 3.8) [103]. Purity of NPC-derived astrocyte cultures were previously assessed by immunostaining for microglia markers (ionised calcium-binding adapter 1-positive cells) and oligodendrocyte markers (O4-positive cells), with no expression of either marker observed, and also negligible amounts of βIII tubulin-positive neuronal cells.

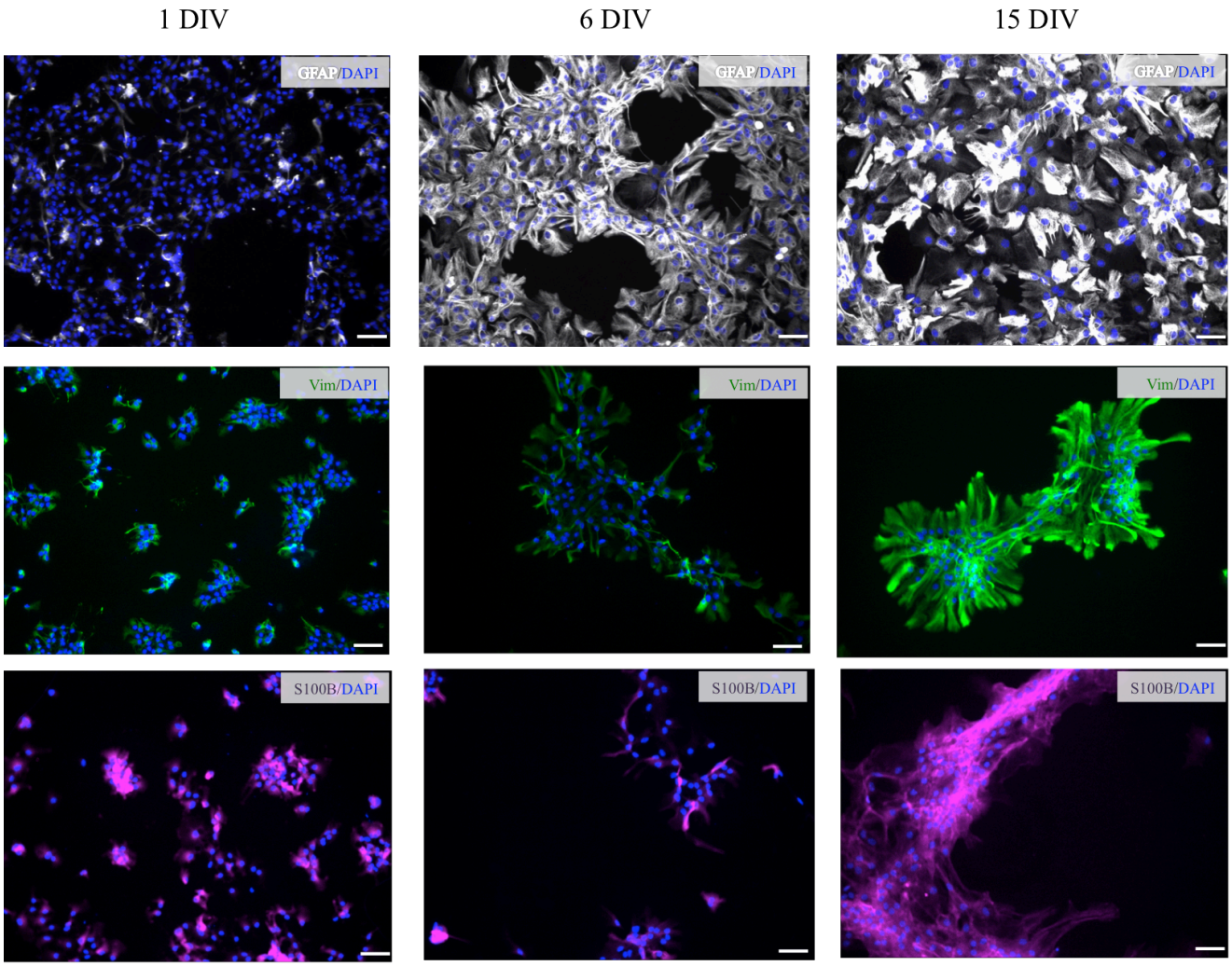

Figure 3.8: Immunofluorescence micrographs of high-FBS/FGF2-free astrocyte differentiation and maturation: 1, 6 and 15 DIV. Scale bar = 50 µm.

A 15-day *in vitro* culture with 10% FBS therefore resulted in pure astrocyte cell cultures characterized by classical markers of mature astrocytes, nevertheless these cells showed high level of basal reactivity, marked by resting cell hypertrophy and high GFAP expression, and thus did not elicit a desirable phenotypic change upon subsequent LPS+IFNγ activation. The ineffectual nature of this protocol was indeed confirmed by qPCR and Western blot analyses: upon activation, qRT-PCR measurements showed that levels of classically activation-induced intermediate filament mRNAs were not significantly changed 48 h following LPS+IFNγ treatment: no induction in either *Gfap* or *Vim* expression levels were observed compared to non-activated control in high-FBS/FGF2-free medium. Interestingly, in all conditions (resting and activation) high-FBS/FGF2-free astrocytes showed a higher induction in *Gfap* and *Vim* compared to the

non-activated control in low-FBS/+FGF2, discussed below (Fig 3.9A), with mean *Gfap* and *Vim* expression levels being 20 and 4 times higher, respectively. This high basal expression (relative to low-FBS/+FGF2 resting), and the fact that LPS+IFNγ stimulation does not induce a change in expression, suggest that astrocytes grown under the high-FBS/FGF2-free conditions are already in a state of activation. This evidence was further confirmed by analysis of protein expression levels, assessed by Western blot, which did not show any significant changes in Vim and GFAP expression upon activation compared to the high-FBS/FGF2-free resting control (Fig. 3.9 B).

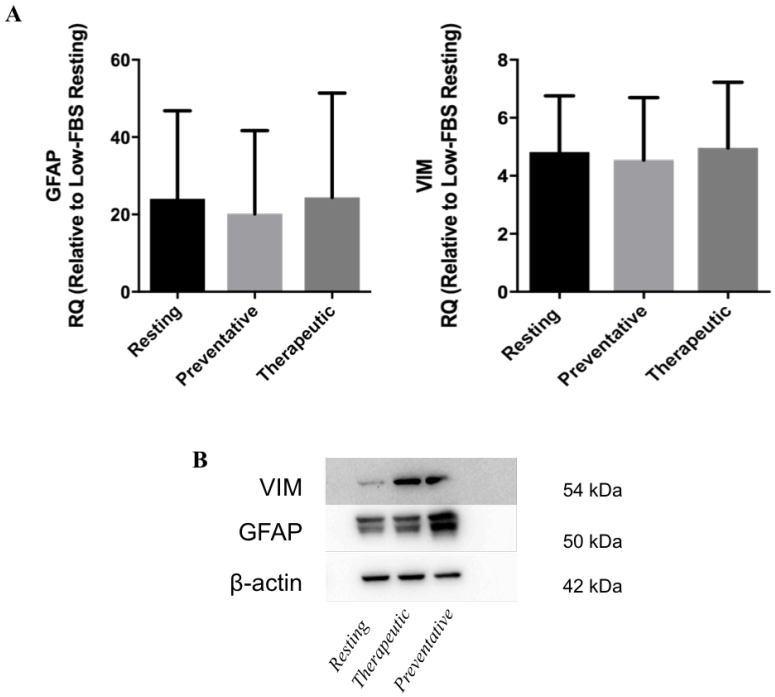

Figure 3.9: **A**: qRT-PCR quantification of *Gfap, Vim* in resting and LPS+IFNγ-treated high-FBS astrocytes. Expression relative to low-FBS/+FGF2 resting controls ($2^{-\Delta\Delta Ct}$ method), *Gapd* reference gene. **B**: Representative Western blots showing GFAP and Vim protein expression levels in resting condition, 7 and 5 days after activation, respectively.

It has been previously described that FBS may have a stimulatory effect on astrocytes similar to that observed in observed in our high-FBS (10%) cultures [104], thus differentiation induced with low FBS media might lead to basally activated astrocytes. Furthermore, it has been shown that the presence of fibroblast growth factors (FGFs) in astrocyte differentiation media can induce a more mature quiescent state in cultured astrocytes [105, 106]. We therefore defined an optimised culture protocol: NPCs were

differentiated in a medium enriched with high (10%) FBS medium for the first 7 days of differentiation and then switched to low (1%) FBS medium supplemented with N2 for the remainder of the maturation protocol (up to 15 DIV or longer, depending on the experimental setting) (Fig. 3.10). Both high- and low-FBS media were enriched with high concentrations of FGF2 (50 ng/ml) for the duration of the experiment.

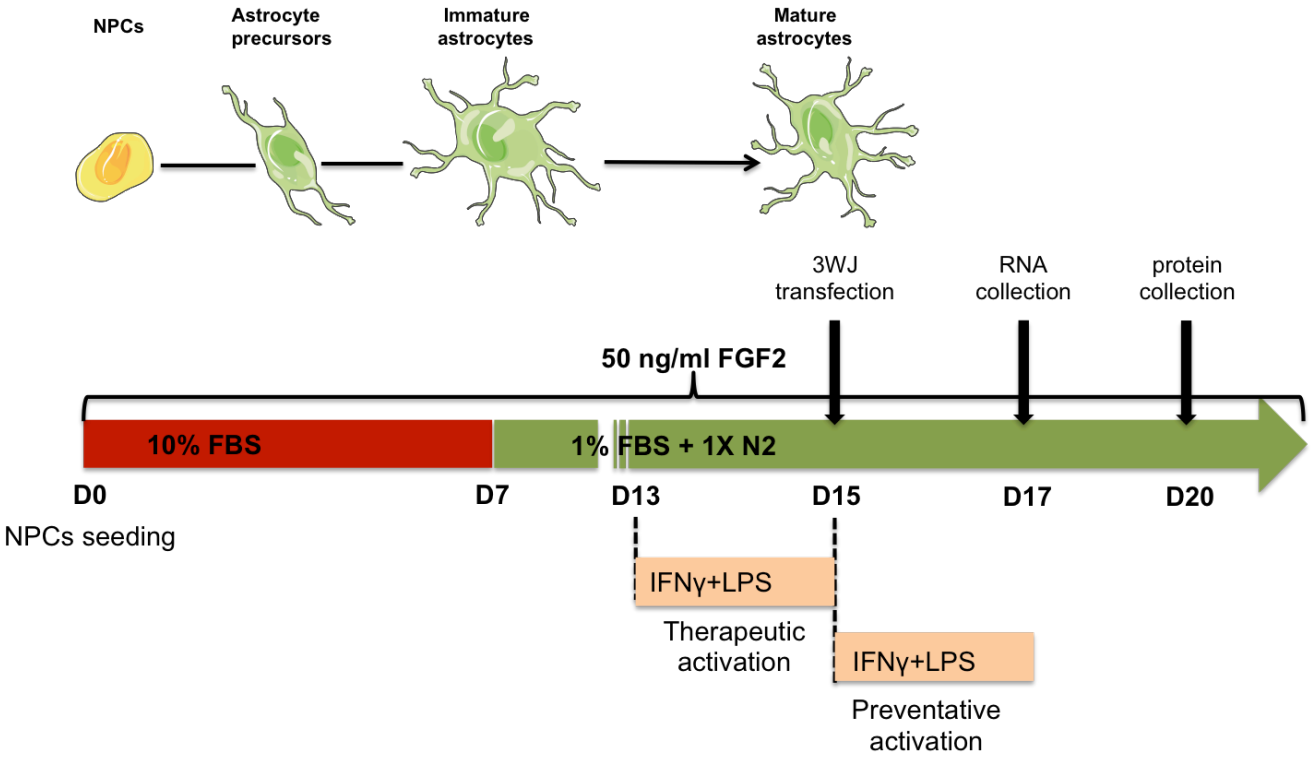

Figure 3.10: Scheme for NPC-derived astrocyte experiments. NPCs were differentiated for 7 days in a medium enriched with high FBS, then switched to a low FBS medium supplemented with N2; both media are enriched in 50 ng/ml FGF2. At day 15 cells were transfected with 3WJs, while RNA and protein expressions were assessed at days 17 and 20, respectively. Astrocytes were activated by adding 2 µg/ml LPS and 3 ng/ml IFNγ to the medium for 48 h at two different timepoints: at day 13 through day 15 for the *therapeutic* treatment profile, from day 15 to day 17 for the *preventative* profile.

NPCs differentiated via the low-FBS/+FGF2 protocol showed a progressive maturation of the astrocytic phenotype and morphology over the course of the protocol, from day 1 to day 15. This progression was primarily observed by immunostaining for GFAP and Vim (Fig3.11); at 1 DIV we observed a homogenous population characterized by few processes (Fig. 3.11). By 6 DIV cells had started to extend processes and by 15 DIV near-confluent cells were characterized by typical astroglial morphology with elongated

processes (Fig. 3.11), notably we observed a remarkable change in cells morphology starting from 7 DIV, when cells are exposed to low-FBS/+FGF2 medium, indeed 6 DIV cells showed a morphology characterized by cell hypertrophy compared to a more thin and thin cell body observed 15DIV (Fig. 3.11). The acquisition of a mature astrocytic phenotype was confirmed by the expression of typical markers for mature astrocytes by immunostaining: at 15 DIV, differentiated NPC-derived astrocytes were positive for GFAP, Vim, S100B, ALDH1L1 and GLT1 (Fig. 3.11).

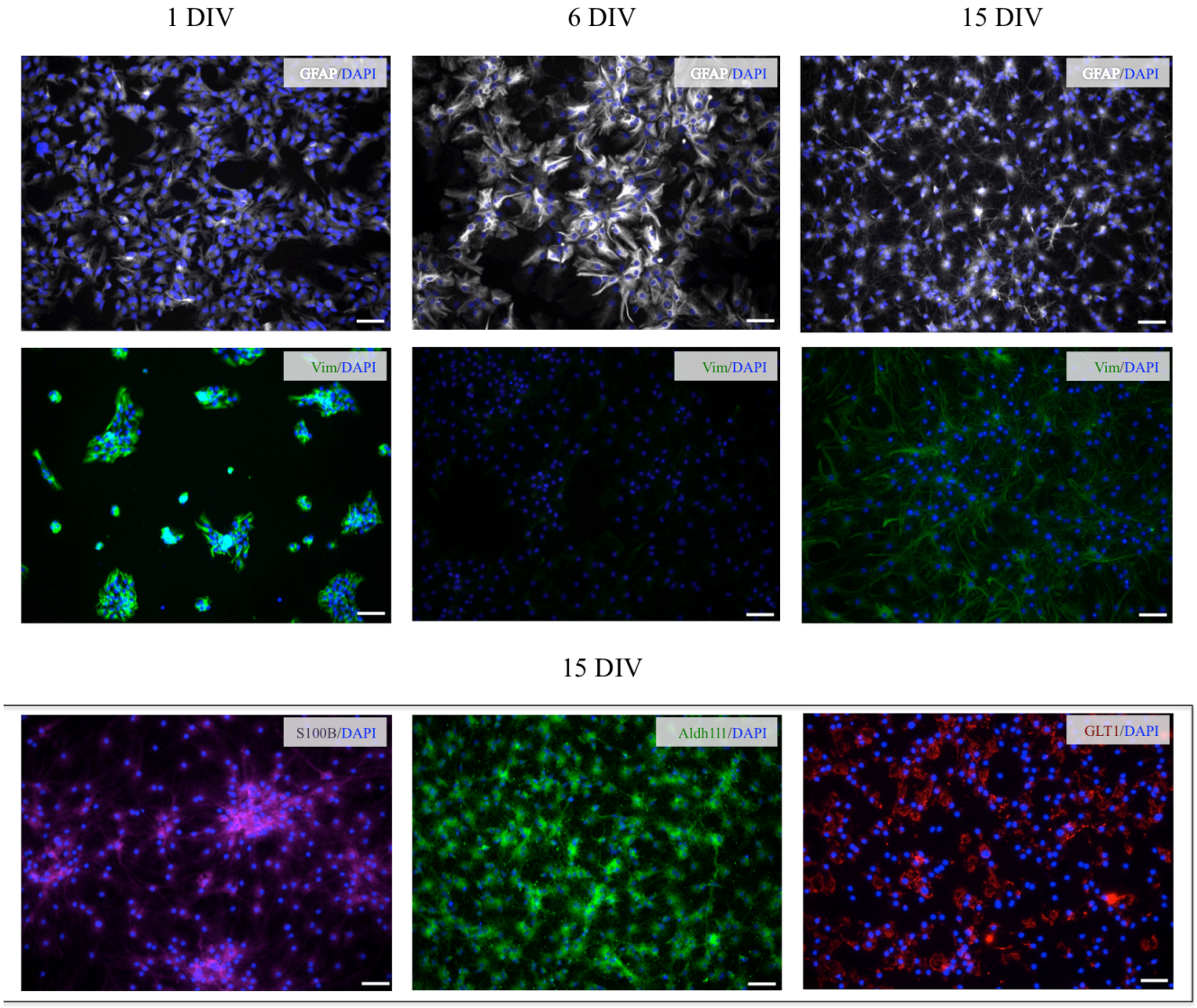

Figure 3.11: Immunofluorescence micrographs of low-FBS/+FGF2 astrocyte differentiation and maturation: 1, 6 and 15 DIV. Scale bar = 50 µm.

We verified the purity of the cell population by immunostaining for neurons and oligodendrocytes; the absence of cells positive for βIII tubulin class (TUBB3) and microtubule-associate protein 2 (MAP2) for immature and mature neurons, respectively, excluded the differentiation of NPCs toward this lineage, and the absence of cells immunopositive for O4 confirmed the absence of oligodendrocytes.

3.5.2 *IN VITRO* ACTIVATION OF NPC-DERIVED ASTROCYTES BY LPS AND IFNγ TREATMENT

After the establishment of a reproducible protocol (low-FBS/+FGF2) to differentiate NPCs into mature astrocytes, we aimed to activate resting astrocytes in order to mimic *in vitro* the molecular and gene expression changes observed upon *in vivo* activation, using the method described by Mor et al. [107]. Therefore, activation was induced by treating astrocytes with lipopolysaccharide (LPS) and interferon gamma (IFNγ): activation was performed by using the low-FBS/+FGF2 astrocyte differentiation medium enriched with 2 μg/ml LPS and 3 ng/ml IFNγ (activation medium) for 48 hours. Activation was induced at two different timepoints during the differentiation protocol: at day 13 (*therapeutic* condition), to mimic a putative *in vivo* approach where astrocytes are first activated through injury and afterwards treated with nanotherapeutics; or astrocytes were exposed to the activation medium at day 15 (*preventative* condition), to assess the capability of the nanotherapeutics to interfere with astrogliosis at the beginning of the phenomenon with the aim of a future combinatorial approach. Resting astrocytes (i.e. quiescent astrocytes not exposed to activation medium), kept in the astrocyte differentiation medium, were used as controls for activated astrocytes in order to evaluate the efficiency of activation protocol.

When treated with LPS+IFNγ for 48 h, astrocytes exhibited an upregulation in the mRNA levels of their associated Toll-like receptor 4 (*Tlr4*) and IFNγ receptors 1 and 2 (*Ifngr1* and *2*) compared to resting controls (Fig. 3.12 A,B,C), although *Ifngr1* did not show a statistically significant increase. When medium was changed back to stimulant-free ‘resting’ medium, expression reverted to basal levels after 48h. Astrocytes become

reactive in response to an infection or inflammation by inducing the expression of class II major histocompatibility complex, transactivator (*Ciita*); we observed an induction in *Ciita* mRNA (Fig. 3.12 D) in the 48h following activation, confirming the activation of cultured astrocytes.

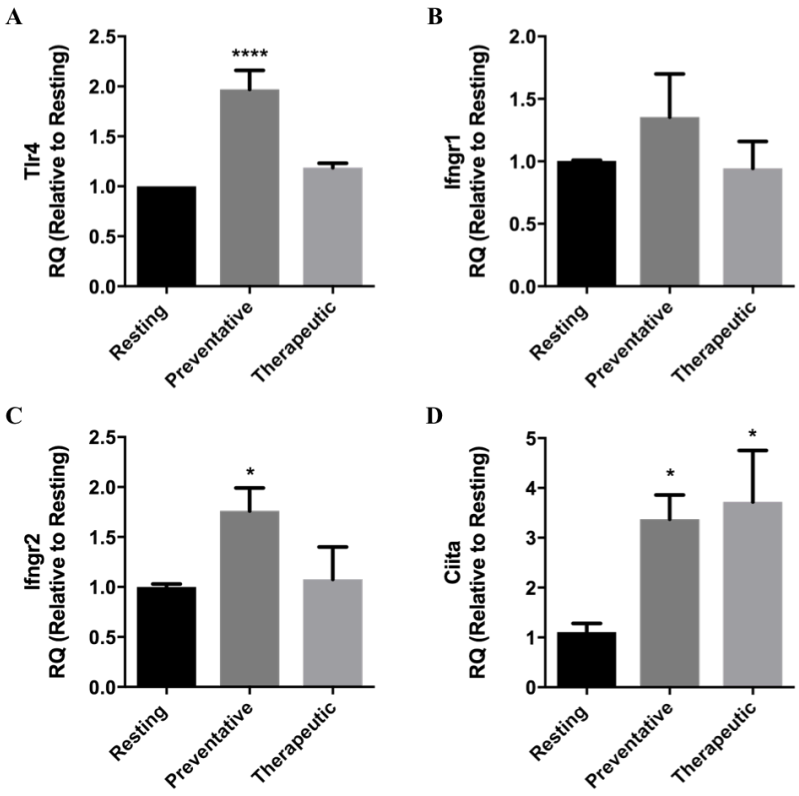

Figure 3.12:. qRT-PCR quantification of relative mRNA expression levels of low-FBS/+FGF2 cultured astrocytes stimulated with LPS+IFNγ. **A** *Tlr4*, **B** *Ifngr1*, **C** *Ifngr2*, **D** *Ciita*. Expression relative to resting controls ($2^{-\Delta\Delta Ct}$ method), *Gapd* reference gene. Data expressed as the mean of N ≥ 3 biological replicates ± SD; * P ≤ 0.05, ** P ≤ 0.01, *** P ≤ 0.001, or **** P ≤ 0.0001 relative to non-activated control samples (one-way ANOVA with Dunnett's multiple comparison test).

To further confirm the reactive state of astrocytes in culture, we assessed the expression of the classical hallmarks of astrogliosis: both *Gfap* and *Vim* mRNA were increased at 48h post-activation: approximately 6-fold and 2-fold, respectively (Fig. 3.13 A,B); the peak of activation was reached after 48 h of activation (*preventative* timepoint) and the expression of these markers decreased after a further 48 h in resting differentiation medium (*therapeutic* timepoint). Due to a large inter-experimental variation in expression, *Gfap* induction failed to achieve statistical significance. A 15,000-fold induction was observed for lipocalin 2 (*Lcn2)* expression upon 48h of activation, and as

observed for *Gfap* and *Vim* it came back to near-basal levels after further 48 h in resting differentiation medium (Fig. 3.13 C).

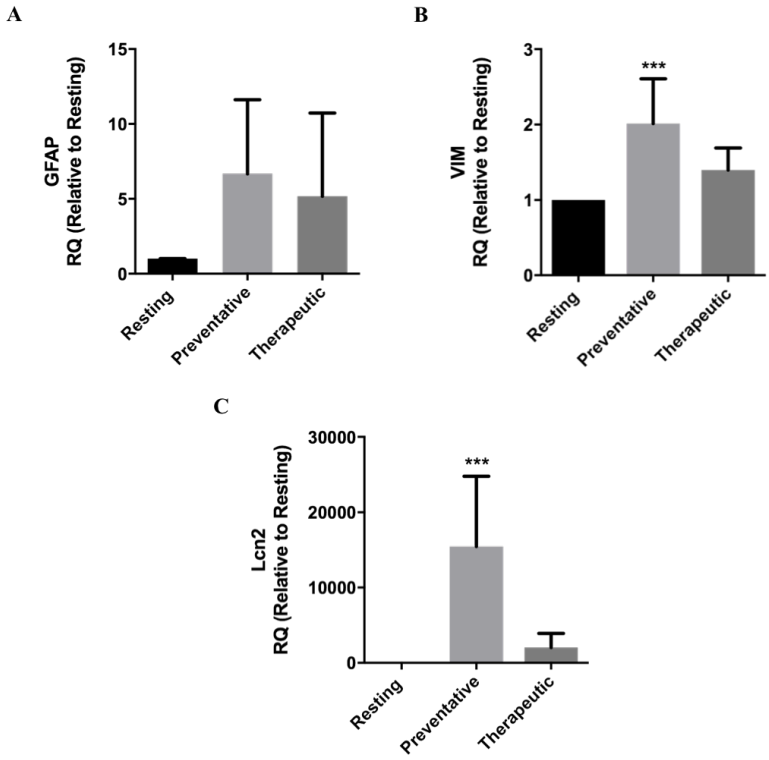

Figure 3.13: qRT-PCR quantification of relative mRNA expression levels of low-FBS/+FGF2 cultured astrocytes stimulated with LPS+IFNγ. **A** *Gfap*, **B** *Vim*, **C** *Lcn2*. Expression relative to resting controls ($2^{-\Delta\Delta Ct}$ method), *Gapd* reference gene. Data expressed as the mean of N ≥ 3 biological replicates ± SD; * P ≤ 0.05, ** P ≤ 0.01, *** P ≤ 0.001, or **** P ≤ 0.0001 relative to non-activated control samples (one-way ANOVA with Dunnett's multiple comparison test).

Several other classical activation/pro-inflammatory genes were upregulated upon activation, including interleukin-6 (*Il6)*, tumor necrosis factor (*Tnf,* although not significantly), and nitric oxide synthase 2 (*Nos2*) (Fig. 3.14 A,B,C); both *Il6* and *Tnf* mRNA expressions revert back to near-basal levels after 48 h of exposure to resting medium, while *Nos2* remained elevated. Notably, expression of the pro-inflammatory cytokine interleukin-1β (*Il1b*) was not significantly affected by activation in this model (Fig. 3.14 D).

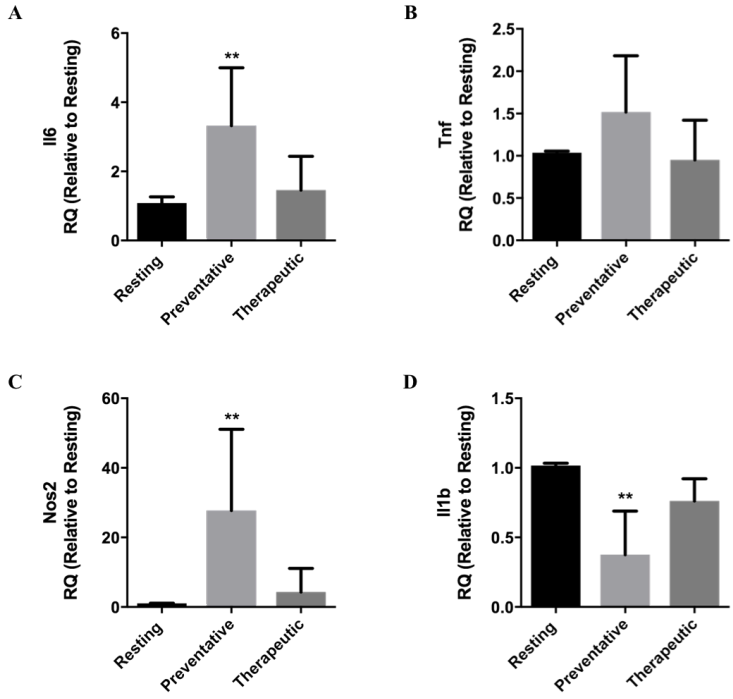

Figure 3.14: qRT-PCR quantification of relative mRNA expression levels of low-FBS/+FGF2 cultured astrocytes stimulated with LPS+IFNγ. **A** *Il6*, **B** *Tnf*, **C** *Nos2*, **D** *Il1b*. Expression relative to resting controls ($2^{-\Delta\Delta Ct}$ method), GAPD reference gene. Data expressed as the mean of N ≥ 3 biological replicates ± SD; * P ≤ 0.05, ** P ≤ 0.01, *** P ≤ 0.001, or **** P ≤ 0.0001 relative to non-activated control samples (one-way ANOVA with Dunnett's multiple comparison test).

The changes induced upon activation in our protocol, low-FBS/+FGF2 cultured astrocytes, were also confirmed by the analyses of protein expression by Western blot technique. Western blots performed at day 20, i.e. 48 h of activation medium with a subsequent 72 h into resting medium, confirmed the upregulation of both GFAP and Vim (Fig. 3.15A) relative to resting controls. Lcn2 expression could not be reliably ascertained by Western blot at this same time point, however a significant induction was evident at earlier time points: at day 16 and day 17, i.e. 24 or 48 h exposure to activation medium compared to resting controls (Fig. 3.15 B,C). To further investigate the reactive state of cultured astrocytes, the expression levels of phosphorylated signal transducer and activator of transcription (STAT3), a critical regular of astrogliosis, were assessed. The active pSTAT3, indicative of JAK/STAT3 pathway activation, was detected after 1 h of activation and slightly decreased at 48h of activation medium exposure by Western blot analysis (Fig. 3.15 D).

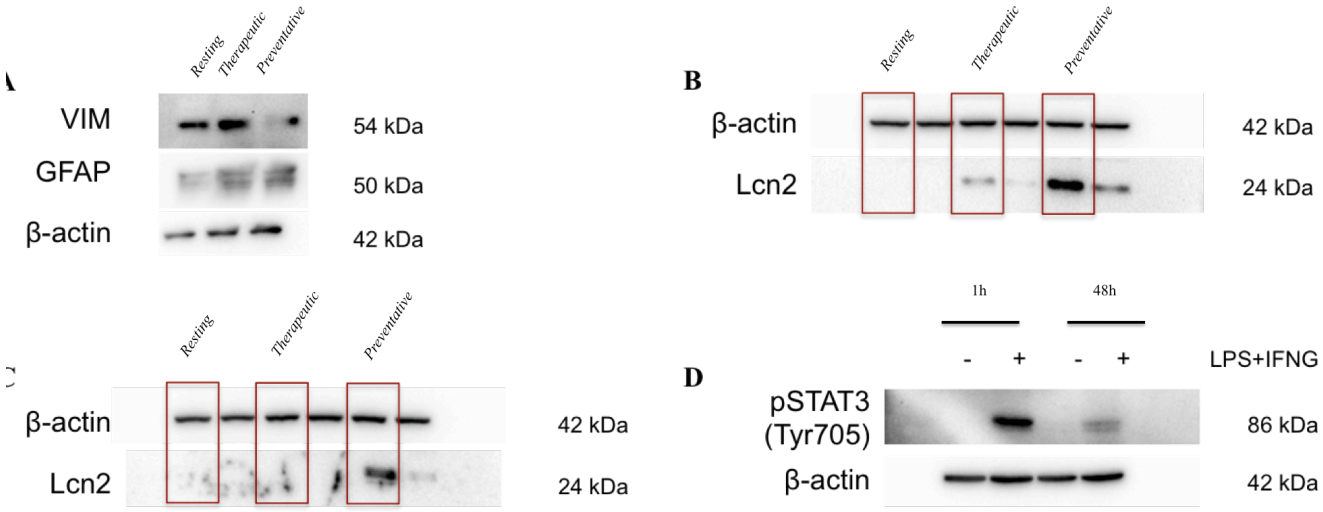

Figure 3.15: Representative Western blots illustrating: **A,** Changes in activation markers GFAP and Vim in resting, therapeutic- and preventative-activation astrocytes, respectively. **B,** Temporal changes in Lcn2 expression (16 DIV), red boxes highlight resting, therapeutic and preventative activated astrocytes, respectively. **C,** Temporal changes in Lcn2 expression (17 DIV), red boxes highlight resting, therapeutic and preventative activated astrocytes, respectively. **D** temporal induction of pSTAT3 upon treatment with LPS+IFNγ after 1 h (first two lanes) and 48 h (latter two lines).

These findings were also confirmed by a qualitative assessment of immunofluorescence micrographs in which the intensity of both markers GFAP and Vim, constitutively expressed in resting low-FBS/+FGF2 astrocytes, increased notably upon activation at day 20, i.e. 48 h of activation followed by 72 h of resting medium (Fig. 3.16). Lcn2 exhibited a remarkable upregulation in immunoreactivity, from a near-absence of expression in resting conditions to a strong labelling of most cells upon activation (Figure 3.16). Curiously, this pronounced induction of Lcn2 occurs at a timepoint (20 DIV, 48 h of activation followed by 72 h of rest) where we were unable to observe expression by means of Western blot (discussed in the next section).

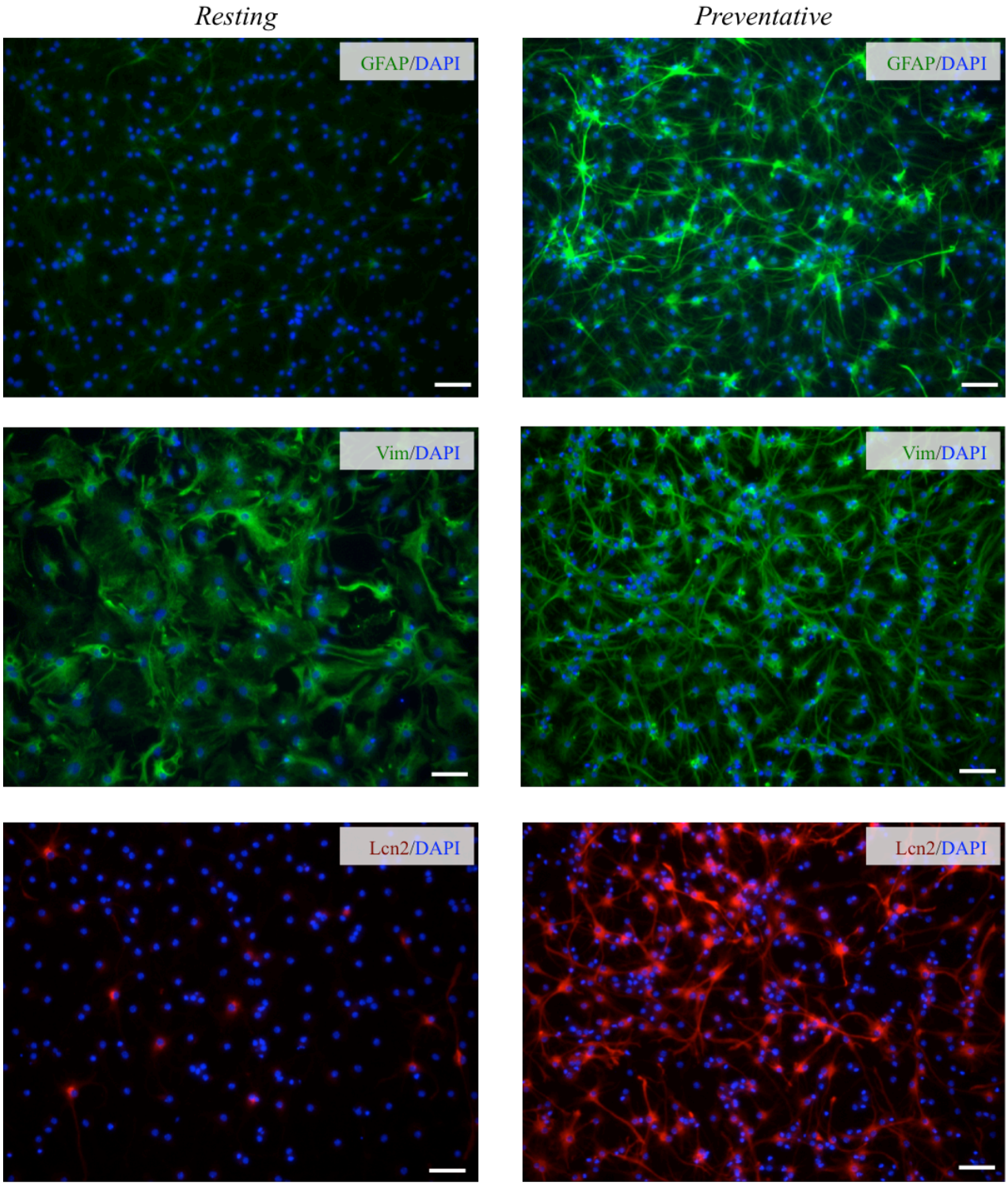

Figure 3.16: Immunofluorescence micrographs of low-FBS/+FGF2 astrocyte in resting and activated (LPS+IFNγ) conditions, 20DIV. Scale bar = 50 µm.

Therefore, both mRNA and protein levels of activation markers demonstrate the reliability and reproducibility of our NPC-derived astrocyte protocol and the expected increase in their expression upon activation.

3.6 DISCUSSION

Astrocytes play a number of fundamental physiological roles within the CNS environment, ranging from the maintenance of the homeostasis through metabolite regulation, modulation of released neurotransmitters, and regulation of synaptic pruning, but they are also able to respond to pathological conditions upon CNS insults. In response to disease and injury astrocytes exhibit a wide spectrum of changes in gene expression, function and morphology, with this broad and heterogeneous reaction referred to as astrogliosis [34, 35, 96]. This reactive state in astrocytes is modulated by a diverse array of instigating stimuli and molecular signals, resulting in a complex phenomenon that occurs across a continuum of intensity depending on the context, severity and proximity to the injury [34, 77].

For many decades astrogliosis has been considered a detrimental and harmful reaction to CNS insults, however more recent evidences involving transgenic loss-of-function models has highlighted its dichotomous nature. On one hand, astrocytes can exacerbate inflammation as a response to signalling pathways involved in pro-inflammatory activation [82], such as the nuclear factor κB (NF-kB) pathway [108], or the astrocytic scar in chronic stages of injury can impede axon regeneration by both secretion of inhibiting factors and as a physicochemical barrier [83]. On the other hand, it has also been shown that, in acute stages of diseases, the ablation or prevention of astrogliosis or the inhibition of astrocyte scar formation is associated with more severe injuries, increased inflammation, and consequently increased tissue damage and worse functional outcomes [91, 92]. Astrogliosis is therefore a phenomenon characterized by a finely coordinated range of potential changes, and the investigation of the physiology and pathophysiology of astrogliosis is providing important evidence for potential therapeutic targets [77, 82, 109]. However, discrepancies between studies could, to some extent, be attributed to complete gene knockout approaches aiming to ablate astrogliosis, since these approaches can also inhibit the beneficial aspects of acute astrocyte reactivity. For example, the ablation of STAT3, a critical regulator of astrogliosis, resulted in a reduced induction of GFAP upregulation in reactive astrocytes, however STAT3 is involved in diverse aspects of astrocyte reactivity [110]

such as the expression of synaptogenic thrombospondins [111], neuroprotective oncostatin M,[112] and proliferation-mediating endothelin receptor type B[113], as well as the response of mitochondria in combatting oxidative stress[114].

From this perspective the overall aim of this project is to modulate astrocyte reactivity by using 3WJ nanoparticles as a new and promising therapeutic platform. Thus, in order to study the efficacy and the effect of our designed 3WJ nanoparticles, we first established a consistent and reproducible *in vitro* protocol for astrocyte culture and the generation of a reactive phenotype.

Commonly, astrocytes cultures are obtained from primary cell derived from rodent brain tissues during the gliogenic stage (newborn pups). The advantages of primary astrocyte cultures are exemplified by a fast expansion, however astrocytes quickly tend towards senescence in the absence of growth factors [104]. Furthermore, primary cultures have been usually grown in undefined culture media, enriched with sera that are generally required for the maintenance of astrocytes [101]. Primary astrocyte cultures are also characterized by a heterogeneous astrocytic population (i.e. astrocytes that, in physiological conditions, differentially express the most classical astrocytic markers) and such cultures may be contaminated by other cell types, such as microglia, which can lead to confounding functional analyses of astrocytes [115]. These two characteristics may then represent major issues for studies that aim to screen *in vitro* compounds or potential therapies targeting astrocytes, since reproducibility between different primary cultures can be compromised.

For these reasons, our first goal aimed to establish an *in vitro* protocol for the differentiation of murine SVZ-derived NPCs, a well-established and characterized self-renewing population of stem cells, into a homogeneous population of mature resting astrocytes. We first followed already established protocols using a medium enriched with 10% FBS [101]; fetal bovine serum is commonly used in mammalian cell cultures since it contains different growth factors and is rich in metabolic substrates. We observed a maturation of an astroglial phenotype through 15 days of differentiation in high-FBS (10%) medium. However, NPCs themselves showed high levels of expression

in the classical astrocytic marker GFAP [101] and it was not possible to observe an increase in GFAP immunoreactivity/immunofluorescence throughout the maturation protocol. Nevertheless, we could observe the maturation in the astrocytic phenotype in other regards; indeed, maturing cells acquired a larger more stellate morphology typical of mature astrocytes with a concomitant increase in the GFAP distribution along the maturing processes. Astrocytes can be characterized by different markers, and besides GFAP expression, S100B has been used as marker for the identification of a terminal maturation state for astrocytes that differentiate from NPCs [103]. Concordant with these previous observations, S100B expression increased during our differentiation protocol (maximum levels were observed at 6 DIV), and it was maintained until the latest timepoints for mature astrocyte differentiation (15 DIV). Therefore, over 15 DIV of differentiation with a medium enriched in 10% FBS we observed a high expression of GFAP and S100B and the characteristic stellate morphology indicated that NPCs had acquired a phenotype typical of mature astrocytes, despite the observed high expression of IF usually associated with a reactive state.

In order to mimic the reactivity state observed *in vivo* upon CNS damages in our NPC-derived astrocytes, and to test consequently the efficacy of our nanoparticles as a modulatory tool, we employed the combined LPS and IFNγ treatment, as previously described by Mor et al. [107]. In that study it was shown that the exposure of primary cortical astrocyte cultures to LPS and IFNγ led to the secretion of pro-inflammatory cytokines Il6 and TNF, reaching a peak at 24-48 hours of exposure, and so we investigated the latter timepoint as being representative of an activated state while coinciding with the gene expression analysis timepoint of a typical siRNA-mediated knockdown experiment. The capability of mouse astrocytes to respond to LPS stimulation has been widely demonstrated [116-119] even though notable differences between human and mouse astrocytes were observed in TLR-ligand and immune activation [120]. In murine astrocytes LPS induces TLR4 dimerization that, through the activation of adaptor molecules, lead to the activation of signalling cascades through NF-κB, MAPK, and Jak1/STAT1 pathways, gene transcription changes, and finally inflammation pro-inflammatory response [117]. The direct relevance of the endotoxin LPS to human astrocyte reactivity in CNS injury is dubious since it has been observed

that human astrocytes exhibit little response to TLR4 stimulation [120], although an *in vitro* and *in vivo* study reported the effect of IFNγ on cultured human astrocytes as a potent mitogen, promoting extensive reactivity in astrocytes *in vivo* [121].

We therefore employed the LPS+IFNγ combination to induce a reactive state in NPC-derived astrocytes, as model for astrogliosis. Nevertheless, astrocytes differentiated into 10% FBS enriched medium showed a high reactivity in ostensibly resting basal conditions that hampered the further induction of a reactivity phenotype through the LPS+IFNγ treatment. While these cells did evoke a classical pro-inflammatory reactive state upon activation, inducing the expression of several pro-inflammatory cytokines and markers, such as Il6, TNF and Nos2 (previously established by our group), the canonical induction of intermediate filaments GFAP and Vim was not observed. Indeed, *Gfap* and *Vim* mRNA levels showed no differences upon activation. This basal reactive state observed in resting condition in astrocytes was attributed to the stimulatory effects of the high concentration of FBS (10%) present in the astrocyte differentiation medium, a well-described phenomenon attributed to the various cytokines, growth factors and hormones present in the serum that can also create variability in results due to inter-vendor and inter-batch variability [104, 105, 122].

Thus, different conditions have been explored in order to establish an *in vitro* system in which culture conditions can induce a reactive or quiescent state in astrocyte-like cells. The use of serum-free conditions aimed to synchronize cultured astrocytes and allows astrocytes to re-enter the cell cycle from a state of quiescence (G0) [123]; the use of chemically-defined media led to the induction of a multipolar stellate phenotype in cultured astrocytes [124, 125]; serum starvation or the withdrawal of serum from the medium prior to the desired assay can be used to reduce the basal activity in many different cell culture systems [126, 127], however the mentioned expedients may induce changes to cell morphology, gene expression and function [127]. The complex morphology observed in astrocytes *in vivo* can be limited by two-dimensional culture systems, and while 3D matrices may provide structural support leading to the development of the typical astrocytic morphology and quiescent astrocytes [128, 129], it

has been shown that astrocytes react to different physical and mechanical characteristics of the substrates [130].

FGF signalling has been found to suppress astrocyte activation, in particular inhibiting activation while promoting proliferation, in the normal brain and after traumatic injury [131]. Furthermore *in vitro* treatment with FGF2 as been found to induce changes in astrocyte structure towards a resting stellate morphology combined with a significant decrease in GFAP mRNA and protein levels [132]. Treatment with FGF2 has also been shown to facilitate the generation of mature, quiescent astrocytes characterized by low GFAP expression from stem cells [105] and recent evidence suggests that FGF can possibly modulate the reactive state of astrocytes through regulation of TLR4/NF-κB pathways [133].

Therefore, to circumvent the basal activation induced by high concentrations of FBS in the differentiation medium, we investigated a two-phase scheme ultimately using low-serum differentiation augmented with FGF. Astrocytic differentiation of NPCs was induced by using high-FBS (10%) medium during the first half of the differentiation protocol, while the promotion of a quiescent state was achieved by changing to low-FBS medium (1%), N2 supplement and FGF2 (50 ng/ml) supplementation for the remainder of the culture. We indeed observed that NPCs differentiated in a low-FBS/+FGF2 protocol were found to ultimately exhibit a resting astroglial phenotype. By 6 DIV NPC-derived cells possessed a ramified morphology with numerous processes; at 15 DIV astrocytes showed a more quiescent and mature phenotype characterized by stellate shape compared to hypertrophic structure of high-FBS/FGF-free cultured cells. Expression of astroglial markers S100B and ALDH1L1 increased over the course of the 15-day culture confirming the maturation of NPCs towards astrocytic lineage, moreover cells acquired a phenotype typical of mature resting astrocytes, characterized by thin and elongated processes and less cell hypertrophy (opposite to what observe in high-FBS/FGF2-free medium). Immunoreactivity and mRNA expression of GFAP, Vim and LCN2 were lower relative to high-FBS/FGF2-free cultured astrocytes, suggesting a lower level of basal activation.

Upon LPS+IFNγ exposure, mature (15 DIV) low-FBS/+FGF2 cultured astrocytes showed evidence of both a classical pro-inflammatory response and canonical astrocyte reactivity. In contrast to high-FBS/FGF2-free conditions, low-FBS/+FGF2 cells did show a response to LPS+ IFNγ-mediated activation observed by the upregulation in the expression of GFAP and VIM at both the mRNA and protein level. *Gfap* and *Vim* mRNA levels were notably higher than resting controls in the 48 h post-activation; while at 96 h post-activation (upon removal of the LPS+IFNγ stimulant) the expression of both IF genes had reduced back to a level intermediate between their resting and 48 h activated state. Protein levels, quantified from Western blots performed 5 days post-activation, were likewise elevated, and, despite the density and complexity of intertwined astrocytes processes, increased immunoreactivity was also evident in fluorescence micrographs.

48 h of stimulation led to an increase in the mRNA expression levels of *Tlr4* and *Ifngr2* confirming the induction of a reactive state in our cultured astrocytes using the activation protocol. Previous studies reported an induction in *Tlr4* expression upon LPS stimulation [117] and *Ifngr* upon IFNγ stimulation [134]. IFNγ stimulates activity of phagocytes by antigen presentation via Class I and Class II major histocompatibility complex (MHC) molecules; recent evidence from screening the transcriptome of astrocytes upon IFNγ activation showed an upregulation in genes involved in the immune response, such as expression of monocyte chemoattractant protein CCL2 and interferon-γ-inducible protein CXCL10 and MHC II pathway [135-137]. Our results confirmed the induction of a transcriptional coactivator of the class II MHC upon LPS+IFNγ stimulation by an increase in *Ciita* expression, supporting the evidence of a potential phagocytic role of astrocytes as immune effector cells. Furthermore, there was a significant induction in *Nos2* mRNA levels upon stimulation, as previously described. As a result of the increased expression of NOS2 by reactive astrocytes, they produce an excessive amount of nitric oxide (NO) in many neurodegenerative and neuroinflammatory conditions, and studies into *in vitro* stimulation with LPS and IFNγ showed an increase of GFAP expression as a consequence of NO production [116, 138].

Il6 has been shown to be involved in the regulation of inflammatory and immunological responses [139], moreover it has been shown that human astrocytes also release Il6 upon injury *in vitro* suggesting an involvement of this mechanism in post-traumatic cerebrovascular dysfunction [140]. A pro-inflammatory activation response was confirmed in our system by a significant induction in the expression of *Il6* and *Nos2* in LPS+IFNγ-treated astrocytes relative to resting controls. Amongst the different signalling pathways involved in astrocyte activation, STAT3 remains a critical regulator of astrogliosis [90, 91]. Studies have shown that IFNγ can directly activate STAT3 (rather than the canonical STAT1 response) upon binding to astrocytes [134]; LPS does not directly trigger the Jak-STAT3 pathway, and thus autocrine/paracrine stimulation by Il6 secreted from LPS+IFNγ-treated astrocytes might be an alternative explanation for STAT3 activation [141]. We did observe pSTAT3 activation induced with LPS+IFNγ stimulation by quantification of protein levels via Western blot. Lcn2, further discussed in the section below, is also regulated via STAT3 activation and it was found significantly upregulated in LPS+IFNγ-treated astrocytes. A large induction in *Lcn2* mRNA was evident 48 h post-activation, an increase reflected at the protein level as seen by Western blot and immunofluorescence, where negligible LCN2 expression was observed in resting conditions.

These data confirm that our low-FBS/+FGF2-cultured astrocytes are able to undergo a canonical response to activation and they showed a classical pro-inflammatory polarisation, thus making them a convenient model system for proof-of-concept studies of pRNA nanotherapeutics. Indeed, both the classical markers of reactivity, GFAP and Vim, and the promising therapeutic target Lcn2 were upregulated in this model of astrogliosis, allowing for the assessment of the efficacy of siRNA-functionalised 3WJ nanostructures to modulate this overexpression.

4) INTRODUCTION

The concept of nanomedicine has developed in recent decades, with the goal of increasing the efficacy of drug delivery through the medical application of nanotechnology [142]. The great improvements in the field has facilitated the development of nanotherapeutics based on a myriad of different materials and strcutures, all exploiting the key properties required for drug and gene delivery systems: biocompatibility, stability in circulation, negligible toxicity, minimal activation of the immune system, and efficiency of accumulation at a target site [143]. One material which has seen particular interest with regards to nanotherapeutic applications is RNA nanotechnology. RNA offers several advantages compare to other nanomaterials, possessing intrinsically defined features at the nanometer scale, being characterized by relatively high thermal stability and structural flexibility, and moreover the capability to perform a variety of different functions, such as RNA interference (RNAi) [144, 145].

4.1 RNA Nanotechnology

In recent years, drug delivery has become an intense field of research, with the major goal of overcoming the limitation that afflicts most classical medicines: an inability to specifically deliver a drug to its site of therapeutic action. Although pharmaceutical advances have led to the circumvention of many potential limitations in drug efficacy, including issues of poor solubility, high toxicity, an *in vivo* stability, specificity of delivery (at a specific rate and at a specific site) remains a goal yet to be substantially realised [146].

Nanotechnology applied to medicine is often referred to as nanomedicine and it offers several potential benefits, such as the possibility to use submicrometer-sized tools for the diagnosis, prevention and treatment of diseases, that has led to a better understanding of the complex pathophysiology of diseases, and also allowed an improvements in the quality of life of patients. Significant efforts have been invested

and substantial progress has been made in the nanomedicine field over the last couple of years [142, 147]. However, the real innovation of nanomedicines over standard low-molecular-weight drugs rely in these features: nanotherapeutics, ranging from ~30 up to 1000 nm, reduce renal excretion and/or hepatic degradation, leading to prolonged circulation times; reduce the volume of distribution, with less chances of accumulation in healthy non-target tissues and allow site-specific delivery, thus they improve the ability of drugs to accumulate at pathological sites, for example by conjugating nanoparticle surfaces to antibodies; [146, 148].
Because of these features, different and multivalent nanoparticles has been developed that offer the possibility of an innovative tools that retains many potentials: in fact nanoparticles can be employed as diagnostic and imaging tools [149, 150] and therapeutic approaches [151-153].

Amongst the diversity of nanomaterials, biological macromolecules (DNA, RNA and proteins) are popular building blocks for top-down approaches or bottom-up fabrication of nanostructures and nanodevices. RNA is particularly appealing for nanotherapeutic applications since it possesses several key advantages [144, 154, Guo, 2010 #1418]:

- RNA molecules are polymers composed of a combination of four bases: adenine (A), uracil (U), guanine (G) and cytosine (C). Therefore, there are copious possibilities to create a variety of polymers; for example, a 30-nucleotide RNA polymer can generate as many as 4^{30} (or 10^{18}) different RNA molecules. Furthermore, the simplicity of a 4-base pool of building blocks leads to an easy and reliable prediction of the formation of various nanostructures by bottom-up assembly;
- RNA molecules have demonstrated a variety of different functionalities. For example, the class of nucleic acid molecules known as aptamers function like protein or chemical ligands and can specifically target a definite cell population or cell type by binding cell-surface receptors. In this role, RNAs can serve as excellent targeting moieties. Another class of RNA of particular interest to nanotherapeutics are represented by RNA interference (RNAi) agents –powerful tools for targeted gene silencing, such as small interference RNA (siRNA);

- The high stability of RNA at lower pH, and thus its resistance to endosome degradation, make it an interesting and useful candidate tool for drug therapy since such barriers must be surmounted prior to dispersal throughout the cell after entry;
- RNA structures are generally characterized by low immunogenicity and toxicity, owing to their biocompatibility, however it has been shown that they can stimulate the host immune system through the activation of members of the Toll-like receptor (TLR) family, specialized in the recognition of pathogen-associated molecules. However proper modification, such as 2′-*O*-methyl modification, can easily eliminate such immune stimulation;
- RNA nanotechnologies can be functionalised with several features, such as desirable chemical or biological activity including ribozymes, aptamers, riboswitches, and RNAi agents, and
- RNAs possess versatile tertiary structures and catalytic functions that mimic some proteins.

The construction of RNA nanoparticles is a multi-step process: first the desired properties of the nanoparticle areidentified, then computational approaches are used to predict the structure and folding of the RNA nanoparticles (Fig. 4.1), then the monomeric RNA building blocks are synthesised by enzymatic or chemical approaches, subsequently assembled into the desired 3D construct, assembly and functional capabilities are characterised, and, finally, they are employed in their therapeutic/diagnostic application (Fig. 4.1) [145].

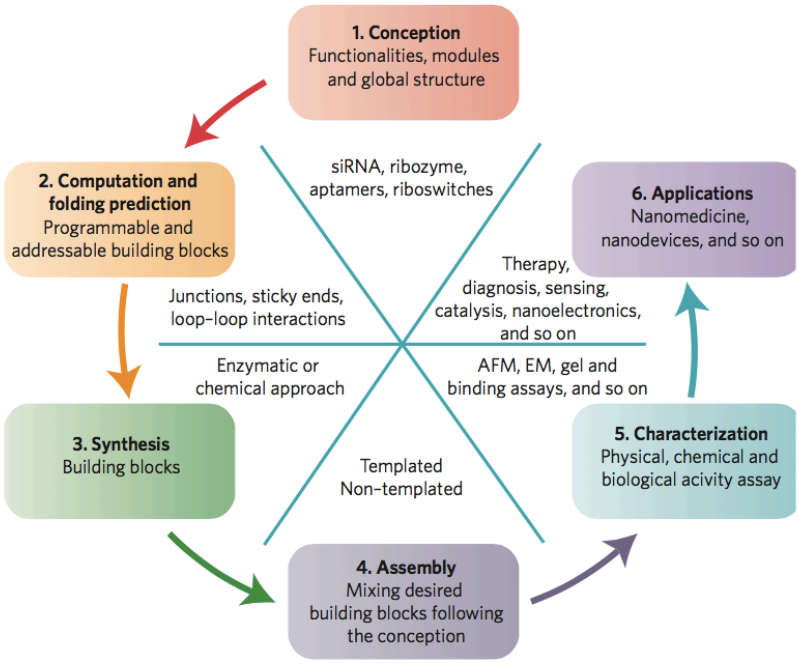

Figure 4.1: Schematic representation of the process for RNA nanoparticle construction. Modified from Guo P. [145].

As mentioned above, RNA molecules are characterized by different functionalities, and the post-transcriptional gene regulation afforded by RNAi in particular has led to the development of various therapeutic strategies [155, Gavrilov, 2012 #1431, Agrawal, 2003 #1433]. RNAi utilises a mechanism of sequence-specific gene silencing based on short double-stranded RNAs (dsRNAs); these siRNAs or micro RNAs (miRNAs) were first found in plants, elaborated upon in nematodes (for which Andrew Fire and Craig Mello would win the 2006 Nobel Prize in Physiology or Medicine), and were later observed in mammalian cells [156, Hammond, 2000 #1440, Zamore, 2000 #1438], paving the way for research-assisting or therapeutic gene knockdown through the design of siRNAs for any gene of interest [157].

siRNA and miRNA shared the same machinery, they are indeed assembled into RNA-induced silencing complexes (RISC), when loaded in the RISC complex one strand of the duplex is bound to Argonaute to direct silencing and the other strand is discarded. These strands are named guide and passenger strands, respectively, and their selection is a key step for silencing function. The guide strand is transient associated with

Argonaute, while the passenger strand will be cleaved and/or dissociated [158]. Therefore, activated RISC contains only single-stranded (antisense) siRNA or miRNA, which guides RISC to its complementary target messenger RNA. It is at this point that the distinction between the two types of RNAi becomes most apparent: siRNA, characterized by perfect sequence complementary with its target mRNA, induces site-specific cleavage of the mRNA, whereas miRNA typically has imperfect sequence complementary which leads to translational repression without mRNA degradation. Nevertheless, both the pathways result in the inhibition of target protein synthesis [159, 160].

Inspired by this cellular mechanism, several artificial methods of RNAi have been developed, such as the transfection of chemically synthesized siRNA oligonucleotides directly into the cytosol, or the use of short hairpin RNAs (shRNAs) synthesized within the cell by DNA vector-mediated production, to mimic endogenous miRNAs [161, 162]. Both techniques present advantages and disadvantages, for example the synthesis of siRNAs is quite fast since it does not require a cellular expression system, complex protein purification, or refolding schemes and a broad variety of reagents is available for siRNA design and synthesis. On the other hand shRNA may be used to generate stable knockdown cell lines, eliminating multiple rounds of transfections, but the creation of a stable shRNA cell line is time-consuming task and the selection of shRNA-positive cells requires a remarkable amount of work [163].

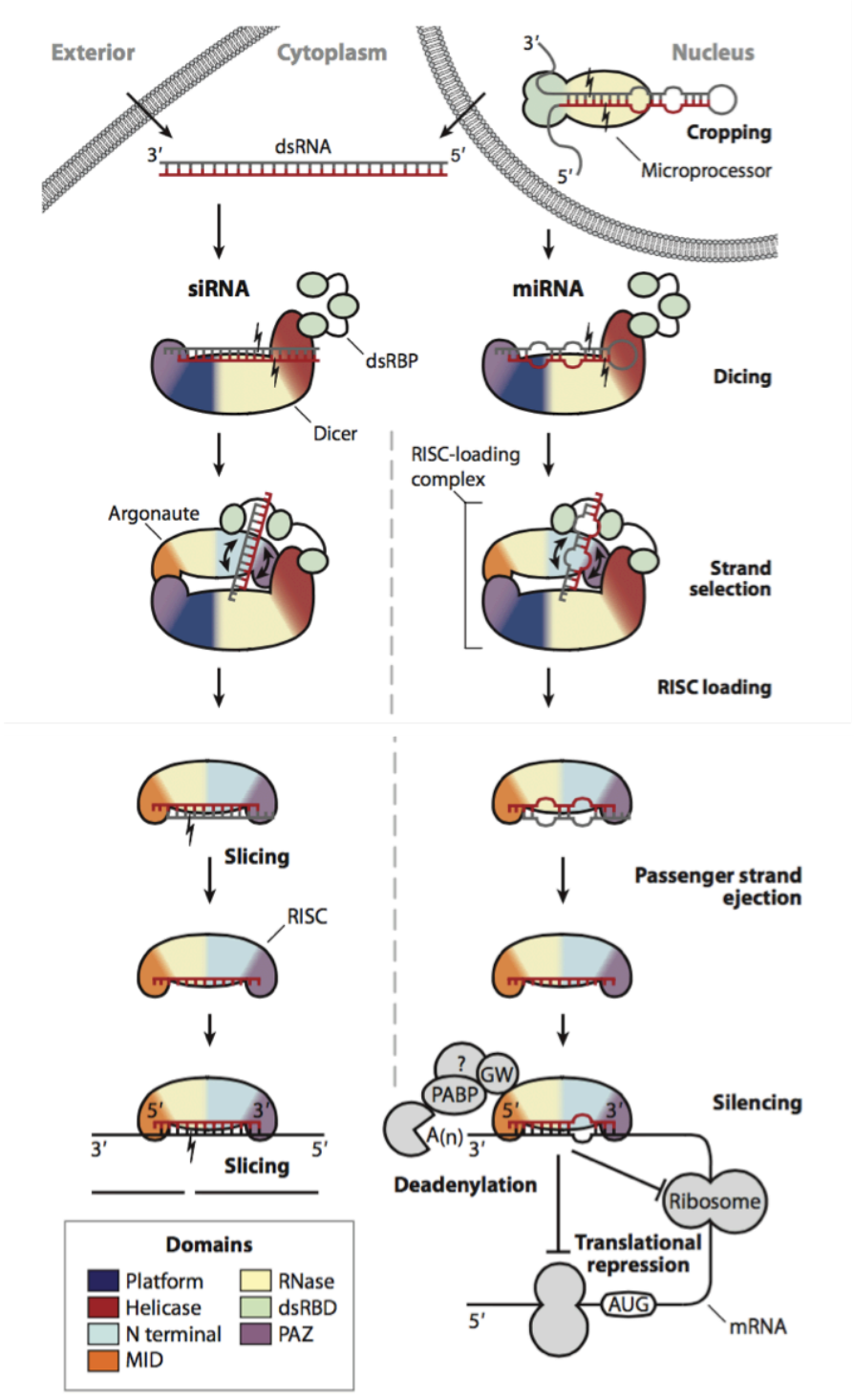

Figure 4.2: Schematic representation of RNA-Induced Silencing Complex (RISC) assembly. On the left is represented the siRNA pathway, while on the right is the miRNA pathway. Briefly, Dicer's cleavage of dsRNA of exogenous or nuclear origin gives rise to siRNA duplex that is loaded onto Argonaute by the RISC-loading complex, which comprises Dicer, a double-stranded RNA-binding protein and an Argonaute protein. The passenger strand (*gray*) is cleaved and the resulting guide strand (*red*) remains bound to Argonaute, forming the RISC. Subsequently, RISC recognizes and binds to a complementary mRNA target sequences (*black*) that are silenced via by slicing activity of Argonaute (in siRNA), or through translational repression (miRNA). Modified from Wilson et al. [160]

The increasing interest in RNAi technology and consequently the amount of data available has highlighted additional concerns of siRNA targeting. Indeed, unbiased genome-scale expression profiling studies revealed off-target activity of siRNA [164, 165].

The siRNA off-target effects can be divided into three main categories: siRNA-induced sequence-dependent regulation of unintended transcripts through partial sequence complementarity to their 3′ UTRs (microRNA-like off-target effects), causing the suppression of genes other than the desired target gene, and potentially diluting the anticipated silencing effect while propagating unintended physiological outcomes. Therefore, when designing siRNA-based therapeutics off-target silencing must be thoroughly investigated and testing should be undertaken for variations in normal protein expression profiles. Indeed, predictive bioinformatic approaches are routinely employed during the design of siRNAs, with the goal of reducing and preventing off-target silencing [166]. Induction of inflammatory response represents another off-target effect, siRNA can trigger the activation of Toll-like receptor pathway with the subsequent induction of interferon-mediated responses, potentially causing cell death [167, Hornung, 2005 #1481], however appropriate chemical modification can rectify this, as discussed earlier. The third class of off-target effects is related to saturation of the endogenous RNAi machinery by exogenous siRNAs and widespread effects on microRNA processing and function, thus making the dosage of putative siRNAs an issue for consideration. In addition to acknowledging these off-target activities and how they can complicate the interpretation of siRNAs effects [168], , siRNAs, and RNAs in general, can be easily degraded by enzymes in serum and tissues, with the half-life of naked, unmodified siRNAs in serum ranging from several minutes to an hour [169, Gavrilov, 2012 #1431]. Again, routine chemical modifications exist which can minimise these potential drawbacks.

To overcome these limitations, and to enhance the efficient delivery of siRNA to target cells, a diverse array of tools has been developed, including advances in delivery vehicle technology, chemical modification, and targeting moiety functionalisation [170].

4.2 pRNA NANOPARTICLES

Within the last decade an innovative bottom-up approach for the construction of RNA nanoparticles was developed, inspired by the molecular machinery of the DNA-packaging motor of the phi29 bacteriophage. Linear double-stranded DNA viruses, including the phi29 bacteriophage, are characterized by the same mechanism: their genome is packaged into a procapsid during their maturation and this energetically unfavourable mechanism is driven by an adenosine triphosphate (ATP)-driven DNA-packaging motor. However, the phi29 DNA packaging process is characterized by a unique feature: small viral RNAs called packaging RNAs (pRNAs) form a hexameric ring on the connector and gears the phi29 DNA packaging motor to package the viral genome into the preformed procapsid [171].

Each monomeric pRNA molecule contains two functional domains, specifically two single-stranded loops (right and left-handed loops) that interact in an intermolecular manner, hand-in-hand, in the assembly of the hexameric ring (Fig. 4.3). These domains are connected by a highly stable three-way junction (3WJ) region that can be manipulated and derivatised in order to obtain multi-armed, multi-functional structures. Since these domains fold independently around the stable 3WJ core, the arms can be readily functionalized by replacing the helical stem or interacting loops with, say, an siRNA moiety without affecting the core pRNA-3WJ structure (Fig. 4.3). 3WJs are common motifs in natural RNA, however the 3WJ-pRNA core is characterized by unique features, described below, that make it a uniquely powerful tool. More importantly, multiple potential functionalities, such as aptamers, ribozymes, miRNAs, fluorophores and imaging moieties, or small-molecule ligands/drugs, can be incorporated into the 3WJs, thus these unique characteristics and the modular, highly-functionalisable nature make pRNA nanotherapeutics promising and attractive tools for gene therapy [151, Shu, 2011 #1486, Guo, 2010 #1428, Guo, 2010 #1418].

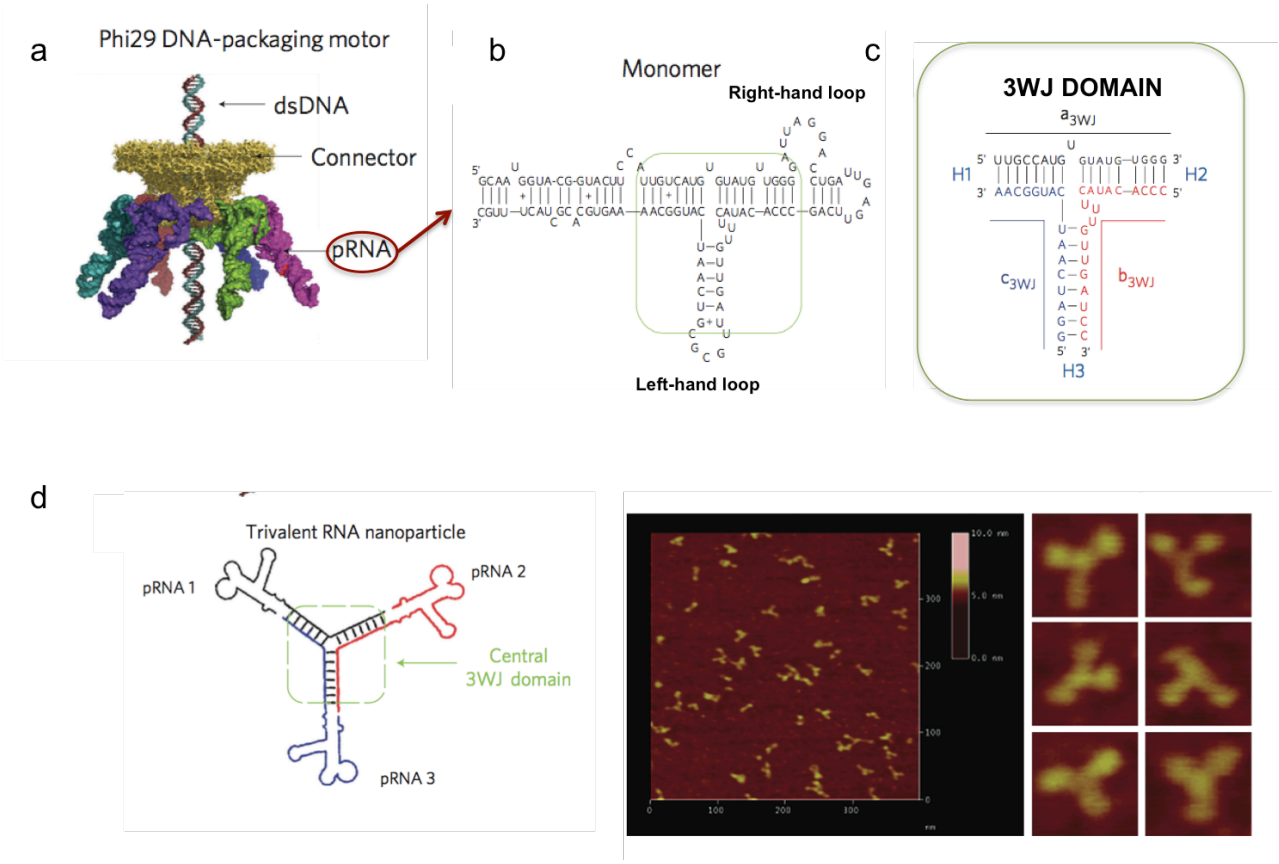

Figure 4.3: Structure of phi29 DNA-packaging RNA. **a**, Illustration of the phi29 packaging motor formed by six pRNAs (in different colours). **b**, Sequence and folding of pRNA monomer. **c**, 3WJ domain composed of three RNA oligomers in black, red and blue. **d**, Example of a trivalent RNA nanoparticle formed by three pRNA molecules bound at the 3WJ-pRNA core sequence, with AFM visualisation. Modified from Shu et al.[151]

Notably, pRNA, when compared to other RNA motifs, exhibits uncommon stability and, as mentioned above, can be used for a broad range of applications as its modular nature can give rise to a myriad of different designs. It has been shown that 3WJ RNA nanoparticles are resistant to denaturation in urea: dsDNA and dsRNA are usually denatured and dissociate in the presence of 5M or 7M urea, while the 3WJ domain remains stable without dissociation at concentrations of 8M. Furthermore, upon 2′-F chemical modifications of pyrimidine nucleotides, 3WJs are more stable in serum, overcoming one of the major challenges of RNA-based technology *in vivo* (2′-F 3WJs are characterized by a half-life of 2-10 hours compared to 5-30 minutes for 2′-F modified siRNAs), and 3WJ-based constructs remain intact at ultra-low concentrations [169, Shu, 2011 #1417].

Three different “toolkits” have been developed for controllable and predictable generation of pRNA-derived nanoparticles with varying shapes and angles, exploiting the versatility of this platform for nanotechnological/therapeutic applications [172, 173]:

- Toolkit 1: Inter-molecular interactions between loop domains (R- and L-loops) on pRNA monomers *via* hand-in-hand interactions. Homo-dimers can be designed by using complimentary sequences in the same pRNA molecule, while a hetero-complex can be created through the combination of a number of pRNAs by matching the sequence of the R-loop and the sequence of the L-loop of another pRNA. These interactions between building blocks lead to the formation of dimers, trimers, and multimeric rings (Fig. 4.4A);
- Toolkit 2: The 5′/3′ open region, in the helical domain of the pRNA, allows for the extension of sequences while maintaining the folding of the entire pRNA molecule. To link pRNA monomers, a palindromic sequence can be added as a bridge for RNA nanostructures via intermolecular interactions, denoted as foot-to-foot interactions, and it can lead to the formation of hexamers, octamers, decamers, and dodecamers (Fig. 4.4B);
- Toolkit 3: The 3WJ core of the pRNA interlocking domain can be assembled from three individual RNA fragments, and its structure allows the functionalisation of this nanoparticle by conjugation of different RNA (or other appropriate chemistries) moieties at each end. Importantly, the conjugation of functional arms does not alter the original folding, and each module maintains its structure and retains its functionality. The higher-order X-shaped motif is inspired by the interlocking domain of the pRNA; it presents a motif similar to 3WJ with the right-hand loop on the pRNA replaced with a short, double-stranded sequence and a final structure characterized by four RNA oligos as a scaffold for the conjugation of four RNA functional motifs (Fig. 4.4C).

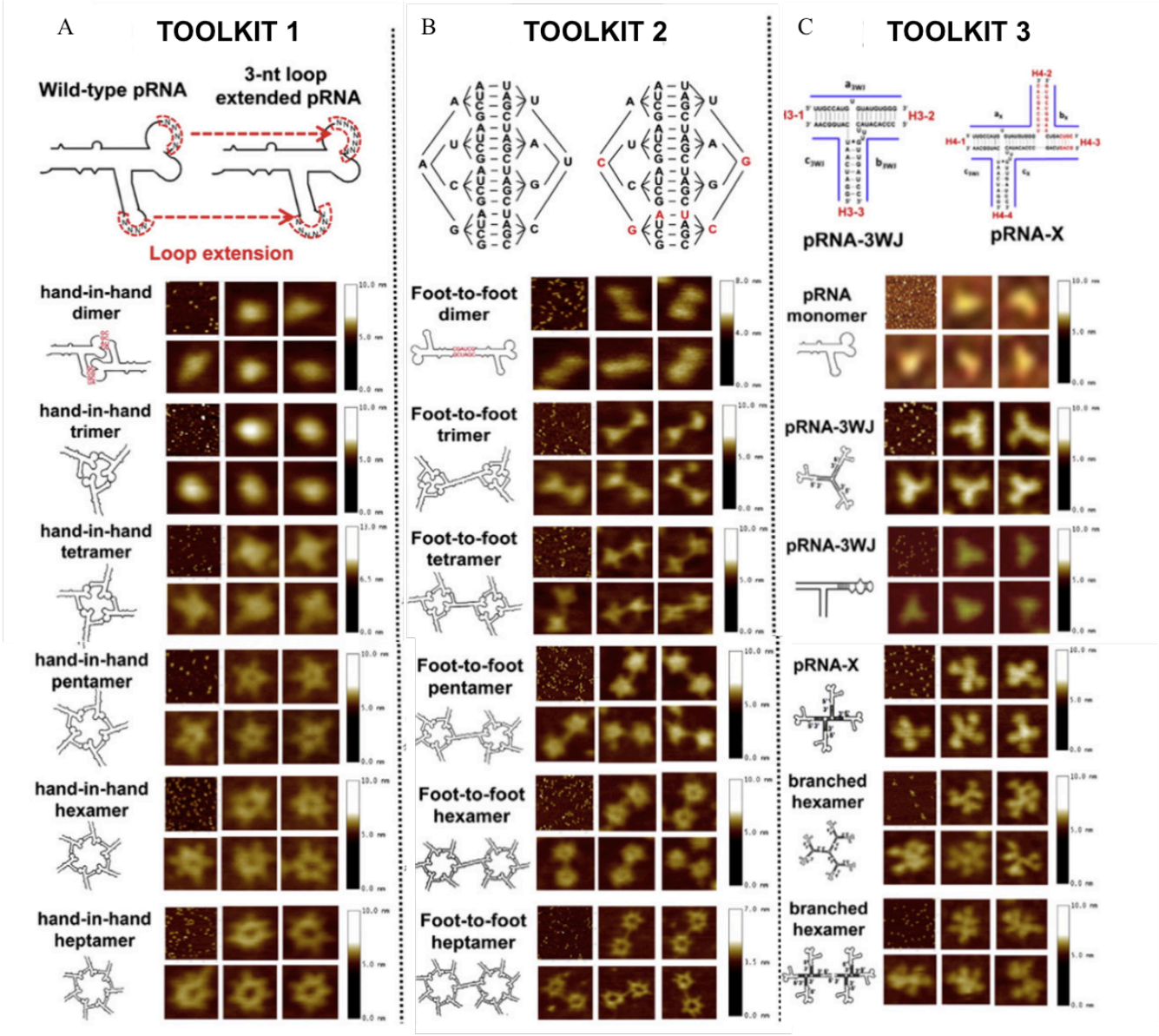

Figure 4.4: Three "toolkits" used for pRNA nanoparticle construction. **A**: Toolkit I: pRNA hand-in-hand interaction. **B**: Toolkit II: foot-to-foot interaction. **C**: Toolkit III: branch extension. Adopted from Shu et al. [172].

The studies described herein employ proof-of-concept 3WJ-pRNA nanostructures, for applications in the CNS niche, bearing siRNA moieties targeting genes overexpressed by reactive astrocytes.

4.3 LIPOCALIN-2

Lipocalin-2 (Lcn2) belongs to a large family of secreted proteins with a common and conserved lipocalin domain that can bind various small hydrophobic macromolecules

including siderophore-bound iron, pheromones, fatty acids, and retinol [174]. Furthermore, lipocalins can bind to specific receptors and deliver ligands and growth factors into cells by receptor-mediated endocytosis [175]. Thus, the lipocalin-protein family act as transporters (some being enzymes) and are associated with a diversity of biological processes, such as immune responses, pheromone transport, olfaction, prostaglandin synthesis, retinoid binding, and cryptic coloration; more locally, they also regulate many cellular processes, such as cell migration, proliferation, differentiation, cell death and survival [174-176].

Lcn2 was first described as neutrophil gelatinase-associated lipocalin (NGAL) but it is also known as 24p3 or 24-kDa superinducible protein (SIP24) [175, 177]. Initially identified murine kidney cells [178], its presence was first described in human tissues in particular bronchial epithelial cells and alveolear type II pneumocytes, which showed an upregulation in the synthesis of Lcn2 during lung inflammation; interestingly, human and mouse Lcn2 showed a 62% homology in amino acid sequence [179, 180]. It has been shown that Lcn2 can bind two cell-surface receptors: brain type organic cation transporter (24p3R) and megalin [181, 182]. 24p3R is expressed constitutively and its presence has been shown in various cell types, such as in kidney epithelial cells [181], epithelia of respiratory tracts (where it is upregulated upon lung inflammation) [180], macrophages, neutrophils [183], microglia (where Lcn2 is constitutively expressed and its expression is upregulated by inflammatory stimulation) [184], astrocytes [185], and neurons [175]. Megalin, a multi-ligand endocytic receptor, is also expressed in different cell types, such as in a sub-population of epithelial cells [175], cells in brain capillaries and the choroid plexus, the ependymal cells of the lateral ventricles where it may contribute to the modulation of this microenvironment [186], and neural progenitors in the embryonic mouse spinal cord [187] where it may play an important role in the development of mature astrocytes.

Lcn2 appears to play myriad roles in the CNS: a recent study focused on oesophageal squamous cell carcinoma employed network-based analyses of protein-protein interactions (PPI) to unravel the complex biological activities of Lcn2. Gene Ontology (GO) annotation revealed the relation of Lcn2 to a group of immunity-related terms,

such as ‘‘regulation of immune response’’, ‘‘activation of immune response’’, ‘‘innate immune response’’(Fig. 4.5 I); another pathway-cluster included ‘‘regulation of transforming growth factor beta receptor signaling pathway’’, ‘‘regulation of Wnt receptor signaling pathway’’, ‘‘immune response-regulating cell surface receptor signaling pathway’’ (Fig. 4.5 II); the third major identified GO term group suggested the enrolment of LCN2 in the regulation of the cell cycle by the discovery of GO terms, such as ‘‘G1 phase of mitotic cell cycle’’, ‘‘G1/S transition of mitotic cell cycle’’, ‘‘G2/M transition of mitotic cell cycle’’ (Fig. 4.5 V) and finally Lcn2 activity was related two other GO terms involving ‘‘cellular response to molecule of bacterial origin’’ and ‘‘extracellular matrix organization’’ (Fig. 4.5 III, IV) [188].

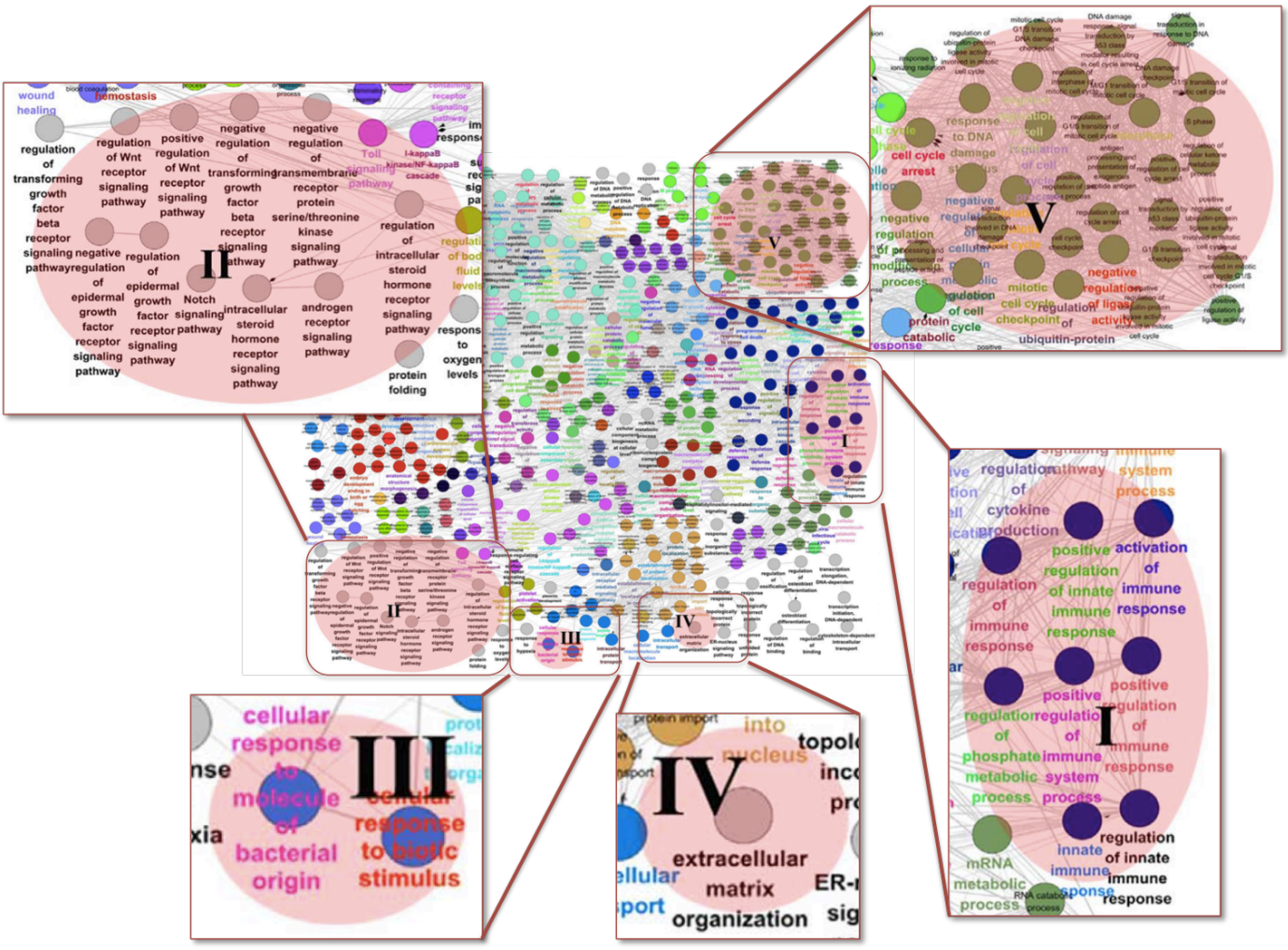

Figure 4.5: Functional map of the total PPI sub-network. Similar GO terms were labelled in the same colour and the GO term group of interest related or potentially related to LCN2 function was indicated by a Roman numeral, magnified in the small boxes. Modified from Wu et al. [188]

Another important role of Lcn2 to bind bacterial ferric siderophores was first unravelled by a crystallography study conducted on Lcn2 that identified its ligand. It was shown that Lcn2 released by neutrophils at sites of infection and inflammation was able to sequester bacterial ferric siderophores, thus playing a role in the antibacterial iron-depletion strategy of the innate immune system with a specificity to sequester iron earmarked for bacterial use [189]. [190]. Siderophores are released by microorganisms under aerobic conditions to scavenge from the environment iron required for a variety of functions, including reduction of oxygen to synthesise ATP, reduction of ribonucleotide precursors of DNA, and a variety of other essential functions [191]. Towards this end, microbes scavenge iron that is bound to proteins in the mammalian host, such as haemoglobin, transferrin, lactoferrin and ferritin. In this context Lcn2 competes with bacteria for iron by binding the siderophores [192]. To support such a role some evidences have shown that, upon bacterial pathogenesis, Toll-like receptors expressed on immune cells stimulate transcription, translation and secretion of Lcn2. The competition and sequestration of iron then attenuates bacterial growth and reduces bacterial infection [175, 192].

Another function attributed to Lcn2 regards the modulation of cell migration and morphology [189]. A recent study showed the capability of LCN2 to modulate the neuronal phenotype in primary cortical neuronal cell cultures and neuroblastoma cell lines as experimental models; cells exposed to Lcn2 increased their cell death rate related to nitric oxide, oxidative stress, and TNF and stimulate neuronal motility and process extension [193]. Furthermore, Lcn2 is able to induce the production of several chemokines, such as CXCL10, in different populations within the CNS, such as astrocytes, neurons and microglia, which in turn modulates their migration and phenotype. Two different *in vivo* models of CNS injury, LPS injection and cortical stab wound injury, showed that Lcn2 secreted mainly by astrocytes promoted the migration of microglia, neurons, and astrocytes themselves, likely acting through the JAK2/STAT3 and IKK/Nuclear fFctor κB (NF-κB) pathways [194].

Lcn2 acts as a cytokine and plays a regulatory role in a broad range of inflammatory reactions. Indeed, its regulation is upregulated during sterile inflammation, infection, injury, or during autoimmune disorders [17, 174, 175, 183, 195, 196]. In the acute phase of inflammation, Lcn2 is overexpressed, leading to an infiltration of granulocytes at the inflamed site that, in turn, synthesize and secrete further Lcn2, mediating local tissue injury or inflammation. Moreover, it has been shown that Lcn2 can also be released in systemic circulation and therefore it may represent a marker for different inflammatory disorders [180, 183, 197]. As part of the innate immune response, Lcn2 contributes to the pathogenesis of several neurodegenerative diseases, but may in fact demonstrate a dual functionality. It has been shown that *Lcn2*-deficient mice in experimental autoimmune encephalomyelitis (EAE) exhibit a worsened disease severity relative to Lcn2-expressing wildtypes, suggesting a protective role for Lcn2 through a modulation of the pro-inflammatory response rather than a promotion of the anti-inflammatory response [196]. On the contrary, the assessment of Lcn2 in a mouse model of spinal contusion injury revealed its detrimental effect in this condition arising from a promotion of neuronal loss, production of proinflammatory cytokines, and immune cell infiltration upon Lcn2 expression [17]. Furthermore, Lcn2 is able to modulate the phenotype of most of cells involved in the immune response. By using a mouse neuroinflammation model it has been shown that Lcn2 plays an essential role in the M1 (pro-inflammatory) polarization of microglia. Upon LPS stimulation of primary microglia and LPS-induced inflammation model *in vivo*, Lcn2 increased M1-related gene expression, while inhibiting M2-related gene expression in microglia lineage [198].

4.4 THE ROLE OF LIPOCALIN-2 IN REACTIVE ASTROCYTES

The important role of Lcn2 as a mediator of astrocyte reactivity was well-characterised with a study published by Lee et al. [185]. This study demonstrated that Lcn2 secreted by astrocytes has a dual role in influencing the morphology and functional fate of activated astrocytes. In fact, it was shown that Lcn2, secreted by astrocytes upon exposure to inflammatory stimuli, was able to cause cell death in activated astrocytes

and induce typical morphological changes, such as GFAP overexpression, associated with reactive astrocytosis *in vivo*. It was speculated that Lcn2 promoted the growth of astrocyte processes and motility by activating the Rho/ROCK pathway (Fig. 4.6), in addition to other parallel Lcn2 pathways. However, by forcing the expression of Lcn2 and using recombinant LCN2, it was hypothesized for the first time that secreted Lcn2 might act as a self-regulatory/feedback control mechanism, sensitizing astrocytes to cell death signals evident in CNS inflammation [185]. More recently these findings have been supported by transcriptomic analysis in models of ischemic stroke and LPS-induced neuroinflammation in which Lcn2 expression was strongly upregulated upon both injuries [82].

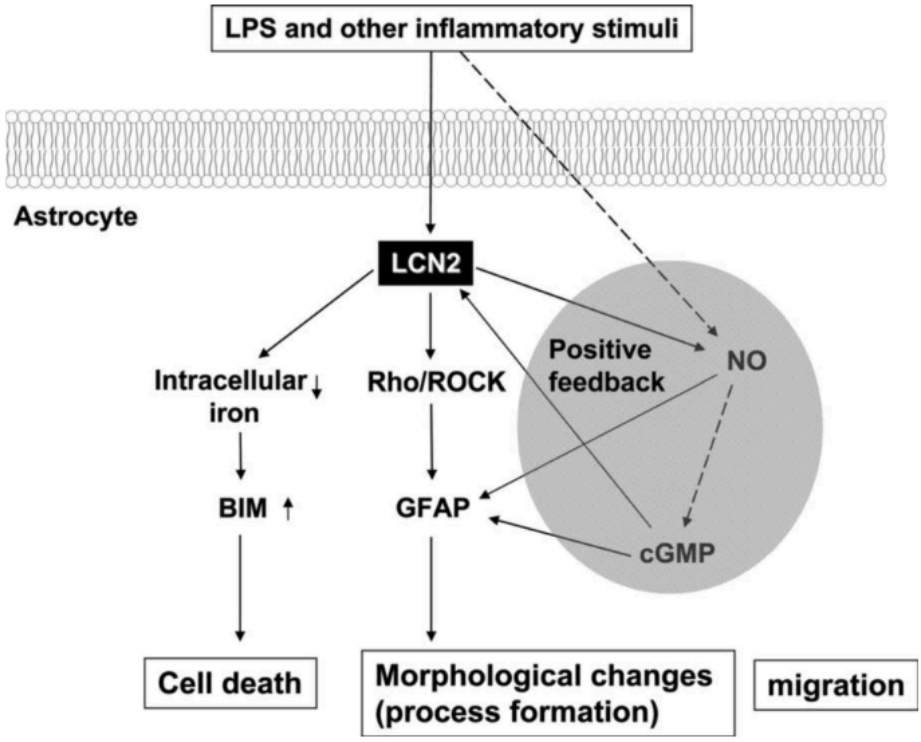

Figure 4.6: Schematic representation of reactive astrocytes under inflammatory condition: secreted Lcn2 may act as a feedback control on astrocytes to induce morphological as well as functional changes. Lcn2 induces morphological changes and promotes migration through the Rho/ROCK pathway in reactive astrocytes. Parallel pathways can lead to cell death signals (BIM pathway). Adopted from Lee et al. [185]

Lcn2 secreted by reactive astrocytes has been shown to play a role as a mediator of astrocytic neurotoxicity during several disease states or neurodegenerative conditions (Tong et al., 2013), in fact *in vitro* studies showed the capability of astrocyte-secreted Lcn2 to induce apoptosis on neuronal cultures[199, 200]. Thus, Lcn2 may contribute to neuronal cell death in injury and disease *in vivo*. These pro-apoptotic effects of LCN2 may be receptor-mediated and dependent on B-cell lymphoma 2 (Bcl-2) family protein BIM [181].

Expression of the Lcn2 gene under conditions related to brain injuries is controlled at the transcriptional level by several different transcription factors. NF-κB is described as one of the most important regulators of Lcn2 gene transcription; indeed, brain injury is inevitably related to an activation of the inflammatory response and NF-κB, as a key regulator in inflammatory signalling pathways, in turn regulates Lcn2 gene expression [201]. It has also been demonstrated that mitogen-activated protein kinase (MAPK) and STAT signalling pathways regulate Lcn2 expression. One particular study employing a mouse model of a chronic neuroinflammatory condition showed the role of astrocytic STAT3 in the upregulation of expression of Lcn2, and although the model does not imply a direct CNS injury, it still emulates the neuroinflammatory characteristic thereof [202]. Notably, the STAT3 pathway is a well-established central player in reactive astrocytosis [91, 92]. Moreover, JAK2/STAT3 and IKK/NF-κB pathways are downstream signalling pathways of Lcn2 and there is evidence demonstrating their activation by Lcn2, resulting in the modulation of chemokine release and cell migration in astrocytes with the likely final outcome of promoting neuroinflammation. Therefore, Lcn2 and the above-mentioned STAT3 and NF-κB pathways are involved in a dual fashion in the role of Lcn2 in reactive astrocytes both in the induction of Lcn2 expression and in its ultimate function [174].
The relevant role of Lcn2 in the inflammatory response has led to further investigation on its ability to modulate the phenotype of immune cells. By analogy to macrophage polarization (i.e. M1 NF-κB being categorized based on their capability to induce classical pro-inflammatory signals, with M2 macrophages grouped based on their anti-inflammatory properties [98]), microglia and astrocytes can also polarise along similar phenotypic axes upon stimulation [82, 203]. In this regard, it has been shown that Lcn2 promotes a classical pro-inflammatory activation in astrocytes and, by inhibiting

STAT6 phosphorylation, it inhibits activation of the alternative phenotype (Fig. 4.7). Indeed, Lcn2 can induce the expression of classical genes related to a pro-inflammatory response, such as IL-1β, NOS2 and TNF, while this induction was reduced in *Lcn2* knockout (KO) mice [204].

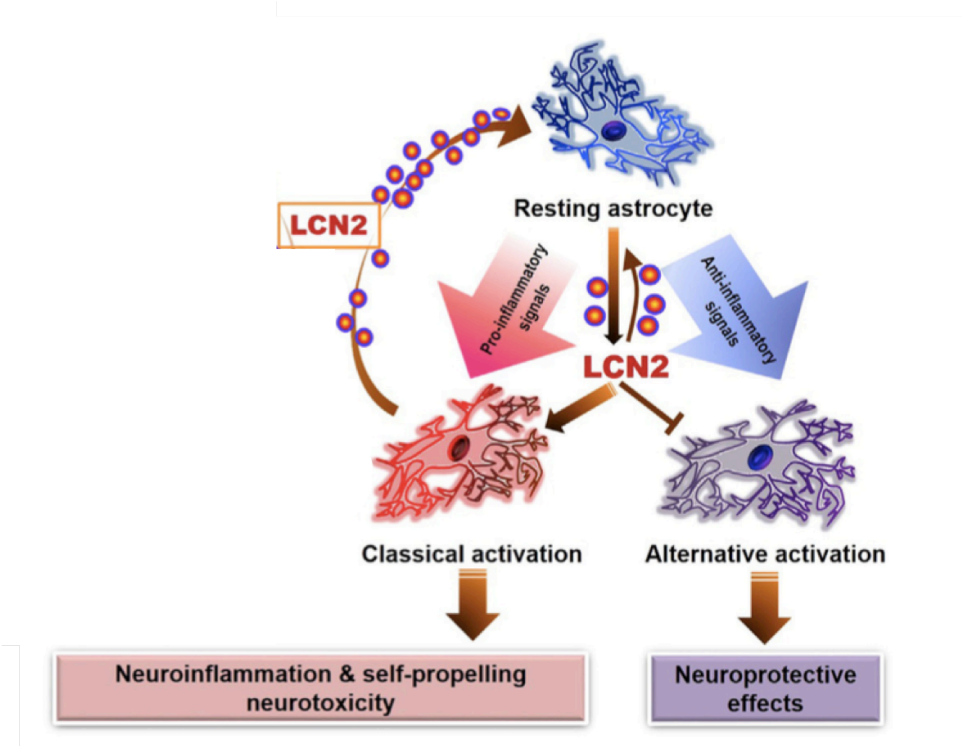

Figure 4.7: Schematic representation of the effect of Lcn2 on astrocytes. Lcn2 promotes classical proinflammatory astrocyte activation and inhibits the alternative anti-inflammatory astrocytic activation, acting through an autocrine mechanism. Modified from Jha et al. [175].

Despite the dual role of Lcn2 in the regulation of the injured CNS environment, its central role in the activation of astrocytes towards a pro-inflammatory state suggests this protein as a valid and promising target for the modulation of reactivity astrocytes. Therefore our aim is to investigate the potential efficacy of 3WJ-pRNA nanostructures in modulating the expression of reactive astrocyte markers, such as GFAP and Vim, herein employ *as a proof of concept* targets, and to investigate the role of astrocyte-secreted Lcn2 in the promotion of a reactive state in astrocytes.

4.5 RESULTS

4.5.1 ASSEMBLY OF SIRNA-3WJ NANOPARTICLES

siRNA-3WJs, of the general scheme depicted in Fig. 4.8, were prepared based on the previously methods described by Shu, et al.[173]. The sequences of the siRNA moieties incorporated in the nanostructures are identical to the commercial sequences provided in the SMARTpool siRNA mixtures (GE Healthcare, Dharmacon), here used as controls, albeit without the proprietary chemical modifications. Each siRNA-3WJ was constructed using three RNA strands that were annealed together in equimolar amounts to achieve the assembly of the 3WJ nanostructure. Strands *A* and *C*, containing the sense and antisense siRNA sequences respectively, were prepared via *in vitro* transcription with subsequent 5′ dephosphorylation using calf intestinal phosphatase, while the short *B* strand was purchased as a pre-synthesised RNA oligonucleotide. Successful assembly of the siRNA-3WJs was confirmed by the decreased gel mobility of the multistranded structures in electrophoretic assays relative to single- and double-stranded controls (Fig. 4.8 b). The chosen nomenclature of siRNA-3WJs refers to their target mRNA (G for *Gfap*, V for *Vim*, L for *Lcn2*, and N for non-targeted negative control sequences) and the identification number of their analogous SMARTpool siRNA analogue (see Table 2.1 in the Materials and Methods section). For uptake assays, Cy3-labelled analogues were prepared by labelling the constituent strands of the siRNA-3WJ with the Cy3 fluorophore using a Mirus Label IT kit prior to assembly.

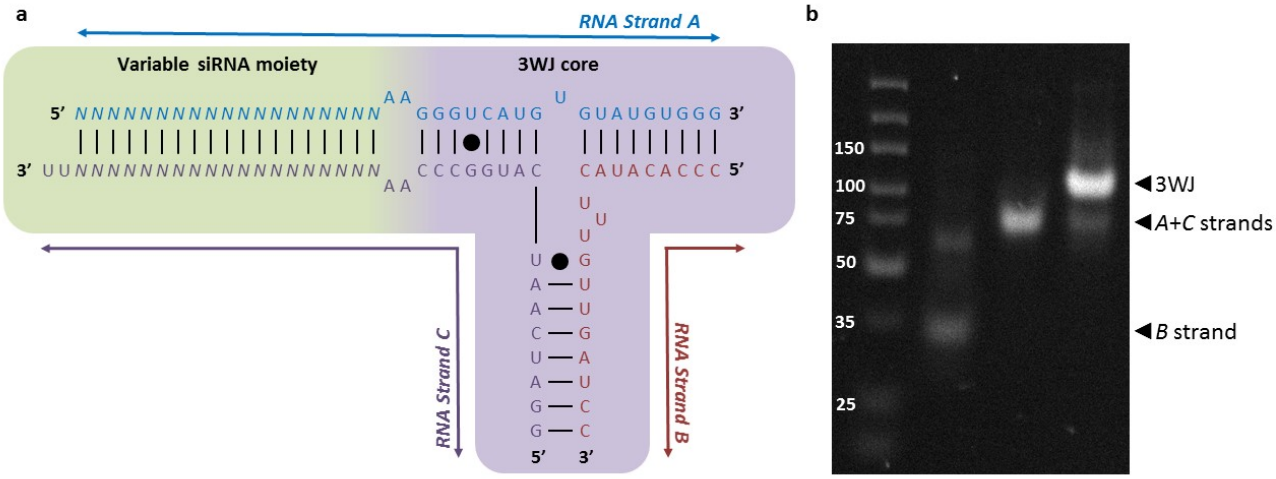

Figure 4.8: Design and characterisation of pRNA 3WJs. **A,** Generic 3WJ scheme showing the three constituent RNA strands, variable siRNA moiety and 3WJ core, unpaired and wobble base pairs (●). **B,** Native polyacrylamide gel (8%) illustrating the characterisation of 3WJ assembly by gel mobility. The assembled 3WJ shows decreased mobility relative to a double-stranded (*A+C* strands) construct or the *B* strand alone. An Ultra Low Range DNA ladder is used as reference.

4.5.2 TRANSFECTION OF NPC-DERIVED ASTROCYTES WITH SIRNA-3WJS

Once assembled, to ensure a high transfection efficiency siRNA-3WJs were delivered to NPC-derived astrocytes *in vitro* via lipofection using Lipofectamine RNAiMAX. Transfections were performed at 15 DIV with subsequent RNA collection for assessment of mRNA levels via qPCR at 17 DIV and evaluation of protein levels via Western blot or immunofluorescent microscopy at 20 DIV. Transfections were performed in three different activation contexts: a *resting* profile, in which the astrocytes were not treated with LPS+IFNγ and therefore quiescent, and two different activation profiles wherein LPS+IFNγ-treatment occurs either in the 48h prior to transfection (i.e. 13-15 DIV) or activation and transfection are concomitant (i.e. 15-17 DIV) (See Fig 3.10, previous section). These two activation profiles are referred to as a *therapeutic* intervention, to mimic an *in vivo* approach upon CNS insult, and the *preventative* intervention, exploring the utility of these putative nanotherapeutics in inhibiting a reactive response, respectively.

4.5.3 SIRNA-3WJS UPTAKEN BY NPC-DERIVED ASTROCYTES SHOW LOW TOXICITY AND IMMUNOGENICITY

To assess the uptake efficiency of the siRNA-3WJs via transfection, high-FBS/FGF2-free astrocytes were grown on poly-D-lysine-coated glass coverslips and incubated with Cy3-labelled N03-3WJs in serum-free medium at a final concentration of 10 nM for 6 hours, thereafter medium was changed and cells were incubated for further 18 hours in high-FBS/FGF2-free medium. 24 hours post-transfection cells were fixed and labelled for immunofluorescence (GFAP, DAPI), with the percentage of transfected astrocytes estimated by confocal microscopy to visualize the co-localisation of punctuate Cy3 staining with $GFAP^+$ cells. Similar high transfection efficiencies were observed across

the different conditions: 89%, 82% and 71% Cy3-N03-3WJ-positive cells were observed respectively in resting, *therapeutic* and *preventative* activated astrocytes (Fig 4.9).

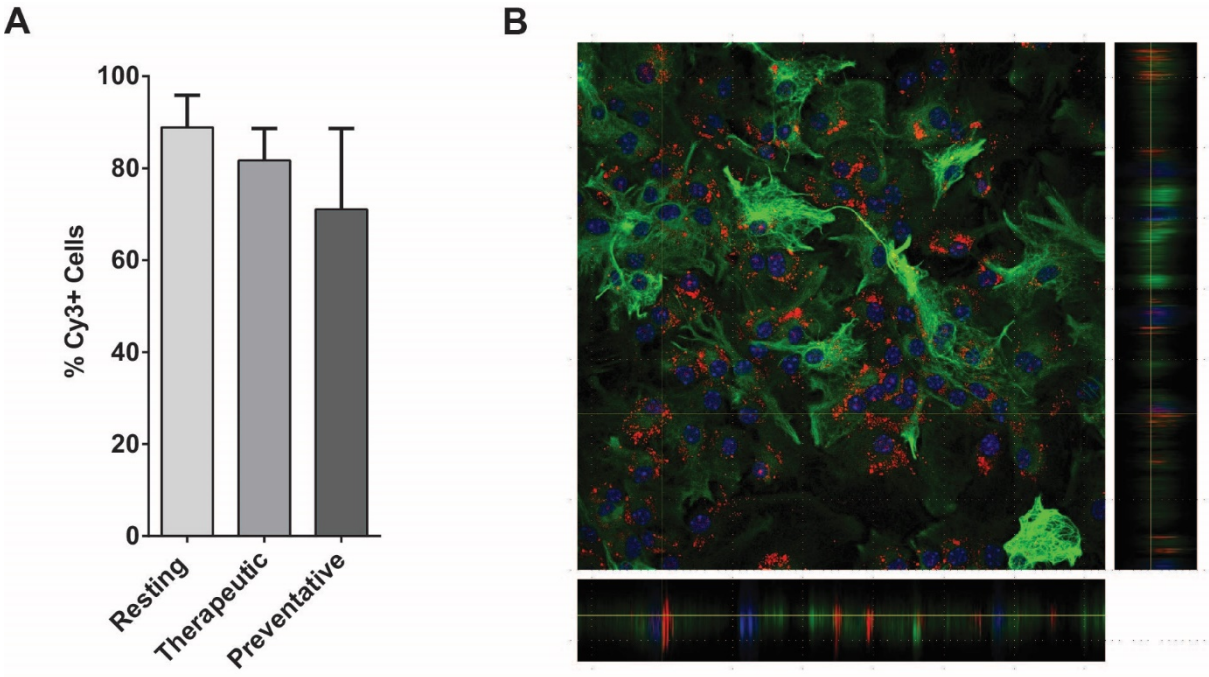

Figure 4.9 A Immunofluorescence quantification of percentage of astrocytes transfected with 20 nM Cy3-labelled 3WJ under resting and activated conditions. Data expressed as mean ± SD; N = 3 biological replicates, 3 coverslips per condition for each experiment, 10 images per coverslip. No statistically significant difference observed between conditions. **B** Confocal micrograph of Cy3-3WJ (red) transfected astrocytes, immunostained for GFAP (green), with nuclei co-stained with DAPI (blue). Orthogonal projections from z-stack images show internalisation of the Cy3-3WJs.

Prior to evaluation of the efficacy in the down-regulation of target genes, transfection of NPC-derived astrocytes with our siRNA-3WJ nanostructures were shown to be non-toxic over the range of concentrations tested (0.5 to 50 nM). By using colorimetric LDH cytotoxicity assays we observed that the viability of cells remained >95% for all siRNA-3WJs (N03, G10, V10 and L12) and at all concentrations, compared to untreated controls (100% viability) and lysed cell samples (0% viability). No significant cytotoxicity relative to untreated controls or mock control, i.e. cells treated with vehicle only (Lipofectamine RNAiMAX), was observed, neither at 24 hours post-transfection when cells remained in serum-free transfection medium, nor at further timepoints corresponding to 48 or 120 h (timepoints of typical RNA or protein quantification) when cells underwent a medium change at 6 h post-transfection (restoring low-FBS medium) (Fig. 4.10).

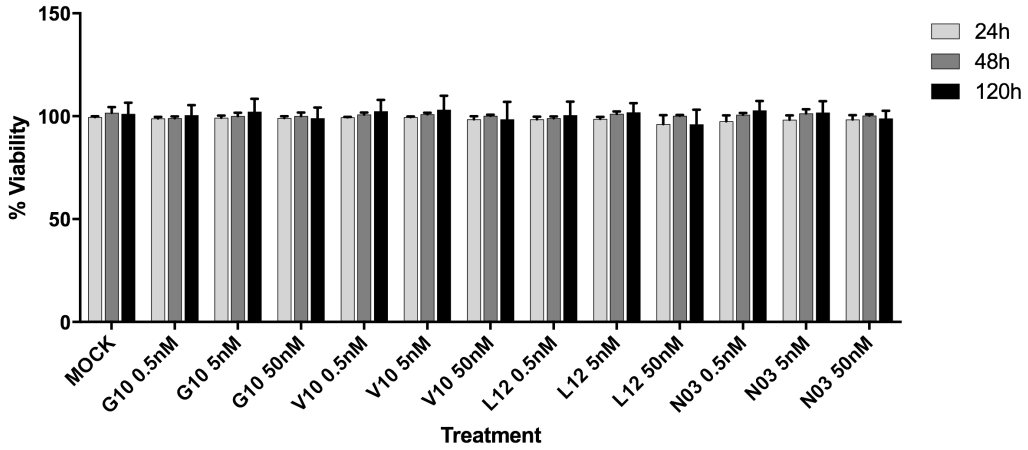

Figure 4.10: LDH-based cytotoxicity assay. Low-FBS/+FGF2-cultured astrocytes were treated with 0.5, 5 or 50 nM doses of anti-*GFAP* (G10), anti-*Vim* (V10), anti-*Lcn2* (L12), or non-targeted negative control (N03) 3WJs. Viability was compared to mock-treated (Lipofectamine RNAiMAX only) or non-treated (control) samples at 24, 48 or 120 h post-transfection. Data presented as mean viability relative to control, N = 3 biological replicates ± SD. No statistically significant difference between treatments observed.

Before analysing gene expression levels we first investigated the stability of several common reference genes (glyceraldehyde-3-phosphate dehydrogenase [*Gapd*], 18S ribosomal RNA [*Rna18s5*], and beta-actin [*Actb*]) via TaqMan gene expression assays in order to establish their suitability in subsequent qPCR assays. The expression of each of these reference genes at 48 h post-transfection showed little variation across treatments (non-transfected control vs mock-transfected control vs N03-3WJ transfected samples) or conditions (resting, *therapeutic*, or *preventative* activation), as determined by comparing mean cycle threshold C_T values across experiments and using the $2^{-\Delta CT}$ method [205] to compare samples of interest to the control sample. *Gapd* was then selected as the reference to report all subsequent gene expression data.

The potential immunogenicity was then evaluated as the capability of siRNA-3WJs to induce the induction of pro-inflammatory cytokines in astrocytes upon transfection. We first tested 3WJs assembled from *in vitro* transcribed ssRNAs that had not been subjected to dephosphorylation, i.e. presenting 5′-triphoshate transcription artefacts. Transfection with 5′-triphosphate N03-, G10- and V10-3WJs (5 nM) were found to cause significant inductions in *Il6* (ca. 50-fold), *Tnf* (ca. 500-fold) and interferon beta 1 (*Ifnb1,* ca. 100-fold) mRNA levels relative to non-transfected controls in high-FBS/FGF2-free astrocytes (Fig. 4.11). However, this polarisation towards a pro-inflammatory phenotype was not observed in mock-transfected astrocyte samples, or in

samples treated with commercial siRNA pools (chemically synthesised and modified). We hypothesized the involvement of retinoic acid induced gene 1 (RIG-1, also known as DDX58)-mediated antiviral immunity, triggered by the 5′-triphoshate transcription artefacts [206]. This theory was further supported by the introduction of a dephosphorylation step to the 3WJ synthesis that resulted in complete ablation of the observed cytokine induction at the mRNA level (Fig. 4.11) Thus, these data suggest that appropriately modified 3WJs are not immunogenic.

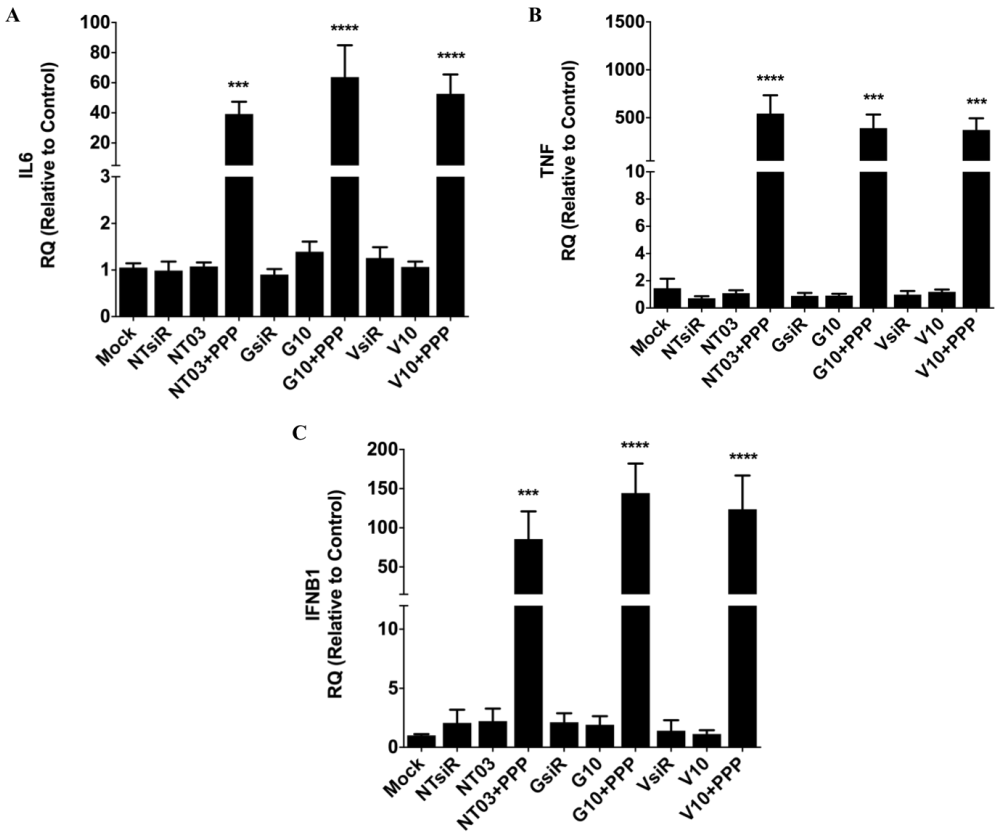

Figure 4.11:Expression of pro-inflammatory cytokines. **A** *Il6*, **B** *Tnf*, **C** *Il1b* in high-FBS/FGF2-free cultured "resting" astrocytes when transfected with 3WJs with (+PPP) or without 5′-triphosphate *in vitro* transcription artefacts. Results expressed as the mean mRNA expression (RT-PCR) relative to non-transfected controls ($2^{-\Delta\Delta Ct}$ method) with N ≥ 3 biological replicates ± SD; *Gapd* reference gene; * P ≤ 0.05, ** P ≤ 0.01, *** P ≤ 0.001, or **** P ≤ 0.0001 relative to control samples (one-way ANOVA with Dunnett's multiple comparison test).

4.5.4 SIRNA-3WJS EFFICIENTLY KNOCK-DOWN TARGET GENES IN REACTIVE ASTROCYTES

The optimal dose of 3WJs for an efficient silencing of the siRNA-3WJs was previously delineated through a dose-response profile by using high-FBS/FGF2-free cultured

astrocytes at three dosages, 0.05, 0.5 and 5 nM, under resting conditions. A dose-dependent knockdown of both *Gfap* and *Vim* mRNA expression levels was observed relative to non-treated controls, comparable to the knockdown achieved by their commercial siRNA SMARTpool counterparts with a statistically significant knockdown by each observed at 5 nM. Furthermore, neither mock transfection nor treatment with non-targeted siRNA (NsiR) or siRNA-3WJs (N03) had a notable effect on *Gfap* expression, nor off-target knockdown effects were observed. Moreover, trials with a 50 nM dosage did not show any differences in silencing efficiency compared to 5 nM dosage (data not shown); this could be attributed to saturation of the RNAi machinery, sincecells indeed have a limited capacity to assemble the RISC complex on exogenous siRNAs [207]. These data thus suggested 5 nM as the appropriate dose sufficient to induce a significant (~50%) reduction in targeted mRNA. This concentration was used in subsequent experiments to further examine the efficacy of the treatments under activation conditions, and to investigate siRNA-3WJ-mediated *Lcn2* knockdown. Transfection was then performed in our low-FBS/+FGF2-cultured astrocyte protocol, under resting or activated conditions. The lipofection of siRNA-3WJs yielded significant reductions of *Gfap* and *Vim* mRNA by the G10 and V10 3WJs, respectively. In particular, both in resting and activation conditions a 5 nM G10-3WJ dose decreased *Gfap* mRNA expression by ≥60% relative to non-treated controls under the same condition (Fig. 4.12A). Similar results were achieved by V10-3WJs, with *Vim* expression knocked down by at ≥50% in each condition (Fig. 4.12B). However, knockdown by L12-3WJs resulted in a stronger downregluation of the absolute expression levels of Lcn2 in resting astrocytes compared to activated astrocytes, with the most significant knockdown (80%) being observed in the resting condition. A significant knockdown was also observed in the *therapeutic* and *preventative* conditions (70% and 50% respectively) (Fig. 4.12C). Notably, no synergistic effects were evident in combinatorial treatments comprising 5 nM doses of both G10 and V10 simultaneously: *Gfap*/*Vim* expression levels were comparable to those samples receiving individual treatments (Fig. 4.12 A,B). No indirect or off-target knockdown (or induction) by targeted 3WJs was observed, nor did the non-targeted N03-3WJ induce any significant change in the expression of the target genes (*Gfap*, *Vim* or *Lcn2*). Despite the efficaciously and specifically knockdown of 3WJs towards their target

mRNAs, the expression of pro-inflammatory markers was unaffected. Levels of *Il6* and *Nos2* mRNA, upregulated upon LPS+IFNγ treatment, were unaffected by 3WJ-mediated modulation of *Gfap*, *Vim* or *Lcn2*. The expression of *Tnf* and *Il1β*, unchanged by activation, were also unaffected by these 3WJs (Fig. 4.13).

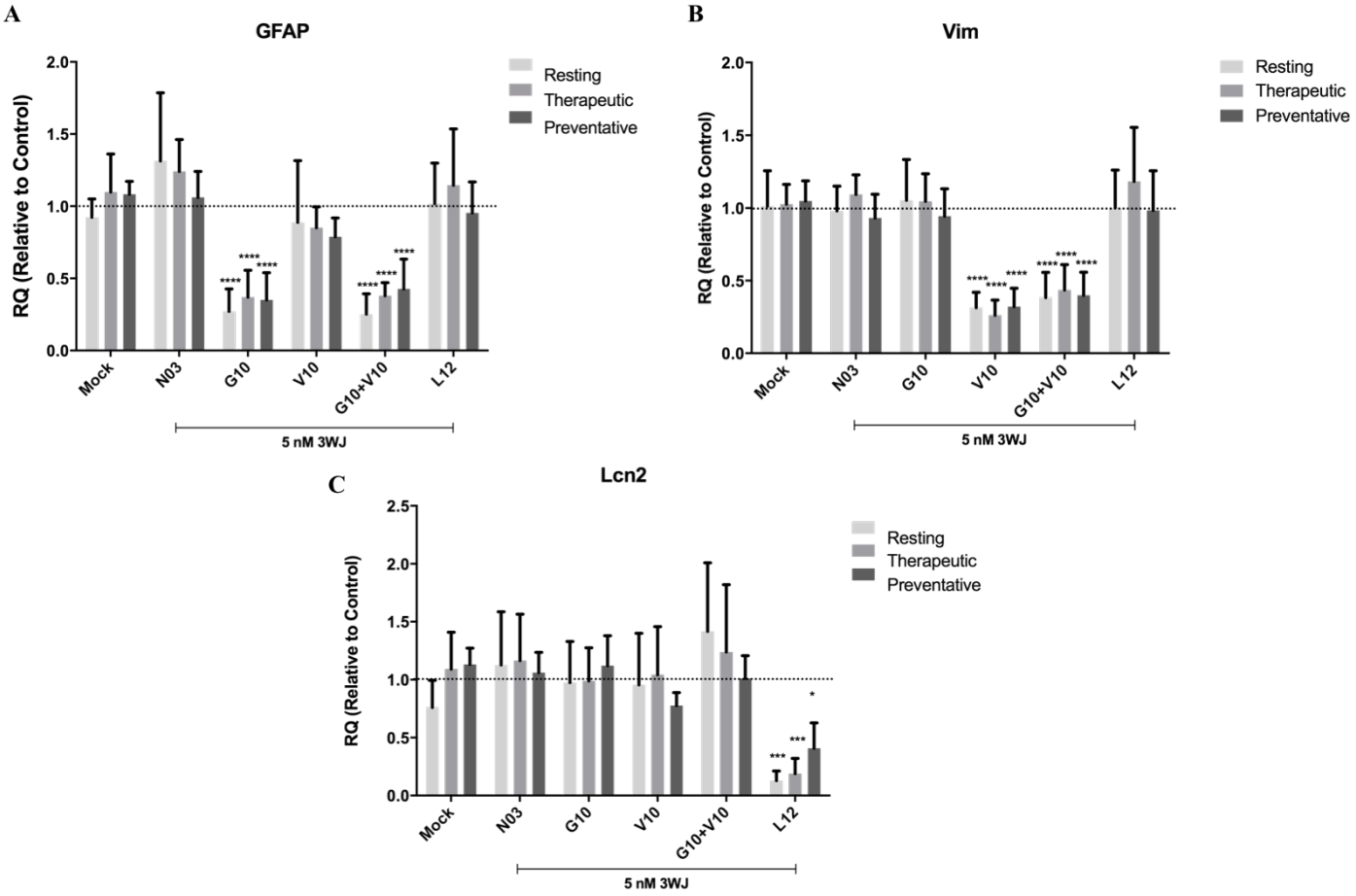

Figure 4.12: 5 nM doses of 3WJ nanostructures induced a significant decrease in the expression of their target mRNA: **A** *Gfap*, **B** *Vim*, or **C** *Lcn2* both under resting and activated conditions 48 h post-transfection, according to RT-PCR assays. No synergistic effects were evident from a combined anti-*Gfap*/anti-*Vim* treatment (5 nM dose of each), nor were there significant off-target modulation of expression. Mock (Lipofectamine-only) or non-targeted negative control 3WJs had no significant effect. Results expressed as the mean of N ≥ 3 biological replicates ± SD; *Gapd* reference gene; * P ≤ 0.05, ** P ≤ 0.01, *** P ≤ 0.001, or **** P ≤ 0.0001 relative to control samples of the same activation condition (two-way ANOVA with Dunnett's multiple comparison test).

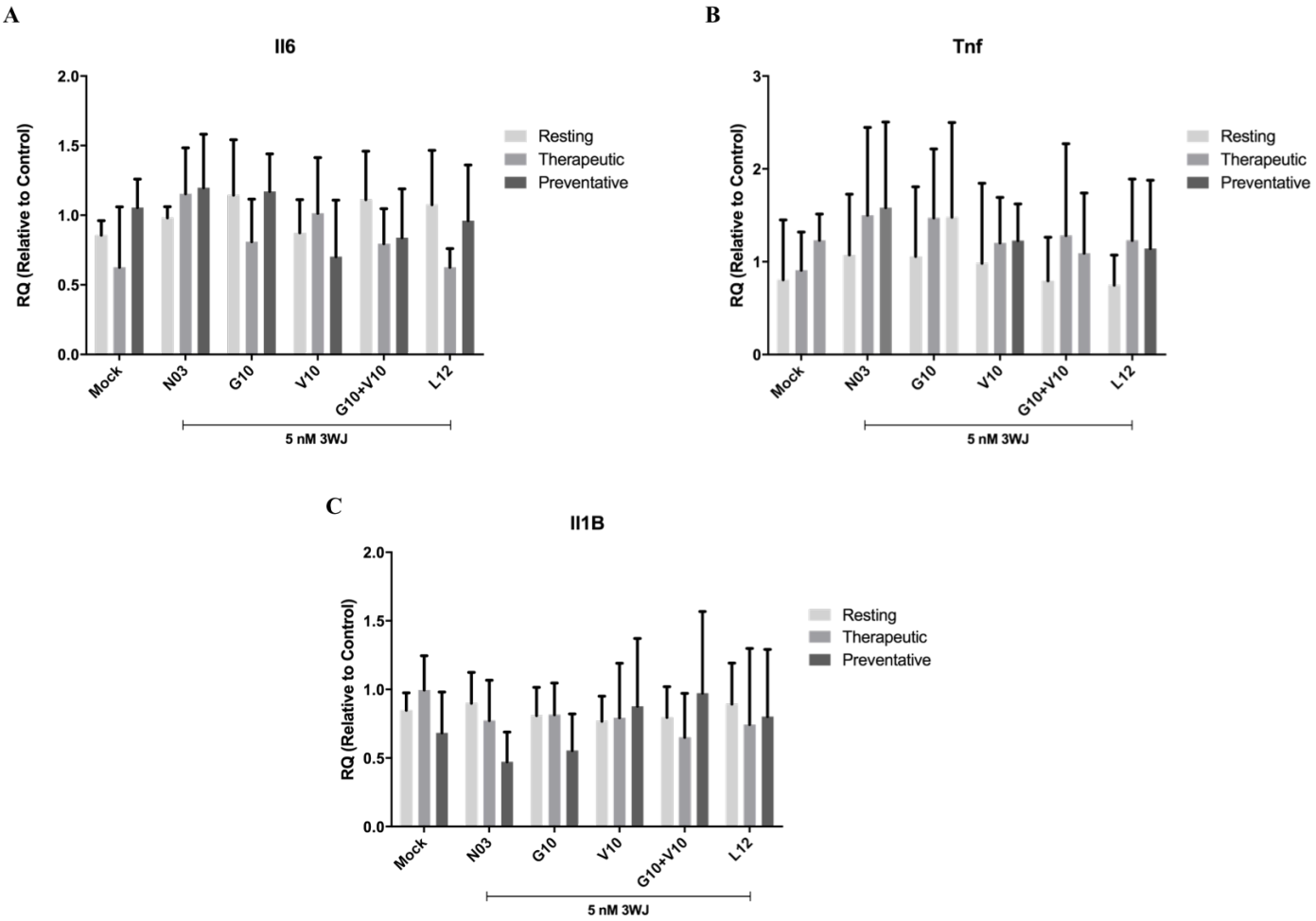

Figure 4.13: mRNA levels of pro-inflammatory markers were not affected by none of the treatments: **A** Il6, **B** *Tnf*, and **C** *Il1b*. Results are expressed as the mean mRNA expression (RT-PCR) of N ≥ 2 biological replicates ± SD; *Gapd* reference gene; * P ≤ 0.05, ** P ≤ 0.01, *** P ≤ 0.001, or **** P ≤ 0.0001 relative to control samples of the same activation state (one-way ANOVA with Dunnett's multiple comparison test).

To further confirm the knockdown efficacy of 3WJs, protein levels were quantified 5-days post-transfection (20 DIV) in low-FBS/+FGF2 cultured astrocytes. Both G10- and V10-3WJs induced significant reductions in GFAP and Vim expression (>70%), in *resting*, *therapeutic*, and *preventative* conditions (Fig. 4.14). As observed for mRNA expression, no off-target effects were evident, and combinatorial treatments with G10 and V10 resulted in a decreased expression of individual proteins comparable to the singular 3WJ treatment, excluding again the possibility of synergistic effects. Qualitative ICC images showed the same decreased expression of protein levels as observed by Western blot analysis (Fig. 4.16). Lcn2 could not be detected by Western blot in *resting*, *therapeutic* or *preventative* activation conditions at 20 DIV, even though

ICC assessments showed observable expression by means of immunofluorescence at 20 DIV in reactive astrocytes (Fig. 4.15). These differences might be due to faster kinetics of the Lcn2 response, with an early peak and subsequent decline in expression in response to LPS+IFNγ exposure, and so we also performed Western blots at earlier timepoints. Lcn2 was detected by Western blot at both 16 and 17 DIV, with a notable induction in activated samples. Moreover, treatment with L12-3WJ showed a reduction in the amount of Lcn2 detected in each condition (Fig. 4.15), however confirmation is ongoing (N=2 for some conditions). This remarkable reduction in Lcn2 expression was mirrored by ICC results obtained at 20 DIV (Fig. 4.16).

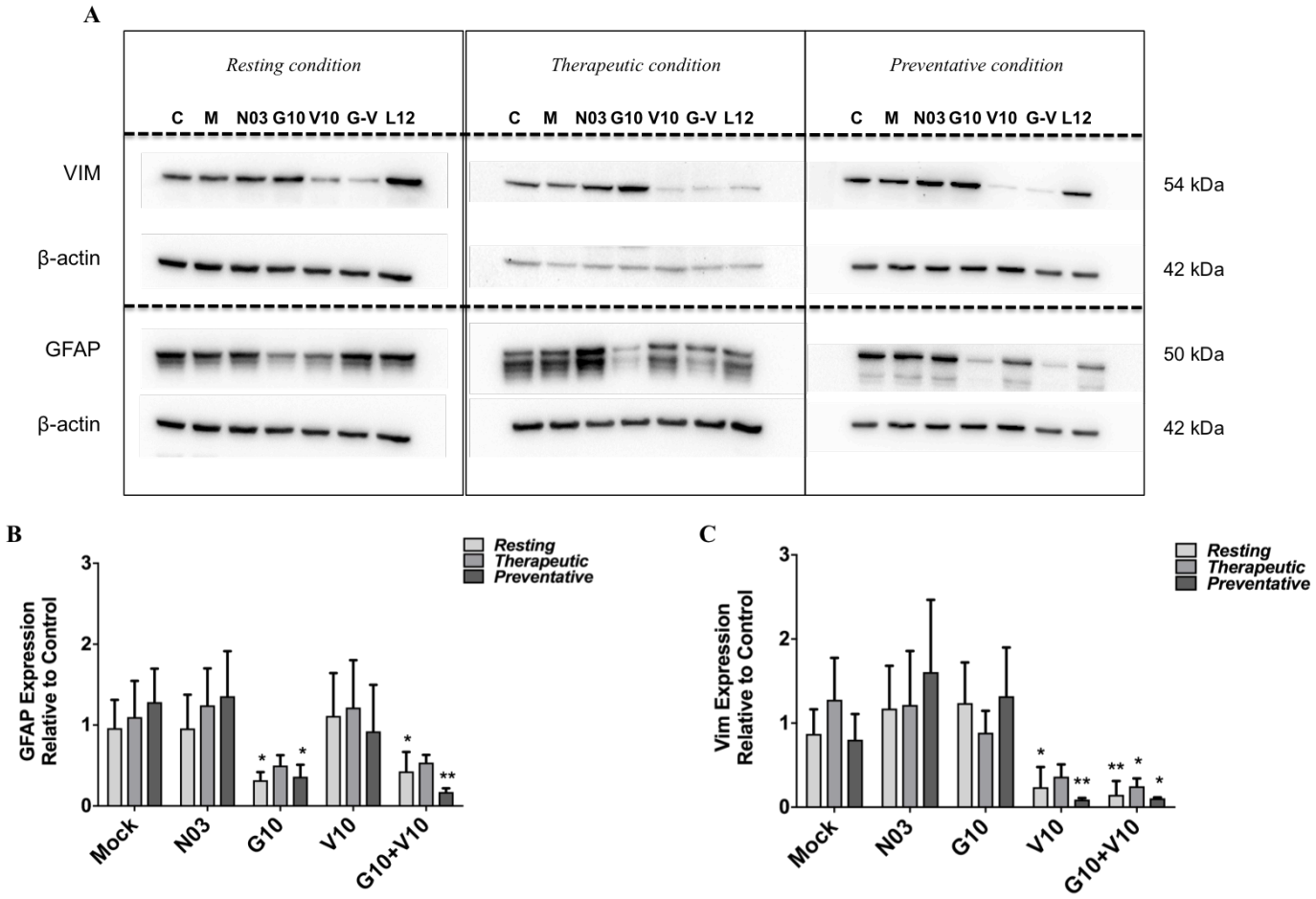

Figure 4.14: **A** Representative Western blots of Vim (54 kDa) and GFAP (50 kDa) in various controls and 5 nM 3WJ treated-samples 5 days post-transfection, under resting and activated conditions. **B** Densitometric analyses showing the expression of GFAP. **C** Densitometric analyses showing the expression of Vim. β-actin (42 kDa) was used as loading controls. Data represent the mean relative to control samples in the same activation condition-treated controls of N ≥ 3 biological replicates ± SD; * P ≤ 0.05, ** P ≤ 0.01 (two-way ANOVA with Dunnett's multiple comparison test).

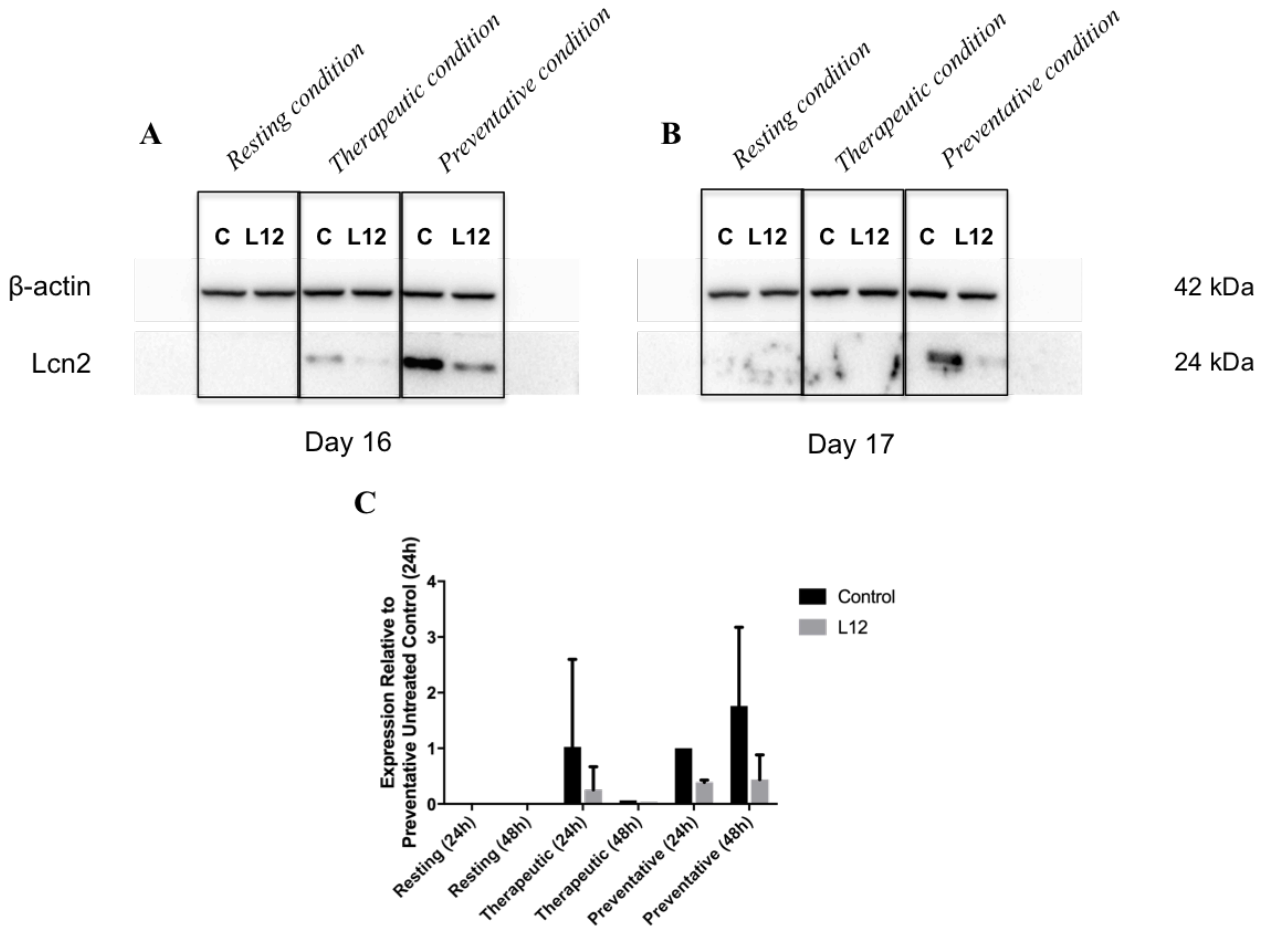

Figure 4.15: **A** Representative Western blots of Lcn2 (24 kDa) expression at 24 h, i.e. 16 DIV. **B** Representative Western blots of Lcn2 (24 kDa) expression at 48 h, i.e. 17 DIV **C** Densitometric analyses showing the expression of Lcn2. β-actin (42 kDa) was used as loading controls. Data represent the mean relative to preventative untreated control at 24h, i.e. 16 DIV, N=2-3 biological replicates ± SD. (two-way ANOVA with Dunnett's multiple comparison test).

Therapeutic condition

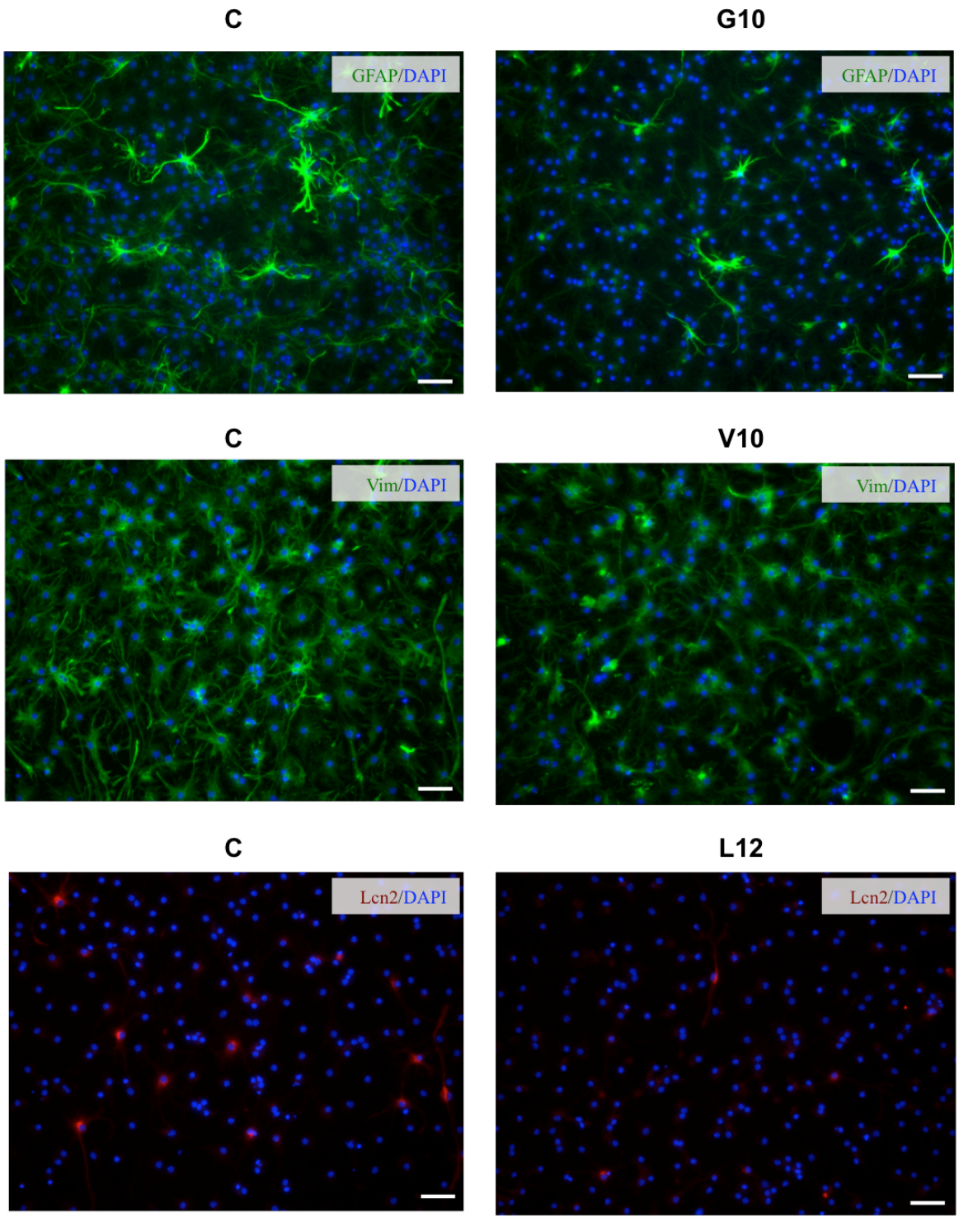

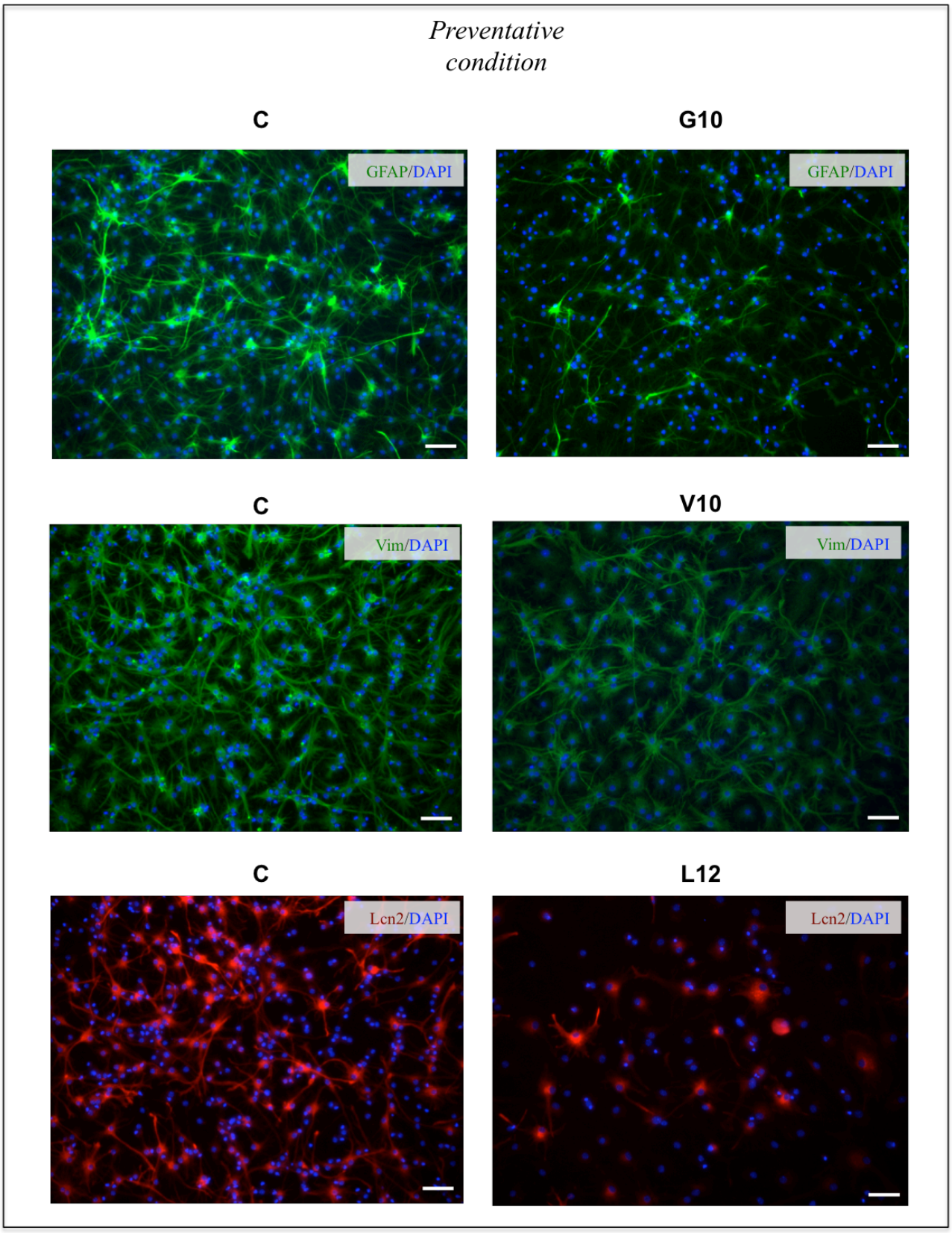

Figure 4.16: Representative immunofluorescence micrographs of low-FBS/+FGF2 astrocytes in *therapeutic* and *preventative* conditions showing reduction in target genes upon 3WJ-pRNA transfection. Scale bar: 50 µm.

4.5.5 THE ABILITY OF LCN2 TO INDUCE MARKERS OF REACTIVITY IN A PARACRINE MANNER IS MODULATED BY 3WJ TRANSFECTION IN REACTIVE ASTROCYTES

To further investigate the role of Lcn2 in the modulation of astrogliosis we assessed the effects of conditioned media from reactive astrocytes, with or without 3WJ treatment, on resting recipient astrocytes. Secreted Lcn2 has been shown to act in an autocrine manner on reactive astrocytes, augmenting the astrogliosis extent in those same astrocytes [185].

We employed donor astrocytes both in resting and *preventative* activation condition. Astrocytes were transfected with L12-3WJ at day 15, and we additionally tested mock and N03-3WJ conditions to exclude any further side-effects. Transfections were performed as mentioned-above. 24 h after transfection we changed media to DMEM which was subsequently conditioned for a further 24 h before being transferred to resting recipient astrocytes. mRNA levels were assessed on recipient astrocytes 24 h after exposure to this conditioned media (Fig. 4.17).

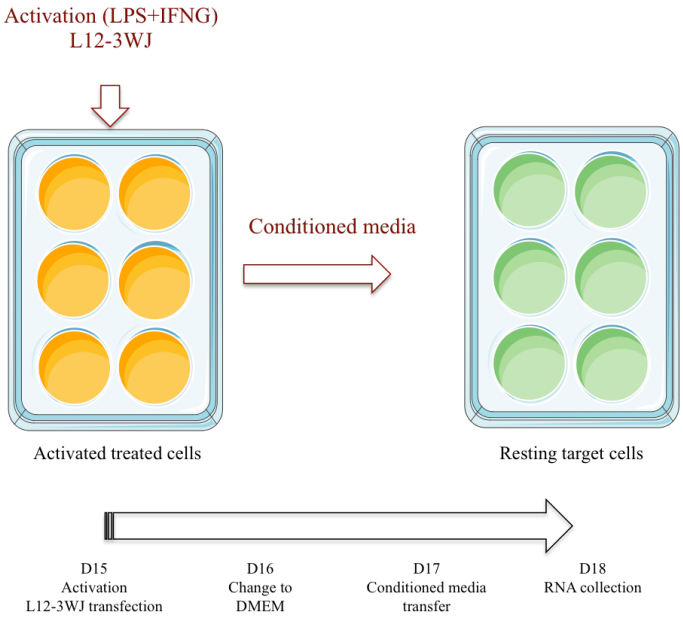

Figure 4.17: Schematic representation of astrocyte-conditioned medium (ACM) experimental setting.

Secreted levels of Lcn2 were measured by ELISA techniques, where we observed a significant induction in the secretion of Lcn2 upon activation: a mean concentration of ca. 18,000 pg/ml, compared to mean concentrations of < 50 pg/ml in resting controls.

These ELISA measurements confirmed results for protein levels obtained by Western blot and immunohistochemistry, showing a significant downregulation in secreted LCN2 upon transfection with L12-3WJ, while both mock and N03-3WJ conditions did not show any significant effect on supernatant Lcn2 levels (Fig 4.18).

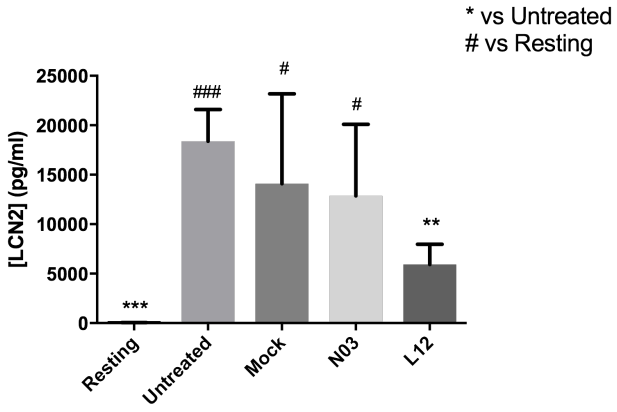

Figure 4.18: ELISA quantification of Lcn2 in the supernatant media of resting or LPS+IFNγ-stimulated astrocytes, as well as activated astrocytes treated with mock, N03 or L12 transfections, 48 h after treatment. Data represent the mean of N ≥ 3 biological replicates ± SD; * P ≤ 0.05, ** P ≤ 0.01, *** P ≤ 0.001, or **** P ≤ 0.0001 relative to control samples in the same activation condition (two-way ANOVA with Dunnett's multiple comparison test).

Astrocytes exposed to conditioned medium obtained from activated astrocytes showed a strong and significant induction in *Lcn2* mRNA levels, while a significant reduction in this level was observed in astrocytes exposed to medium derived from L12-3WJ-treated activated astrocytes, in correlation with ELISA Lcn2 measurements. Conditioned medium from resting donor astrocytes showed negligible induction of *Lcn2* levels in recipient astrocytes (Fig. 4.19A). Interestingly, *Nos2* was also significantly induced in recipient astrocytes upon treatment with non-transfected conditioned medium. But, as for *Lcn2*, *Nos2* levels were found significantly downregulated when astrocytes were exposed to L12-3WJ conditioned medium (Fig. 4.19 B). Nevertheless, we did not observe any changes upon different conditions in the modulation of *Gfap* and *Vim* expression (Fig. 4.19 C, D).

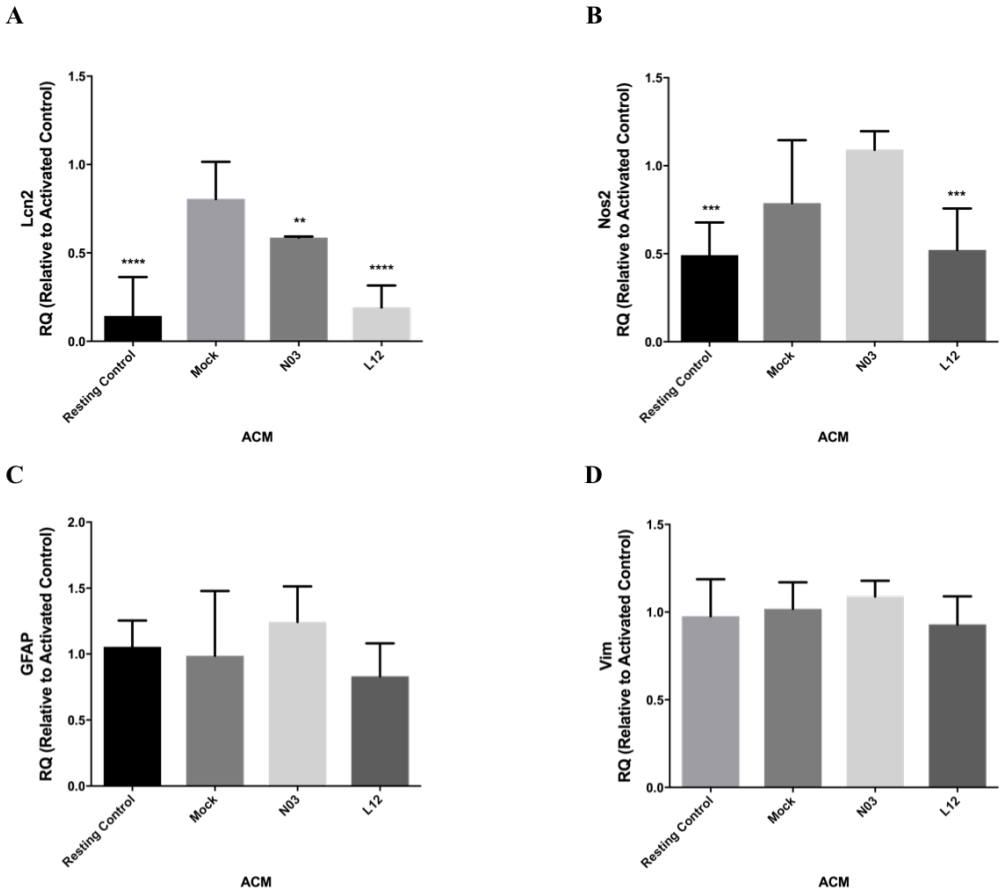

Figure 4.19: qRT-PCR quantification of activation-related genes in recipient cells 24 h after transfer of media from treated astrocytes. **A** *Lcn2,* **B** *Nos2*, **C** *Gfap*, **D** *Vim*. Results expressed as the mean mRNA expression relative to those cells receiving conditioned media from activated controls ($2^{-\Delta\Delta Ct}$ method), *Gapd* reference gene. Data represent the mean of $N \geq 3$ biological replicates ± SD; * $P \leq 0.05$, ** $P \leq 0.01$, *** $P \leq 0.001$, or **** $P \leq 0.0001$ relative to control samples in the same activation condition (two-way ANOVA with Dunnett's multiple comparison test).

4.6 DISCUSSION

pRNA-derived 3WJs were designed based on the technology developed in the Guo laboratory: a novel and efficacious RNAi-delivery platform inspired by structural and molecular characteristics of the phi29 bacteriophage DNA packaging motor [151]. The modular nature of this technology makes it versatile and nanoparticles can be functionalized with multiple components [208]. Recent application of the pRNA system have showed promising results in the targeted delivery of RNAi or small-molecule drugs for anti-cancer and anti-viral applications *in vitro* and *in vivo* [209, 210]. Indeed, one recent application of 3WJ-pRNA nanotherapeutics in a triple negative breast cancer (TNBC) murine model has shown the capability of the nanoparticle to specifically bind and internalize into TNBC cells, efficently knocking down the target RNA, miR-21, and showing specificity for the target tumors with poor accumulation in healthy organs and tissues [210]. However, the studies reported herein represent one of the first applications in the CNS environment [211]. The proof-of-concept 3WJ design used for this project incorporate a single siRNA sequence per structure, each of which were selected to match the target sequences employed in commercially-validated anti-*Gfap*, -*Vim*, -*Lcn2* and non-targeting siRNA pools (which we also employed as controls in these studies). siRNA-3WJ mechanisms of action rely on the formation of RISCs: after reaching the intracellular environment, the siRNA moiety is cleaved from the 3WJ by the endonuclease Dicer before entering the RISC and guiding the cleavage of mRNA strands complementary to the target sequence [160]. It has been suggested that Dicer-substrate based RNAi such as this is more potent than that produced by standard 21-nucleotide double-stranded siRNA agents since Dicer assists in loading the siRNA into the RISC assembly [212]. Other design considerations, such as the inclusion of two-nucleotide overhangs on the free 3′ end of the antisense (guide) strand to promote Dicer recognition, and 5′ guanine residues as needed to facilitate efficient T7 RNA polymerase transcription of RNA strands, were addressed as previously as described by Shu et al [172].

The two longer RNA strands of each 3WJ (***A*** and ***C*** strands) were prepared via *in vitro* transcription and dephosphorylated to remove 5′-triphosphate groups, an artefact of

transcription using nucleotide triphosphates. In mammalian cells, the innate receptors involved in the recognition of nucleic acid are classified in two families: the transmembrane Toll-like receptors (TLRs) that detect viral RNA or DNA in the endosomal compartment, and the cytoplasmic RIG-I receptor [213]. RIG-I like receptors (RLRs) act as cytoplasmic sensors of pathogen-associated molecular patterns (PAMPs) for viral RNA, in particular recognising RNA sequences marked with 5′ triphosphorylated (5′-ppp) ends and triggering a type I interferon inflammatory response [206, 213-215]. It has also been shown that the activation of RIG-like receptor signalling is involved in the onset of astrogliosis, such as in the induction of GFAP and Vim upregulation, and so for our purposes we therefore aim to avoid RIG-I mediated interferon responses [216]. After dephosphorylation with calf intestinal phosphatase, transcripts were annealed together with a third, synthetic ***B*** strand to allow for the assembly of the construct. This process was monitored using PAGE migration assays; consistent with previously described characterisation of 3WJs the assembled construct ran as a compact band, considerably slower than single- or double-stranded assemblies. Targeted delivery is one of the major challenges in drug delivery; therefore, size is an important parameter to consider in order to allow the diffusion of therapeutics into the CNS. The size of siRNA-3WJs (ca. 20-40 nm) represents an optimal size to be taken up into cells, to avoid renal filtration or stimulation of the innate immune response or without being recognized by the reticuloendothelial system (RES) [154]. Moreover, components in a range between 35-64 nm are suitable to diffuse uniformly within the brain [217].

siRNA-3WJs were designed and synthesised for each of the four siRNA target sequences found in each commercial siRNA pool (i.e. sixteen siRNA-3WJs total), but based on transcription yields and previously preliminary silencing assays only one siRNA-3WJ of each class was selected (anti-*Gfap*, anti-*Vim*, anti-*Lcn2* and non-targeting) for further characterisation. To test the uptake efficiency of transfections, 10 nM doses of Cy3-labelled N03-3WJ were transfected using Lipofectamine RNAiMAX and immunostaining assays was conducted 24 hours post-transfection. The presence of labelled siRNA-3WJ, as punctate cytoplasmic Cy3 fluorescence, was detected in >70% of previous established protocol high-FBS/FGF2-free astrocytes, with no statistically

significant difference between resting and activated cells, and no uptake was observed without the use of Lipofectamine. After testing the efficiency of delivery, safety of siRNA-3WJ treatment *in vitro* was investigated by confirming that the constructs were both non-cytotoxic and non-immunogenic upon transfection. qRT-PCR assays were performed to profile the expression of genes of interest. To obtain an accurate and reproducible gene expression analysis, we first aimed to identify putative reference genes (housekeeping genes or internal control genes) with the most stable expression to use for normalization of gene expression data, an important validation for experiments utilising the $2^{-\Delta\Delta Ct}$ method of assaying relative gene expression [218]. Our reference gene of choice, *Gapd*, was unaffected by activation or transfection, with or without 3WJ-treatment. Another critical step to be investigated in siRNA knockdown techniques concern the cytotoxicity of the tool employed and considering the different mechanisms through which siRNA can interact with the immune system, the possibility to invoke pro-inflammatory effects is an important consideration to be addressed [219]. Colorimetric quantification of LDH activity in the supernatant of astrocytes treated with 5 nM doses of G10, V10, L12 and N03 showed negligible impact on the viability of low-FBS/+FGF2-cultured cells for at least 120 h post-transfection, confirming 3WJs were non-toxic. Moreover, cytokine expression in cells transfected with 3WJs comprised of dephosphorylated RNA strands were compared to those using their phosphorylated analogues. Those siRNA-3WJs retaining their 5′-triphosphate groups induced a significant pro-inflammatory response in transfected astrocytes, with average mRNA levels of the cytokines *Ifnb1*, *Il6* and *Tnf* increasing approximately 100, 50, and 500-times, respectively. On the contrary, no such induction was evident upon transfection with the dephosphorylated constructs. This observation is consistent with previously discussed involvement of RIG-I-mediated antiviral responses upon triphosphate activation: this has been shown to trigger signalling cascades involving both interferon response factor 3 and NF-κB pathways, resulting in the upregulation IFN-β1 and pro-inflammatory cytokines respectively [220, 221]. Thus, these preliminary results suggest 3WJs as a safe therapeutic platform in a CNS context, however more extensive profiling would be required before any translational application, especially regarding potential off-target activity, due to the different transcript regulation across species [168].

Previous results in our lab demonstrated that upon transfection, the siRNA-3WJs were successfully able to knockdown the expression of their target genes in high-FBS/FGF2-free astrocytes in a dose-dependent manner, with a maximal efficacy at 5 nM. 50 nM did not show any increase in the knockdown efficiency, probably related to a saturation of RNAi machinery. Indeed it has been shown that cells are characterized by a limited capacity to assemble the RISC complex on exogenous siRNAs, and this might affect microRNA expression levels and function, although we did not observe any non-specific effects in the few genes we examined in this proof-of-concept study [207]. Based on the substantial silencing observed in these preliminary studies, a 5 nM dose was selected as the basis for further investigation (i.e. in our reactive astrocyte model). At this 5 nM dose, in both resting and activated conditions, both G10- and V10-3WJ caused a >60% reduction in the expression of their target mRNA (*Gfap* and *Vim*, respectively) in low-FBS/+FGF2 cultured astrocytes relative to non-transfected controls. The use of siRNA-3WJs resulted in gene-specific knockdown, with each of the siRNA-3WJs showing no observable effect on the expression of the other analysed genes at any of the doses studied. Furthermore, combinatorial approaches employing both G10- and V10-3WJ at 5 nM doses each did not reveal any synergistic, antagonistic or compensatory effects, at least at the mRNA level, despite the interfunctionality of these two intermediate filaments [96]. Such results are promising given the relatively low concentration of the siRNA-3WJs employed compared to other studies, 30-40 nM in one similar study, for instance [14]) which also lead to a modulation in IF expression by inducing a *reduction*, rather than complete silencing; the low-dosage may also limit both off-target effects and potential saturation of natural RNAi pathways [222]. Moreover, while the analogous commercial siRNA pools GsiR and VsiR were capable of inducing similar reductions in target intermediate filaments (IF) mRNA levels (i.e. >60% tested in high-FBS astrocytes), this was accomplished using pools of four siRNA sequences targeted against each mRNA and the siRNAs themselves have unspecified modifications to enhance stability/activity. The possibility of inducing side effects upon transfection was excluded by using both the non-targeted N03-3WJ as a negative control that showed no effect on either *Gfap* or *Vim* expression levels at any of the concentrations tested, and also by showing that mock transfections showed no

significant effect on *Gfap* or *Vim* mRNA levels, excluding any obvious side-effects of Lipofection, at least with regards to IF expression. L12-3WJ, investigated in low-FBS/+FGF2 cultured astrocytes at the 5 nM concentration, was found to significantly reduce the expression of *Lcn2* in resting and activated astrocytes, with no effect on the other target genes.

The increasing of number of silencing studies has led to the investigation of which features may influence the efficacy of siRNA, including such properties as the mRNA internal stability, and characteristics of the target mRNA, such as the secondary structure of the siRNA target site [223]. Furthermore, several studies have shown that the abundance of target transcripts correlate with silencing efficacy, demonstrating that transcripts with low expression levels are less susceptible to siRNA-mediated degradation [223, 224]. Nevertheless, both *Gfap* and *Vim* were expressed at relatively high levels in our astrocytes, even in the resting condition. *Lcn2* knockdown seems to follow the trend (if not the magnitude) of post-activation induction. While still potent, the relative silencing in *therapeutic* (>70%; 96 h post-activation, 48 h in basal medium) and *preventative* conditions (ca. 50%; 48 h post-activation) is less than that observed in resting astrocytes, perhaps due to the magnitude of the induction upon LPS+IFNγ treatment.

To further confirm the siRNA-3WJ efficacy, protein level modulation has been assessed. Silencing observed at the mRNA level was reflected at the protein level as evidenced through Western blots and immunofluorescence micrography. IF proteins, once synthesized, tend to be very stable [225]: GFAP and Vim are structural in nature and therefore expected to have a relatively long cellular half-life compared to signalling proteins such as cytokines. Indeed, it has been reported that these IFs exhibit biphasic decay kinetics in primary astrocytes, with 40% of the IF population being in a fast-decay phase ($t_{1/2}$ = 12-18 h) and 60% in a slow-decay phase ($t_{1/2}$ = 8 d) [226]. Preliminary data conducted in the lab showed that, by comparison of several timepoints post-transfection, maximal silencing (ca. 90%) was observed at 4-6 days post-transfection, therefore protein levels have been assessed 5 days post-transfection. Strong reductions in GFAP and Vim expression were observed in low-FBS/+FGF2 cultured

astrocytes at this 5 days post-transfection timepoint, in each of the different resting, *preventative* and *therapeutic* conditions. Significant reductions of GFAP and Vim were observed upon transfection with 5 nM doses of G10- and V10-3WJs, respectively, by Western blot assay, while a combined treatment of G10- and V10-3WJs efficiently reduced their expression simultaneously, supporting results obtained for mRNA levels. Qualitative assessment by ICC techniques showed a decrease in the GFAP and Vim intensity upon transfection in activated astrocytes as compared to controls. Substantial Lcn2 knockdown was also evident in immunofluorescence images of activated astrocytes at 20 DIV (i.e. 5 days post-transfection). However, as mentioned earlier, Lcn2 could not be detected by Western blot assay at this timepoint. Results suggest that Lcn2 expression might reach a peak between 24h and 48h and decreases throughout time, as observed between 16 DIV and 17 DIV by Western blots. Although its expression remains higher compared to control, as observed in immunofluorescent images, it is possible that the high sensitivity of immunofluorescence techniques could detect its cellular expression while such signal could be not enough to be detected in Western blot, likely Lcn2 protein quantity in the total 20 μg protein loaded for Western blot assay might be insufficient to be detected as such later timepoints. Results obtained from Western blots performed on reactive astrocytes at 16 and 17 DIV showed a substantial upregulation in Lcn2 expression compared to resting condition, and, upon L12-3WJ transfection, a strong decreases in Lcn2 expression was observed.

Thus, it is evident that low doses of siRNA-3WJs are capable of downregulating astrogliosis-associated molecular markers at both the mRNA and protein levels in astrocytes, however potential therapeutic approaches require more substantial investigation. For this purpose, we examined the effect of 3WJ treatments on the expression of several pro-inflammatory cytokines and markers. *Il6*, *Tnf*, and *Nos2* expression levels, each found to be elevated in LPS+IFNγ-treated low-FBS/+FGF2 astrocytes, both at mRNA and protein levels (from ELISA data), were unaffected by the substantial reductions in *Gfap*, *Vim*, or *Lcn2* afforded by our siRNA-3WJs, at least at the 17 DIV (48 h post-transfection) timepoint at which qRT-PCR experiments were performed. The inability to modulate pro-inflammatory signals upon siRNA-3WJ treatment may be due to a differential kinetics between protein knockdown and

subsequent secondary effects on cytokine/chemokine mRNA expression at the assayed timepoint. However, considering that Il6 and NO synthesis (by NOS2) are upstream pathways in the induction of IFs [91, 116], an effect on the expression of these signalling mediators is not necessarily a certainty following the knockdown of our selected targets. Therefore, downregulation of GFAP/Vim is likely to be too late an intervention in the astrogliosis response to modulate the pro-inflammatory polarisation of astrocytes. Lcn2, however, is known to be a secreted autocrine/paracrine mediator of astrogliosis, playing a dual role in STAT3 and NF-κB pathways, both being induced via activation of these signalling pathways but also by activating those same pathways upon secretion and subsequent binding to the 24p3R receptor on recipient astrocytes [174, 185, 194]. Despite this dual relationship between Lcn2 induction and astrocyte reactivity, we did not observe changes in cytokine or IF expression, by qRT-PCR, Western blot, or immunofluorescence upon L12-siRNA-3WJ transfection. This might be related to a strong induction in reactivity via stimulation with a large LPS+IFNγ dose that may consequently mask or inhibit therapeutic actions resulting from siRNA-3WJ treatment.

To further investigate this hypothesis, we aimed to unravel the paracrine effects induced by reactive astrocyte-secreted Lcn2 on recipient resting astrocytes, by transferring media conditioned by the activated astrocytes (with or without L12-3WJ treatment) to non-reactive astrocytes, and characterising the extent of the induced secondary reactivity. ELISA measurements performed on the supernatant/conditioned media of reactive astrocytes confirmed the presence of secreted Lcn2 in conditioned media, showing a significant upregulation in the secretion of pro-inflammatory Lcn2 upon activation, while treatment with L12-3WJ was able to downregulate this Lcn2 secretion. ACM obtained from LPS+IFNγ-stimulated astrocytes was found to induce a significant induction in *Lcn2* and *Nos2* expression in recipient resting astrocytes. Remarkably, both upregulated genes were reverted back to levels comparable to resting ACM controls when exposed to media obtained from L12-3WJ activated astrocytes (in which secreted Lcn2 levels were downregulated), confirming the capability of Lcn2 to act as a paracrine mediator in regulating itself and its capability to regulate pro-inflammatory signals, such as NO production. Further investigations are currently being undertaken

by us in order to elucidate the interconnected roles of these genes in the modulation of reactive state in astrocytes. Nevertheless, both genes are indeed crucial in astrogliosis and these results confirmed the significant role of Lcn2-mediated reactivity as Lcn2 is known to upregulate NO production (via NOS2 induction), which in turn may drive astrogliosis-associated GFAP overexpression [116, 185].

Therefore these proof-of-concept studies confirmed the powerful potential of siRNA-3WJ constructs. 3WJ nanotherapeutics did not show any cytotoxic or immunogenic effects and in particular their employment showed an efficacious knockdown of astrogliosis-associated genes (*Gfap*, *Vim* and *Lcn2*), confirmed by a significant reductions in mRNA and protein expression using relatively small doses of siRNA-3WJ. Moreover, no off-target effects were observed in our limited study. Furthermore, we confirmed the key role of Lcn2, as protein secreted by reactive astrocytes, as a potentially significant contributor to the propagation of inflammation and astrogliosis, and consequently the potential of therapeutic intervention employing anti-*Lcn2* 3WJs to ameliorate astrocyte reactivity.

5) INTRODUCTION

Spinal cord injury (SCI) is a devastating neurological disorder that affects thousands of individuals each year. During the last few decades enormous progress has been made in understanding the molecular and cellular events initiated by SCI, leading to a better knowledge of crucial mechanisms that contribute to tissue damage and regenerative failure of injured neurons. Surgical procedures soon after the injury aim to stabilize and decompress the spinal cord to reduce secondary complications and rehabilitative care [227], however fully restorative treatments are not yet available. Due to the multifaceted nature of SCI, different therapeutic approaches have been investigated, amongst which stem cell transplantation has emerged as a promising tool [8]. Stem cells retain the capability to differentiate into different cell types, an appealing approach for cell replacement in the injured CNS; neural precursor cells (NPCs) in particular have received considerable attention for their committed nature to differentiate towards the neural lineage. Intriguingly, recent evidence pointed out bystander mechanisms alternative to cell replacement [228].

5.1 SPINAL CORD INJURY

SCI can be defined as a damage or trauma to the spinal cord that results in impairment in sensory, motor or autonomic functions, leading to a devastating and debilitating condition that adversely affects a patient's quality of life. In 2013 the World Health Organization reported a global estimation for SCI incidence at around 40 to 80 new cases per million population per year, based on quality country-level incidence studies of spinal cord injury from all causes, meaning that every year, between 250 000 and 500 000 people become spinal cord injured [229]. Traumatic injuries (i.e. caused by trauma or damage resulting from the application of an external force of any magnitude, such as in the event of road traffic crashes, falls or acts of violence) have a higher rate of incidence compare to non-traumatic injuries (i.e. congenital/genetic malformations,

damage caused by infection, loss of blood supply (infarction), compression by a cancer or tumour, or by slow degeneration of the vertebrae because of osteoarthritis) (Fig 5.1) [229, 230]. Demographic distribution of SCI also influence the etiology of spinal cord injuries -- traumatic spinal cord injuries, for example, affect predominatly young people between 18-32 years, and while life expectancy of people with SCI has greatly improved over time as a result of advances in medicine and improved access to medical care, rehabilitation and systems of support, this leads to a noteworthy cost in terms of medical and support resources [227].

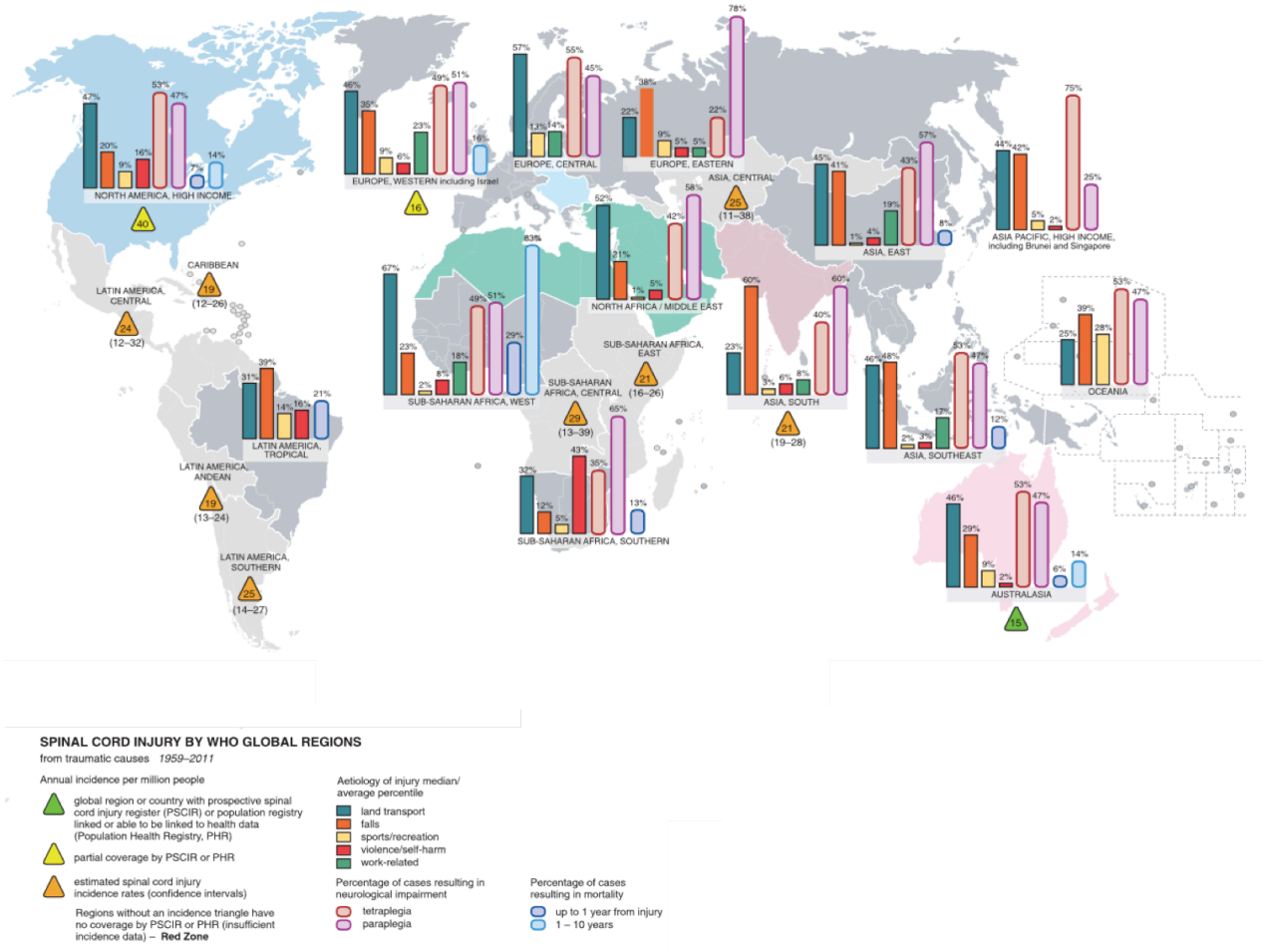

Figure 5.1: Traumatic spinal cord injury causes from 1959-2011, WHO global regions. Adopted from Lee et al. [231]

Spinal cord injury in humans has been classified into 4 different categories based on gross findings [232, 233]:

- Solid cord injury (representing 10% of cases) – despite the normal appearance of the spinal cord by a gross evaluation, without signs of softening or cavity formation, a clear damage in the spinal cord is evident by deeper histological examinations compared to normal appearing spinal cord (Fig. 5.2 A,B);
- Contusion/cavity (representing 49% of cases) – this type of injury develops from a haemorrhagic event and subsequent necrotic area, eventually forming a cyst into the cord developing from the rostral to the caudal side of the cord, along the ventral parts of the posterior columns. However, the surface of the cord does not show any disruption (Fig. 5.2C);
- Laceration (representing 21% of cases) – this is the result of a disruption of meningeal layer and underlying parenchyma by a sharp object. Compared to contusion, formation of cavity in this type of injury is minimal and the lesion is mostly characterized by the deposition of collagenous connective tissue (Fig. 5.2D). Notably, complete transection of the spinal cord is a rare condition in patients, with most of the cases still presenting small amount of residual tissue traversing the cord, although complete transection is a common paradigm in experimental research;
- Compression (representing 20% of cases) – with this type of injury the spinal cord appears macerated and the degree of the damage depends on the severity of the compression. This lesion presents characteristics similar to contusion, with the development of extensive scarring over time and similarities with laceration (often as consequence of vertebral body fractures) (Fig. 5.2E).

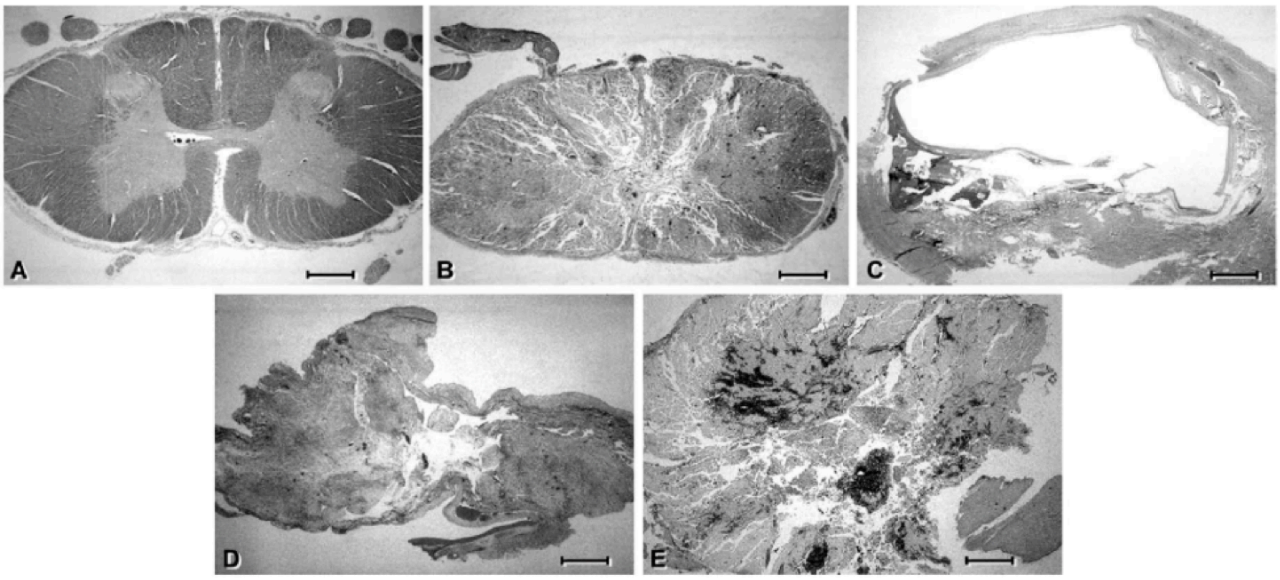

Figure 5.2: Pathophysiology and histopathology of SCI. **A,** Coronal section of normal appearing spinal cord. **B,** Solid cord injury with loss of the normal architecture and myelin loss. **C,** Contusion/cavity with cyst. **D,** Laceration injury and disruption of the pial surface. **E** Massive compression showing haemorrhagic area. Bar = 2 mm. Modified from Norenberg et al. [233]

Spinal cord injury develops in different phases (Fig. 5.3). The initial trauma, as a consequence of any of the above-mentioned causes, leads to the primary injury, damage of blood vessels, disruption of axons, and breakage of neural-cell membranes; however, in most of the cases no abnormalities are observed during this early phase (unless resulting from a consistent compression or laceration) suggesting that secondary phenomena contributes to a significant extent to the pathology [1, 233, 234].

This initial injury is followed by acute and sub-acute phases, lasting for days and weeks, respectively, which are characterized by the activation of a cascade of biological events, referred as "secondary injury", that exacerbate the pathology throughout the time (Fig. 5.3). Finally, in the chronic phase, occurring from days to years after the injury, neurological impairments in both orthograde and retrograde directions are observed, including in the brain [235].

The relevant role of the secondary injury in the development of the pathology has underlined the need for a better understanding of the biochemical and cellular events driving these phenomena in order to provide significant information for the

development of promising therapies to minimize the injury and to improve regeneration. Towards this goal, several studies have unravelled the complexity of these secondary events, highlighting a number of key contributory mechanisms (Fig. 5.3):

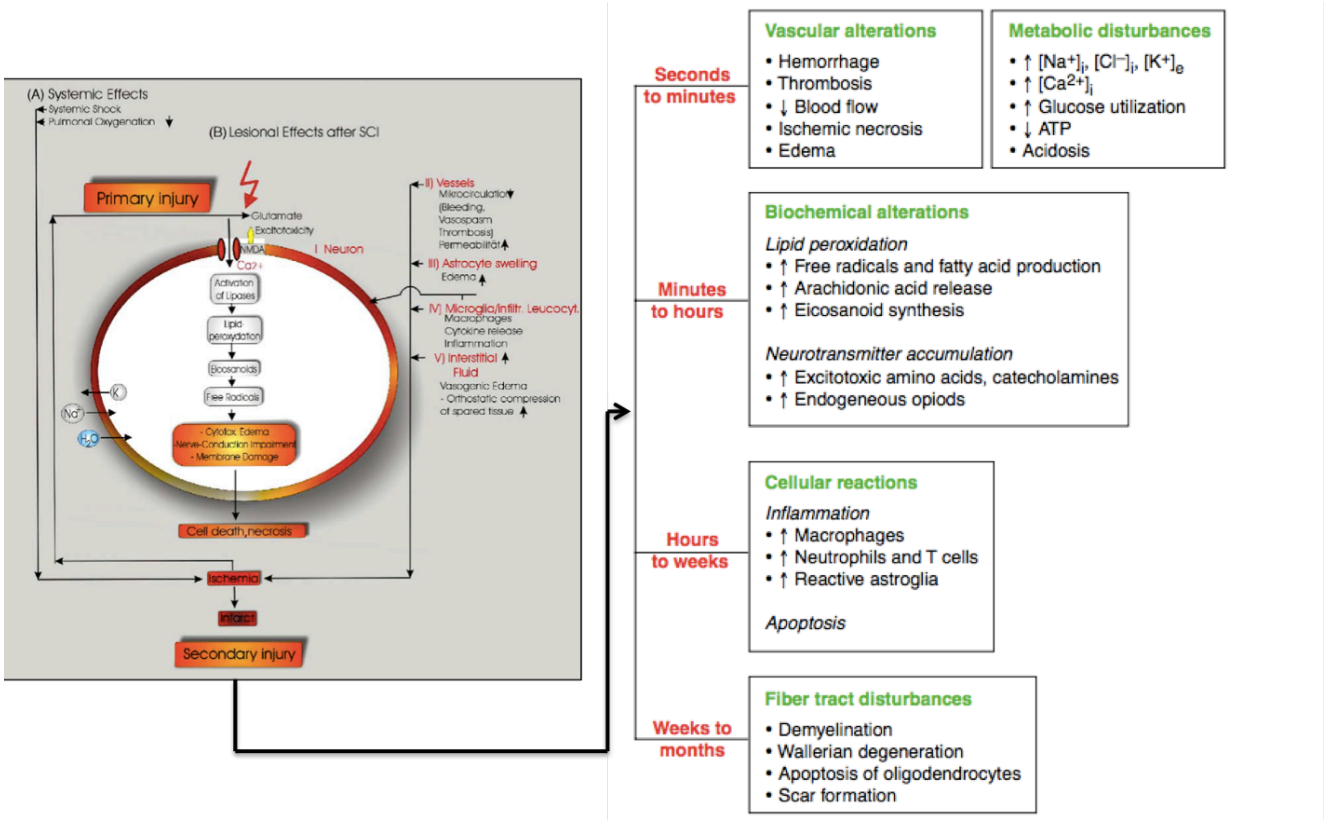

Figure 5.3: Schematic representation of the pathophysiology of the secondary damages in SCI. The illustration on the left depicts a neuron represented with the cascade of secondary damages. Modified from Schwab, et al.[5]. On the right, a schematic representation of the temporal progression of secondary damages after SCI. Modified from Bareyre et al. [236].

- Vascular changes: these are characterize by haemorrhage, breakage of the blood brain barrier and infiltration of inflammatory cells, which leads to oedema, necrosis and a period of ischemia followed by reperfusion which increases the production of oxygen-derived free radicals that further exacerbate the secondary damage [234, 236, 237];
- Free radical formation and lipid peroxidation: these biochemical events lead to hypoperfusion, oedema, failures in axon conduction and energy metabolism, and

Wallerian degeneration [238]. Peroxidation of phospholipids results from degradation of the cell membranes of damaged cells by the enzyme phospholipase A2, which in turn releases arachidonic acid. The metabolisation of this acid by cyclooxygenases produces pro-inflammatory prostaglandins, such as PGE_2. As a consequence, free radicals are produced and trigger the progression of inflammation and apoptosis [5];

- Disruption of the ionic balance of K^+, Na^+, Ca^{2+}, and glutamate excitotoxicity: following injury, extracellular levels of glutamate rise rapidly. Glutamate excitotoxicity has been shown to play a key role in neuronal cell death and in delayed post-traumatic spinal cord white matter degeneration. Indeed, oligodendrocytes are particularly vulnerable since they express a variety of glutamate receptors, such as the alpha-amino-3-hydroxy-5-methyl-4-isoxazoleproprionate (AMPA) receptors [239]. AMPA receptors present on the myelin sheets in turn activate Ca^{2+}-sensitive proteases that lead to cytoskeleton degradation and myelin disruption [240].
  Finally, impairment in calcium and sodium regulation induces a depletion of potassium and magnesium, with subsequent depolarization and interference with metabolic processes [241];
- Apoptosis: morphological and biochemical evidence has showed the presence of apoptosis after SCI, occurring in neurons, oligodendrocytes, microglia and likely astrocytes [242]. The activation of caspases, proteases with a crucial role in the apoptotic programme, occurs in neurons at the injury site within hours and it extends to oligodendrocytes. The widespread nature of this phenomenon may lead to long-term deficits after the injury, and to the damage of cells unaffected by the initial trauma [243], as observed in several different animal model, as well as in humans[244, 245];
- Inflammatory response: this includes different cellular components, such as neutrophils, macrophages and T cells, and the release of cytokines, prostaglandins and complement factors [236]. After the injury, infiltrating neutrophils rapidly increase in the tissue and start to release cytokines [246] to recruit other inflammatory cells and to further promote activation of resident microglia and astrocytes [247]. However, it is now clear that inflammation can

play a dual role, both exacerbating the damage and promoting neural tissue repair.Therefore, therapeutic modulation of the immune system, as well as of the injured environment, is still a challenge for pre-clinical research [248]. For instance, TNF, a central player in inflammation signalling, is significantly upregulated in neurons, glia, and endothelial cells within hours of SCI [249]. Yet, while the reduction of TNF signalling has been demonstrated to improve functional neurological recovery following SCI [250], the use of TNF-deficient mice led to an increase in apoptotic cell numbers, increased lesion size, and worsened functional recovery when compared with wild-type mice after SCI [251];

- Glial scar: it is well known that astrocytes react to CNS injury, and reactive astrocytes can lead to the formation of a glial scar that surround the injured environment, incorporating newly proliferated cells and in which astrocyte processes overlap in ways not seen in healthy tissue [34, 77]. Furthermore, it has been observed that the glial scar is characterized by a gradient of severity, with astroglial proliferation and density of astroglial cells diminishing with distance from the SCI lesion, gradually assuming a density similar to that seen in healthy tissue [252]. Traditionally, it was thought that this structure represented only a simple mechanical barrier, later studies suggested that regeneration was inhibited even when a dense glial scar does not form, unravelling the production of inhibitory molecules by astrocytes and the molecular composition of the scar as contributing factors for regenerative failure [83, 95, 253]. Reactive astrocytes, concomitant with other cells present in the scar, exert inhibitory effects due to the secretion of three main axon growth inhibitory molecules in the extracellular matrix such as Semaphorin 3, ephrins and chondroitin sulfate proteoglycans (CSPGs) [95, 254-256]. Semaphorin 3 is mainly secreted by meningeal cells that enter CNS lesions and contribute to the lesion core, which are highly inhibitory to axons that express the relevant receptors and they may therefore represent an important cause of regenerative failure [257]. Axon regeneration is affected also by the upregulation of members of the eph/ephrin family of tyrosine kinases and their ligands, mainly by astrocytes in SCI [258]. Finally, reactive astrocytes secret several of the inhibitory CSPGs major factor in blocking axon

regeneration, in particular neurocan, NG2, versican and brevican [95]. The mechanisms by which the GAGs inhibit axon growth are not well understood, probably related to the small GTPase Rho, however hey also bind to other extracellular matrix molecules such as laminin and tenascin, masking their growth-promoting properties [259, 260];

- As with inflammation, the experimental ablation of the glial scar in animal models of SCI has shown that this structure plays a dual role in the pathology (Fig. 5.4) [261]. The enzymatic removal of scar-associated molecules has shown to lead to a restoration of post-synaptic activity and the promotion of functional recovery of locomotor and proprioceptive behaviours [262, 263]. Nevertheless, the manipulation of some the hallmarks for astrocyte reactivity, and thus glial scarring, have shown detrimental effects on locomotor recovery. The ablation of reactive astrocytes from the injury site during acute phase in a moderate contusion injury model showed increased tissue disruption, pronounced cellular degeneration, and worsened motor deficits [9]. Moreover, (STAT3-CKO) mice, i.e. presenting conditional deletion of STAT3 from astrocytes, showed similar results with marked widespread inflammation, demyelination and neural disruption, increased lesion volume, and attenuated motor recovery [91, 92]. Thus, these evidences emphasize the dichotomous functions of reactive astrocytes, during the early phase of the injury they can preserve and protect the tissue from spreading of the damage, while a persisting presence of glial scar in the chronic phase can inhibit the axonal regrowth and neuronal survival [261].

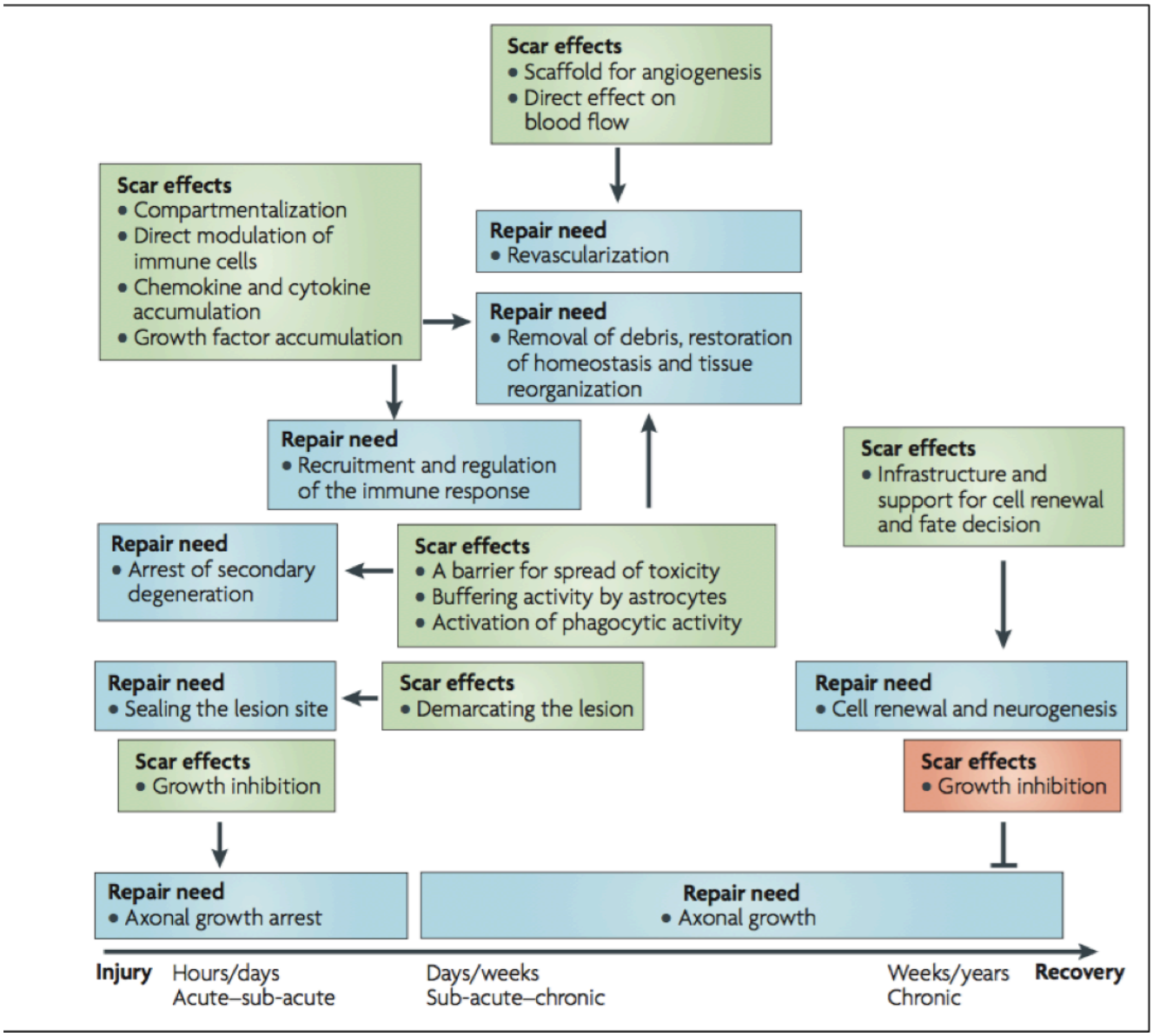

Figure 5.4: Representation of the roles of the glial scar in the development of SCI. Green boxes and arrows show the beneficial effects of the scar tissue, red box show the harmful growth-inhibitory properties of the scar tissue on axon regrowth in the chronic phases of the repair process. Adopted from Rolls, et al.[261].

Animal models have been developed in order to mimic the aspects that characterise the different types of human SCI. The use of animals has facilitated a deeper understanding of the anatomical, biological, and functional consequences of the injury [264] and, in fact, great advances have been made in the comprehension of the cellular and molecular reactions involved in acute and chronic SCI. Animal models can also offer advantages over clinical observations, especially for testing new therapeutic approaches, in that

they are characterised by reproducibility, relatively low-costs allowing for the employment of large numbers of deep histological and molecular analyses [265], and they lend themselves to standardized functional outcomes [266].

The choice and the design of models is usually dictated by the following characteristics: similarities to clinical conditions, reproducibility and reliability, and the desire for the use of a simple technique [267]. Certainly, rodents are the most common models employed in SCI research. Indeed, compared to other species they more readily allow for the generation of a reproducible injury model, one of the more crucial points for screening therapeutic approaches and treatments; the rapid availability of mice and rats of specified age, weight and sex, combined with the relative low cost and ease-of-care (a distinct advantage for chronic studies), have also increased their value for SCI. For these reasons a vast array of SCI-induction techniques have been modified to their size [268].

Despite their universal adoption, rodent models present some limits for translational applications, such as the substantial difference in size of the spinal cord compared to humans [269]. Indeed, most studies that aim to investigate potentially regenerative approaches targeting axons deal with very small distances in the rodent spinal cords, typically millimetres, while longer fiber distances are instead required to reinnervate injured areas in humans [270]. Another important limit of rodent models is represented by corticospinal tract (CST) organization. CST location, as result of evolution, differs between species and these differences are also reflected in the responses to SCI, since CST damage does not completely compromise stepping in rodents [271, 272].

As mentioned above, human SCI can be classified in different categories and so animal models aimed to mimic the pathology of these SCI are likewise categorised:

- Contusion: contusion and compression are the most common injuries in human. For recapitulation in animal models, a controlled weight-drop contusion model was developed by Allen in 1911. This device is based on the kinetic energy released when a set weight falls from a measured height onto the exposed

surface of the spinal cord, resulting in compression and displacement of the tissue [273]. Different types of injuries (mild, moderate or severe) are obtained by changing the combination of weight and height. The major advantage of this model relies in the close similarity between pathology developed in the most common animal models, such as rodents, and human pathology. In fact, starting from the acute stage arising from the first initial mechanical damage, secondary reactions develop into chronic stage comparable to that observed in human SCI patients in the chronic stage. The original impact device has been improved during recent decades and various models has been developed, nowadays the most commonly used device is the Infinite Horizon (IH) impactor; it is based on a force-controlled impact, in which a sensor measures the force inflicted to the tissue and, when the established force is reached, a stepping motor automatically and immediately withdraws the tip. This excludes the weight-bounce phenomena, and consequently the introduction of errors encountered with the other devices [274]. Similar in nature to the IH impactor, the Ohio State University (OSU) impactor is a computer feedback-controlled electromagnetic impactor.

- Compression: this model resembles the contusion as both apply a pressure on the spinal cord, however this model allows prolonged compression of the cord, mimicking the residual compression after column displacement observed in patients. Compression can be obtained by using clips, calibrated forceps or balloon compression [275].

- Transection: this model consists of complete or partial transection of the spinal cord performed with spring scissors, making it a suitable and reproducible model for evaluation of the effectiveness of interventions aimed at axonal regeneration, tissue engineering, plasticity or implantation of specific devices, therefore for assessment of axonal regeneration and subsequent functional recovery [276, 277], although spinal cord transections are not common in clinical settings.

- Photochemical: photochemical injury is based on the reaction between a photosensitive dye with light source, resulting in the production of singlet oxygen molecules on the spinal cord vessel surface and subsequent ischemia in the tissue. This model technique may provide an appropriate milieu to better understand the aspects of the vexing problem of post-traumatic syringomyelia in the human [278].

- Excitotoxic model: this model is obtained with intraspinal or intrathecal injection of some excitotoxins, such as quisqualic acid or other amino acids [278]. The employment of chemicals is aimed to mimic a specific aspect of the secondary injury cascade in traumatic SCI, their investigation and the effect of various therapies on specific pathways.

- Canal stenosis: canal stenosis is obtained by compression of the cauda equina and/or lumbar nerve roots and models a clinical problem derived from impairment of walking [278].

It is important to remember that both species and models for SCI are relevant for the design of an experimental study, in particular the type of the approach and the potential therapeutic interventions (aim of the study) are the most relevant and essential factors that should influence the choice of a model. The correct choice of a model could improve the translational value of a treatment, whereas the non-appropriate model could underestimate the potential of a treatment or lead to negative results when translating into humans [267].

5.2 THERAPEUTIC APPROACHES FOR SCI

The first intervention for SCI patients consists of early spinal decompression and stabilization surgery [279], with subsequent therapeutic approaches being divided into neuroprotective or neuroregenerative treatments. Neuroprotective therapies aim to interfere with or prevent the progression of the secondary injury, while

neuroregenerative therapies aim to repair neuronal circuitry of the spinal cord [234]. However, due to the complexity of the pathology, a combination of multiple therapeutic modalities (Fig. 5.5) should be considered, including: (i) limiting secondary damage by surgery, (ii) re-myelination of axons or replacement of oligodendrocytes, (iii) elimination of inhibitory factors, (iv) enhancement and support of neuronal growth and axonal regeneration by delivering neurotrophins or growth factors, (v) employing cell grafts as a replacement approach and as a source for creating bridges, (vi) implanting biomaterials to create bridges, and finally, (vii) the removal of dead cells [227].

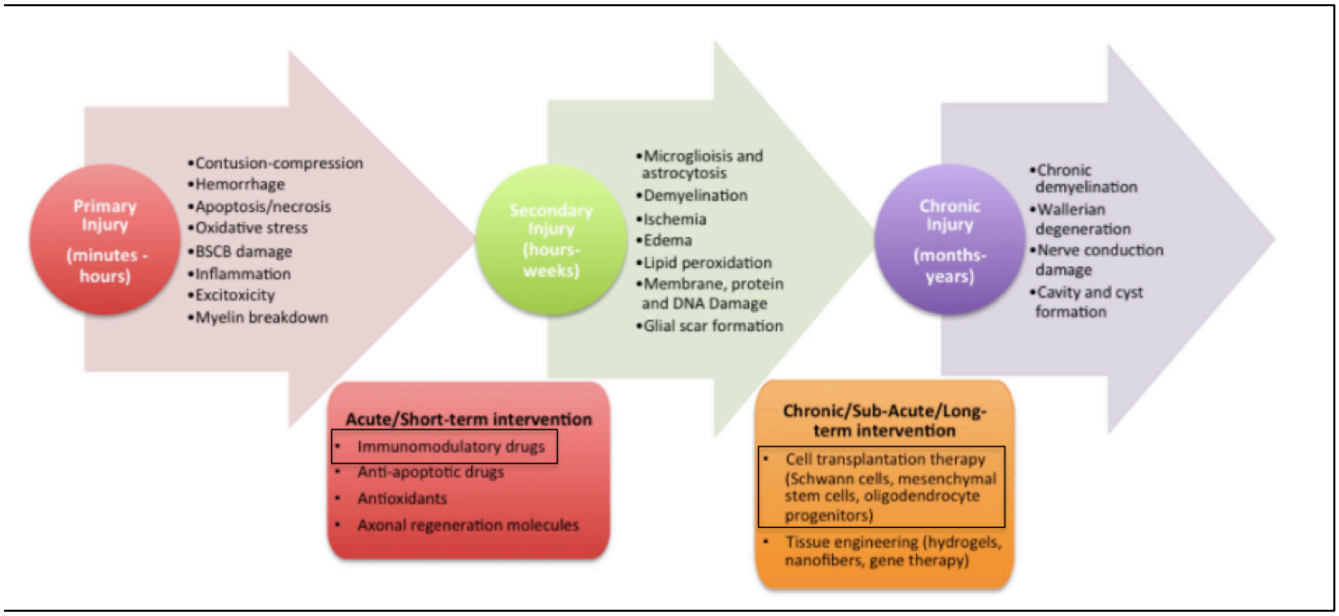

Figure 5.5: Schematic representation of different therapeutic strategies in conjunction with the progression of the spinal cord injury pathology. Modified from Kabu et al. [280].

Therapies focused on preventing the progression of the secondary injury target mechanisms such as apoptosis, oxidative stress or inflammation. For instance, immunomodulatory therapies aim to modulate the inflammatory response to SCI, an extremely complex phenomenon that has been shown to have both beneficial and detrimental roles in the recovery process [281]. Clinically, the glucocorticoid methylprednisolone (MP) was thought to yield neuroprotection by suppressing secondary inflammation and lipid peroxidation, however its safety and efficacy for acute SCI is controversial [282-284]. In fact, beneficial effects depend on the type of

injury and the time of intervention (3-8 hours after injury), with prolonged or delayed treatment, or treatment applied in penetrating SCI having been shown to be detrimental [283]. The employment of the glycolytic enzyme chrondroitinase ABC (ChABC) to degrade the CSPG inhibitory activity in the glial scar has shown significant restoration of neuronal regeneration and plasticity in both small and large animal models [262, 285]. In fact, ChABC gene therapy led to significantly reduced secondary injury and showed immunomodulatory properties through the modulation of macrophage phenotype towards the anti-inflammatory M2 polarisation [286]. However, ChABC has different disadvantages as clinical treatment: a single injection is insufficient since CSPGs are continuously synthetized and it ChABC has a short functional half-life, and also it is a biological product (synthesised by the bacterium *Proteus vulgaris*) and so repeated injections could induce a potential immune reaction [287].

One of the most attractive approaches for translational medicine and clinical trials in SCI research is cellular transplantation. Indeed, cellular transplantation aims to bridge cysts or cavities at the injury site, replace dead cells (such as neurons or myelinating cells), and create a more amenable environment for axon regeneration [8, 280]. Amongst the different cell types that can be transplanted in order to promote recovery, stem cell-based therapy is one of the most promising treatments, although some concerns arise about potential side effects and safety, including potential immunological rejection or tumour formation, as well as ethical issues regarding the acquisition of the cells [288].

One promising cell candidate is neural stem/precursor cells (NPCs): multipotent cells capable of self-renewal, readily expandable *in vitro*, and committed to the neural lineage. During recent decades it has been shown that both fetal and adult brains contain NPCs [50, 289], with the cells residing within specific niches – the subventricular zone lining the lateral ventricles of the forebrain [52], the dentate gyrus of the hippocampus [55], and the periventricular region of the spinal cord [48]. Reynolds and Weiss demonstrated for the first time the possibility to isolate neural stem cells from the adult mouse brain and their culture protocol, now widely used, is known as the neurosphere assay. Neurospheres are obtained by culturing NPCs in a chemically defined serum-free

medium enriched with specific mitogenic growth factors, such as epidermal growth factor (EGF) and FGF2 [290].

A systematic review published in 2011 summarized the application of NPCs as a treatment for SCI, both in mice and rats. These studies showed that significant clinical improvements could be attained upon transplantation, even though in some of these studies co-treatments were applied, such as myelin vaccination or infusion of trophic factors cocktails [291-294]. Indeed, our current interest in stem cell transplantation arose from remarkable outcomes observed in sub-acute transplantation of NPCs into a murine model of moderate contusive SCI. A number of noteworthy outcomes were observed including a survival capacity *in vivo* of up to 2 months after transplantation, the localisation of transplanted NPCs to clusters in very close proximity to macrophage/microglial cells and blood vessels, highly reminiscent of the 'atypical ectopic perivascular niche-like areas', as previously described [22, 295, 296], and the ability of transplanted NPCs to significantly skew the polarisation of inflammatory infiltrates of the injured spinal cord segment towards a tissue remodelling/repair (M2-like) phenotype leading to the promotion of tissue healing [26]. Interestingly, it has also been shown that transplanted undifferentiated NPCs exert a long-term bystander effect. Studies in rodents and non-human primates with experimental autoimmune encephalomyelitis (EAE, an experimental model of multiple sclerosis) demonstrate the accumulation of systemically injected NPCs around the perivascular space in the proximity of reactive astrocytes, inflamed endothelial cells and blood-borne infiltrating T cells [22, 297, 298]. These areas, called '*CNS atypical ectopic niches*', display a molecular cross talk between the different constituents of the atypical niche where undifferentiated stem cells promote neuroprotection by *in situ* release of immunomodulatory molecules and neurotrophic factors [228]

Therefore, NPCs constitute an attractive option for transplantation because they can be readily expanded and are committed along the neural lineage; however, transplanted embryonic stem cell-derived neural cells may give rise to ethical issues for the use of these cells, as well as immunocompatibility concerns and accessibility limitations [291, 299]. These limits have been overcome by the generation of induced pluripotent stem

cells (iPSCs); through the administration of four key transcription factors mature somatic cells can be reprogrammed into pluripotent stem cells that in turn can be differentiate into neural-lineage cells [300]. Other new and alternative methods have been developed for reprogramming, such as zinc-finger nucleases (ZFN), transcription activator-like effector nucleases (TALENs) and the CRISPR–Cas9 system [301]. However, iPSCs do present some limits, such as the possibility of tumorigenesis upon transplantation [302], and, although this issue is often understated, individual iPSC lines may show variability in their potential to differentiate into functional cells of a given lineage [301].

5.3 INDUCED NEURAL STEM CELLS (iNSCs)

Advances in iPSC methods led to new approaches allowing for the generation of neurons by direct induction of fully mature neurons from somatic cells by using forced expression of various key neuronal transcription factors [303, 304]. The major advantage of this technology is the more rapid and easy induction of the neuronal phenotype compared to iPSC generation. However, these techniques showed some disadvantages, especially for clinical applications, such as the limited rate of expansion of these derived cells. Therefore, new induction processes have to be started for every experiment and mature-differentiated cells are more difficult to transplant due to their increased sensitivity to manipulation [305]. To overcome these limitations, an alternative approach has been developed to derive induced neural stem cells (iNSCs) from somatic cells as an expandable cell type, retaining the potential to differentiate into all neuroectodermal lineages. This novel approach is based on a combination of various key fate-determining transcription factors and has shown success in generating stable and expandable iNSCs from somatic cells which exhibit the major properties of primary NSCs [6, 306].

Indeed, it has been demonstrated that it is possible to obtain stably expandable NSCs, forming neurosphere-like clusters, from fibroblasts through a curtailed version of reprogramming toward pluripotency. The innovation of this protocol resides in the

limited induction (up to 5 days) of the expression of Oct4 (which would rather favour iPSC induction), based on the observation that NSCs endogenously express a subset of iPSC reprogramming factors, namely transcription factors Sox2 (Sry-box containing gene 2), Klf4 (Krüppel-like factor 4), and c-Myc, but not Oct4 (Pou5f1 - POU domain, class 5, transcription factor 1) (Fig. 5.6). iNSCs exhibit similar morphological and molecular features of NSCs such as the expression of Nestin, Olig2 (oligodendrocyte transcription factor 2), Sox2, Blbp (brain lipid binding protein), and Pax6 (paired box 6) (Fig. 5.6), and all the three transgenes employed were determined to be silenced in all iNSC-derived lines analyzed, confirming that a stable conversion had been achieved. Concomitantly, endogenous Sox2 has been shown to be upregulated in iNSCs, demonstrating that self-renewal capability of iNSCs is not dependent on sustained transgene expression, but triggered by activation of the intrinsic NSC transcriptional program. Furthermore, when exposed to appropriate culture media, iNSCs showed the capability to differentiate into the three main neural lineages: astrocytes, oligodendrocytes and neurons [6].

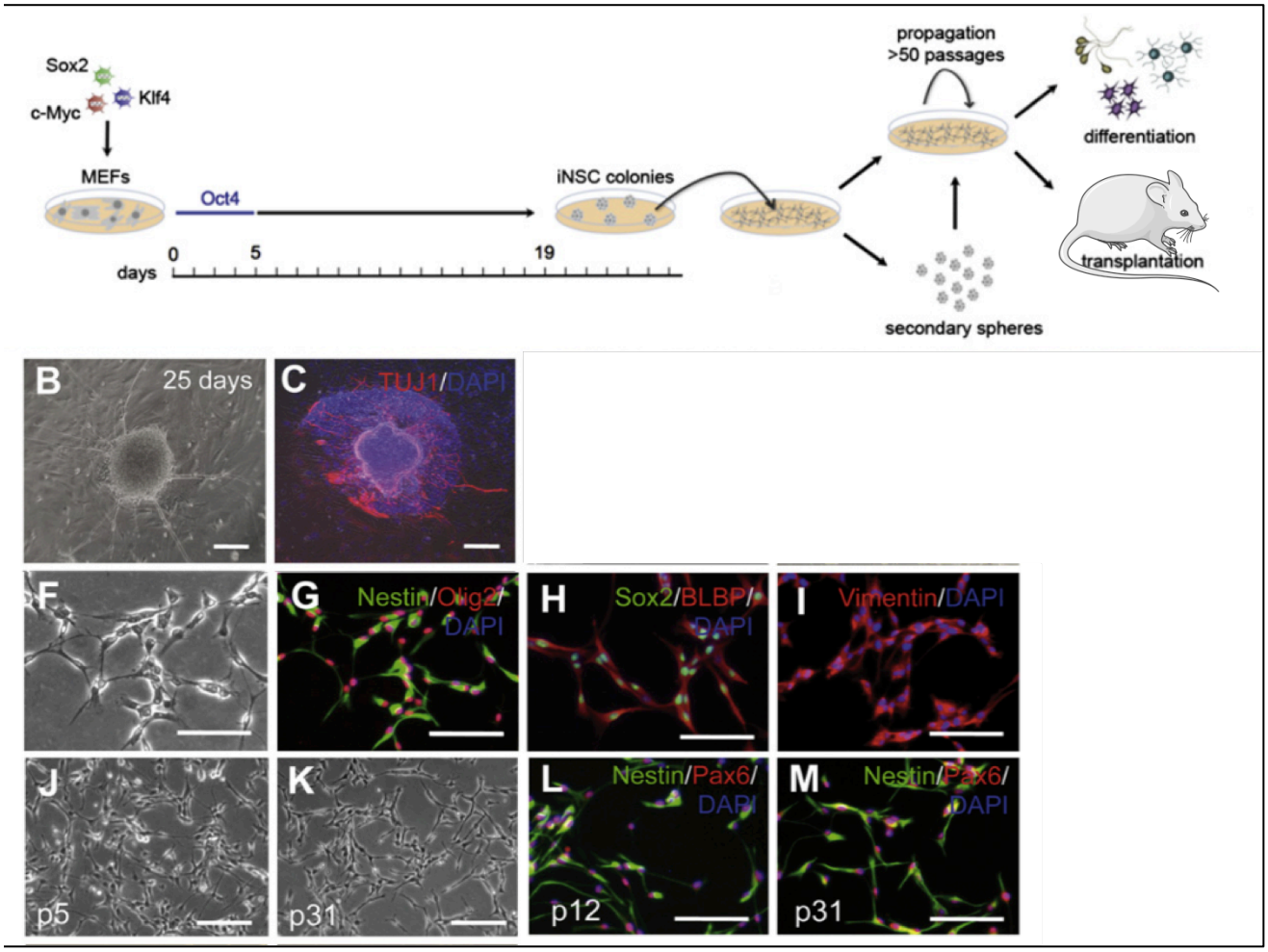

Figure 5.6: **A,** Schematic representation of the experimental protocol to derive induced neural stem cells (iNSCs). **B,** Phase contrast micrograph of neurosphere-like colony at day 25 and axonal structures processing out of the sphere. **C,** Immunofluorescence analysis using a specific antibody directed against the neuronal marker b-III-tubulin performed on neurosphere-like colony at day 27. **F,** A phase contrast micrograph of iNSCs. Immunofluorescence analysis of the NSC marker proteins in iNSCs: Nestin and Olig2 (**G**), Sox2 and BLBP (**H**), and mesenchymal marker Vimentin (**I**). **J** and **K**: Phase contrast pictures of iNSCs in neurosphere propagation medium at passage 5 (**J**) and 31 (**K**). **L** and **M**: iNSCs at passage 12 (**L**) and passage 31 (**M**) were stained for NSC markers Nestin and Pax6. Modified from Thier et al. [6].

Therefore, considering the promising results obtained from NSCs transplantation in SCI models, and the translational potential inherent to iNSCs as a potential source for autologous transplantation, our aim is to assess the therapeutic potentiality of sub-acute iNSC transplantation in a murine contusion model of SCI. In particular, with the overall aim of a combined approached using reactive astrocyte-ameliorating pRNA-3WJs nanotherapeutics and stem cells, our first goal is to verify the potential of iNSC transplantation compared to the already well-characterized NSC approach.

5.4 RESULTS

5.4.1 TRANSPLANTATION IN A MURINE MODEL OF CONTUSIVE SPINAL CORD INJURY

The therapeutic potential of sub-acute transplantation of iNSCs was assessed in a moderate contusive model of SCI, 70 kDyne (IH Horizon impactor), applied in a total of n = 55 C57Bl/6 mice at day 0. Locomotor activity of SCI mice was assessed at day 1, 3 and 5 by using the Basso Mouse Scale (BMS) score in the open field arena; SCI mice presenting an abnormal (asymmetric) BMS score (10/55; 18.2 %) were excluded from further studies, in line with previously described methods [27], while 4 mice were excluded based on the force/displacement outcomes from initial impactor treatment (force above 75 kDyne, displacement above 900 μm). Deficits in bladder functions, such as cystitis or inflammation of the bladder, are common in both human SCI and rodent SCI models [307]; in our experiments 5 mice were sacrificed due to bladder infections.

7 days after SCI, mice were randomized into a total of three different treatment groups based on individual BMS scores assessed on the same day:

- Control group - PBS group: SCI mice received sterile PBS 1X at 7 days post injury (dpi) in a total of n = 4 injection sites (250 nl/site) bilaterally from midline at both the anterior aspect of T13 and the posterior aspect of T11 (fig. 5.7) (n = 4 for 28 days post transplantation (dpt) evaluation; n = 9 for 49 dpt evaluation);
- NPCs group: SCI mice received single cell-dissociated 150 x 10^3 farnesylated-GFP^+-NPCs at 7 dpi in a total of n = 4 injection sites (250 nl/site), as described above (n = 6 for 49 dpt evaluation);
- iNSCs group: SCI mice received single cell-dissociated 150 x 10^3 farnesylated-GFP^+-iNSCs at 7 dpi in a total of n = 4 injection sites (250 nl/site), as described above (n = 3 for 28 dpt evaluation; n = 10 for 49 dpt evaluation).

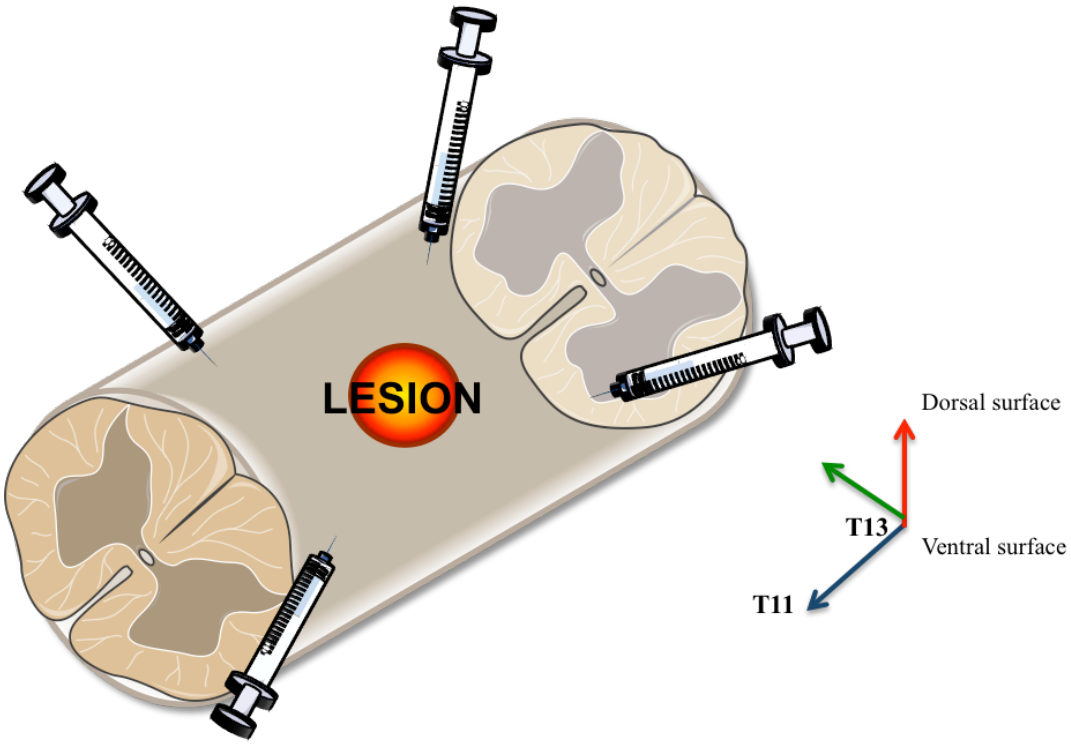

Figure 5.7: Schematic representation of the transplantation setup. 4 injections were performed bilaterally from midline at both the anterior aspect of T13 and the posterior aspect of T11, 250 nl/injection, a total of 150 x 10^3 farnesylated-GFP$^+$ NPCs/ iNSCs were injected.

Functional performances were then tested 1 and 3 days after transplantation, and then weekly for the entire duration of the experiment by using BMS score and, upon reaching a BMS score of 5, BMS subscores. Mechanical allodynia was tested weekly by using Von Frey testing on the hind limbs; the lowest filament associated with an animal's withdrawal was assigned as a threshold the day before the injury. Thermal nociception was assessed weekly by using Hargreaves' method on the hind limbs, withdrawal response observed the day before the injury was assigned as the threshold.

Tissue samples obtained 35 dpi (28 days after transplantation) and 56 dpi (49 days after transplantation) were analysed for preliminary data on the localisation and survival of transplanted cells.

The evaluation of hind limb-locomotor recovery by using BMS scores for the transplanted groups, both NPCs and iNSCs, did not reveal any significant differences compared to control group (Figure 5.8).

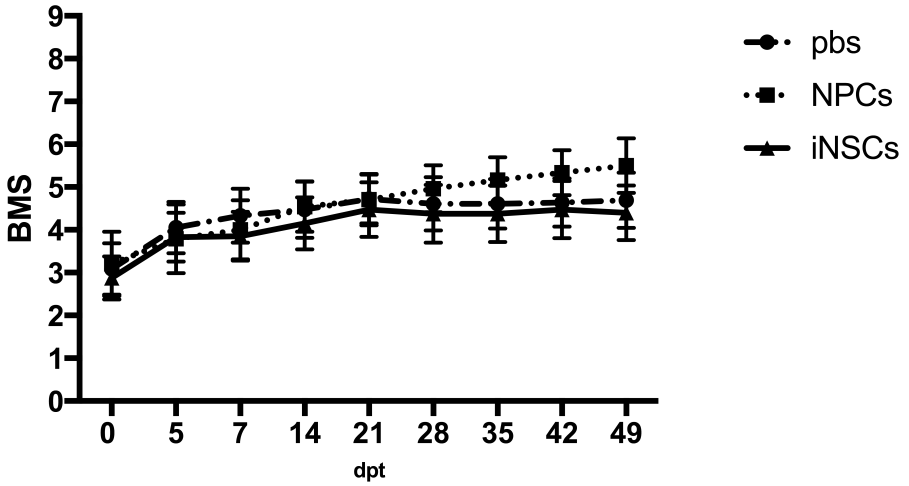

Figure 5.8: BMS score evaluation of the three different SCI treatment groups. No statistically significant differences were observed. N = 9 PBS group; n = 6 NPC group; n = 9 iNSC group (mean ± SEM). Two-way ANOVA and Bonferroni post-hoc test, $p < 0.05$. dpt = days post transplantation.

However, significant spontaneous recovery occurs in moderate injury and the use of the BMS scale, a gross evaluation of locomotion, may not allow one to appreciate the recovery in more fine locomotor capabilities. For this reason, we also performed BMS subscore analyses on mice that reached a 5/9 score with BMS (Figure 5.9). The small number of subjects for each group only allowed us to observe a trend in the improvement of NPC and iNSC-treated groups compared to the control group (Figure 5.10).

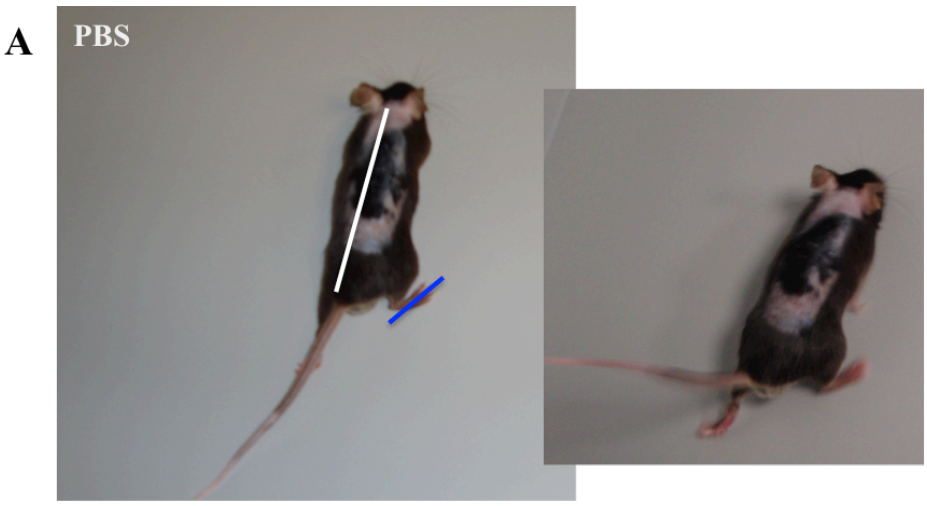

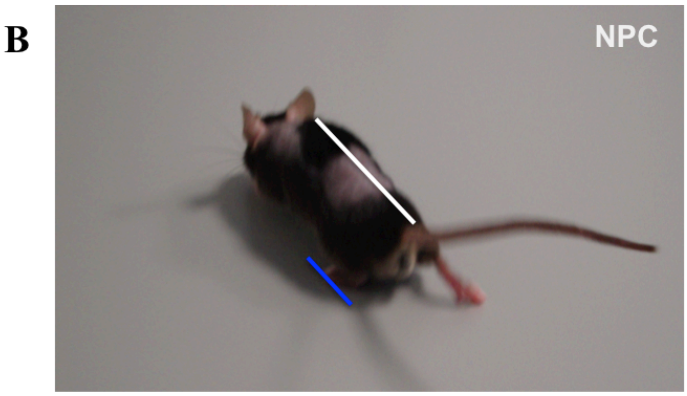

Figure 5.9: Representative images of BMS appraisal. BMS subscore was evaluated as previously described by [27]. Mouse belonging to PBS group in **A**, NPC group in **B**. Paw position is evaluated by the orientation of the middle digits of the paw (blue line) compared to the long axis of the body (white line).

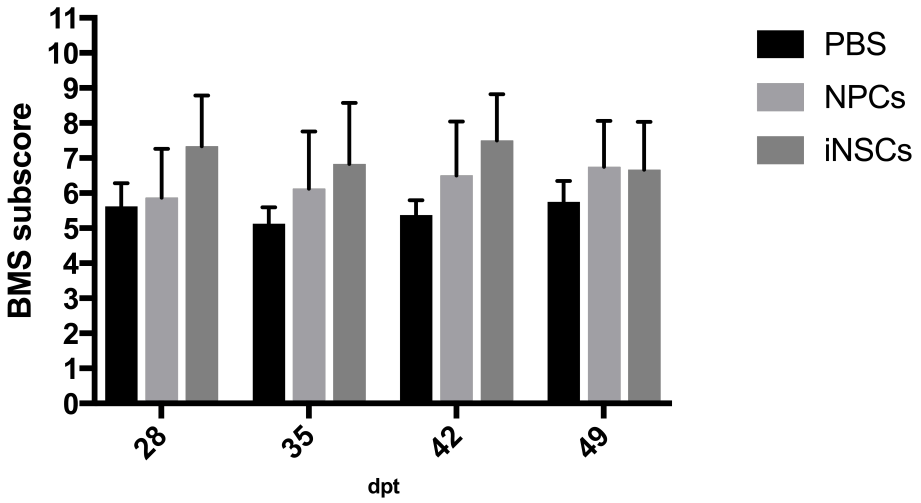

Figure 5.10: BMS subscore evaluation of the three different SCI treatment groups. No statistically significant differences were observed. n = 9 PBS group; n = 6 NPC group; n = 9 iNSC group (mean ± SEM). Two-way ANOVA and Bonferroni post-hoc test, $p<0,05$. dpt = days post transplantation.

5.4.2 MECHANICAL ALLODYNIA AND THERMAL STIMULUS TEST ASSESSMENTS

In order to evaluate the possibility of development of hind limb allodynia upon transplantation or an increased sensitivity to noxious thermal stimulus applied to the hind limbs, Von Frey hair test and Hargreaves' test were assessed the day before the surgeries in order to establish a threshold for each mouse, and then weekly for the entire duration of the experiment.

Von Frey's hair test was applied to the hind limbs following the up and down approach, as previously described [28]. Transplantation of both NPCs and iNSCs did not show any decrease in the threshold of response to mechanical allodynia or statistically significant differences between groups (Figure 5.11).

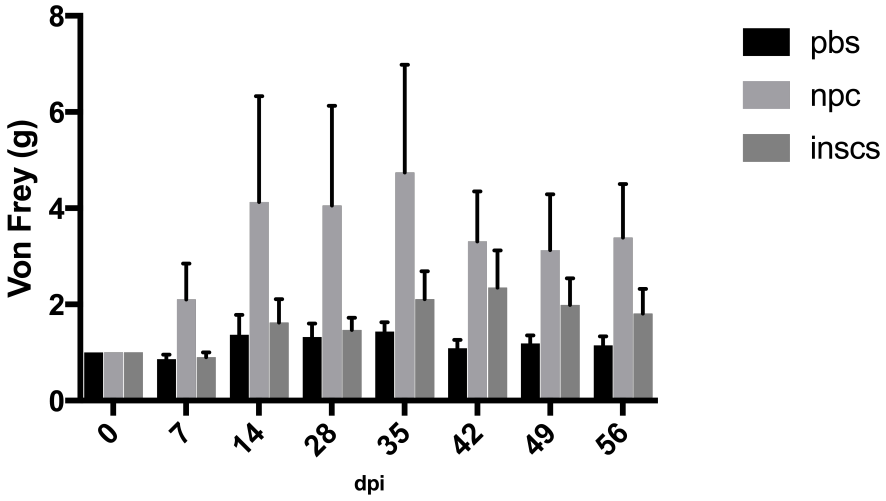

Figure 5.11: von Frey analysis of mechanical allodynia in the hind limbs. Data are normalized to the threshold measured the day before the spinal cord injury surgeries (mean±SEM). Two-way ANOVA and Bonferroni post-hoc test, $p < 0.05$. dpi = days post injury.

The Hargreaves method measures cutaneous pain thresholds in rodents [308]. Pain thresholds are evaluated as hind limb withdrawal latencies from a painful stimulus, a standard baseline temperature applied to the skin in unrestrained rodents. As observed with the Von Frey test, no induction in pain sensitivity was recorded upon transplantation in both NPC and iNSC-transplantation groups, with no statistically significant differences between groups (Figure 5.12).

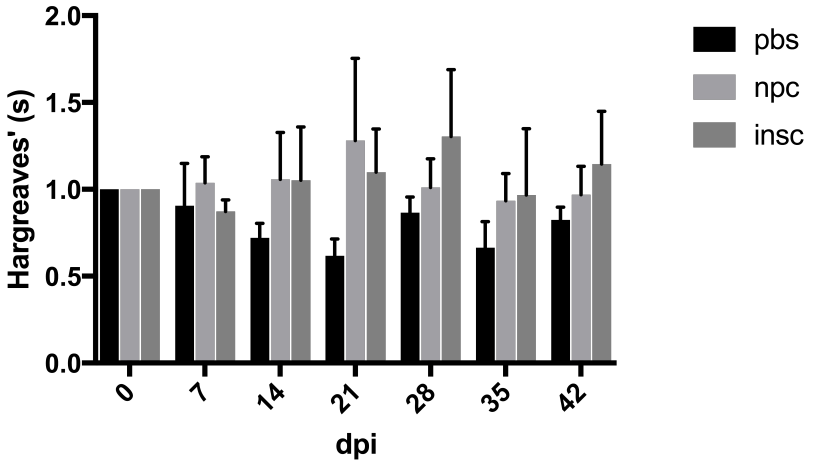

Figure 5.12: Hargreaves' method for thermal pain sensitivity in the hind limbs. Data are normalized to the threshold measured the day before the spinal cord injury surgeries (mean ± SEM). Two-way ANOVA and Bonferroni post-hoc test, $p < 0.05$. dpi = days post injury.

5.4.3 CELL SURVIVAL AND MIGRATION EVALUATION

To investigate the survival of transplanted cells, mice from iNSCs were sacrificed 4 and 7 weeks after transplantation. We observed successful cell engraftment in all transplanted mice; specifically, quantification at 4 weeks (n = 3) revealed the presence of an absolute number of 2057.67 ± 357.39 GFP^+-engrafted iNSCs (Fig 5.15), decreasing to an average of 350.83 ± 78.32 at 7 weeks after transplantation (n = 6), corresponding to a percentage of surviving cells on the total number of transplanted cells of 5.23 ± 1.34 % and 1.94 ± 0.43 %, respectively (Fig. 5.13). Nevertheless, limited graft survival has previously been reported in SCI models, with less than 10% of grafted NPCs usually observed upon transplantation [26]. Further evaluations are being assessed to compare iNSC and NPC survival upon transplantation.

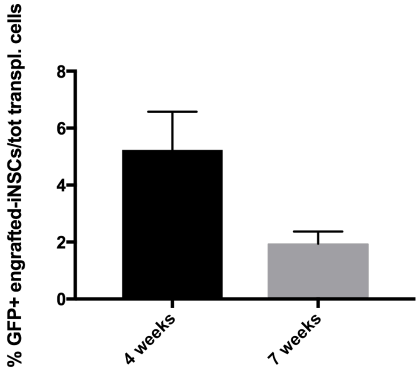

Figure 5.13: Preliminary evaluation of survival percentage of grafted iNSCs. Percentage of surviving cells decreased during over time reaching a percentage of 1.94% of the total amount of transplanted cells that survive in the host parenchyma at 7 weeks after transplantation (mean ± SEM).

Additionally, we estimated the migration capabilities of transplanted iNSCs into the parenchyma. It has been shown that transplanted cells migrate both toward rostral and caudal direction [26, 309], and while we found that transplanted cells did not migrate extensively, we did observed an increased accumulation of cells around the lesion site 7 weeks after transplantation (Figure 5.14).

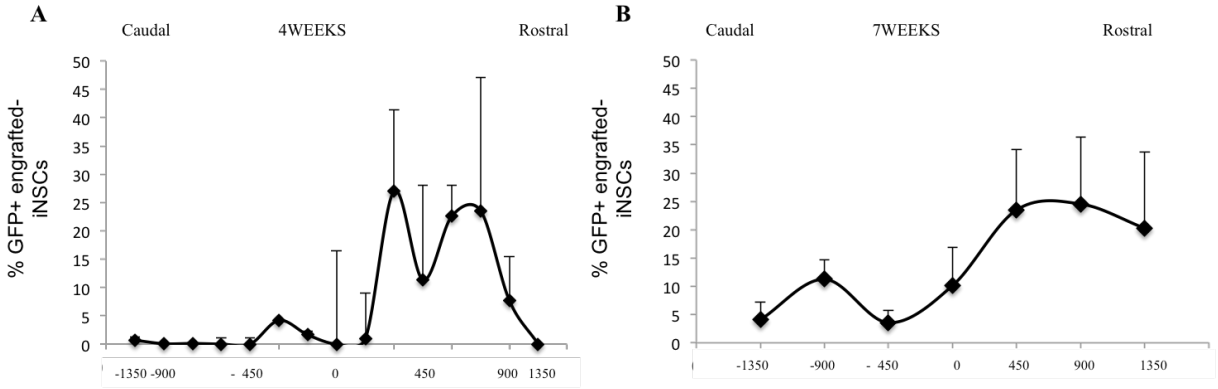

Figure 5.14: Evaluation of migrational properties of GFP+-transplanted iNSCs 4 weeks (**A**) and 7 weeks (**B**) after transplantation. Percentage of grafted-cells are represented (± SEM).

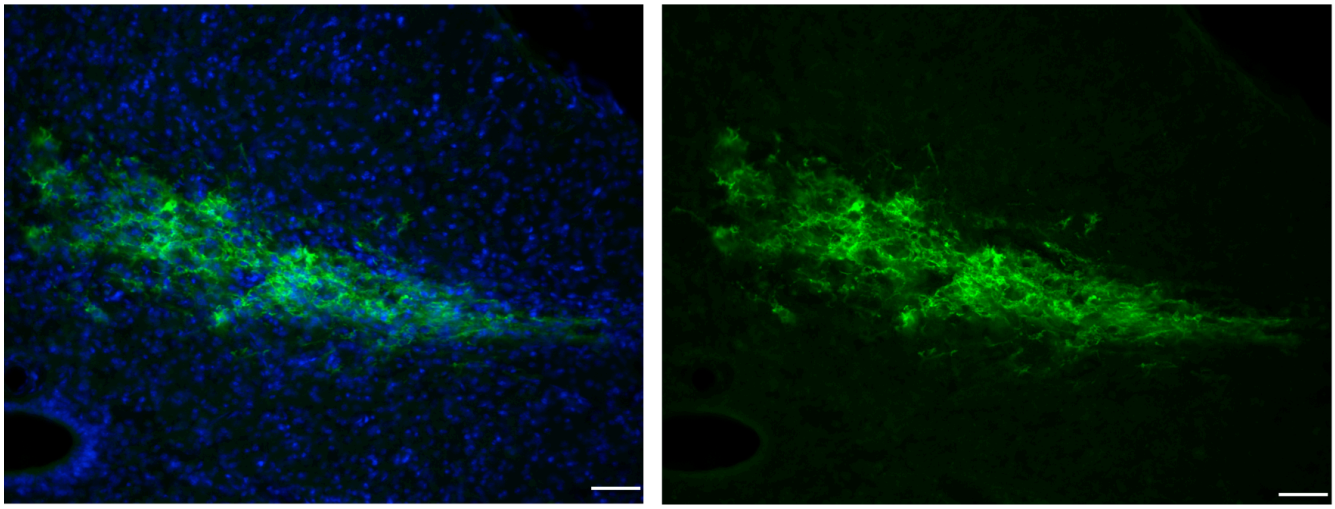

Figure 5.15: representative image of grafted-GFP+ iNSCs 28 dpt. Coronal section of spinal cord, 30 μm thickness. DAPI is represented in blue, GFP in green. Scale bar = 50 μm.

5.5 DISCUSSION

Spinal cord injuries (SCI) are highly debilitating pathologies characterized by an initial mechanical insult that is subsequently exacerbated by secondary damages such as inflammatory responses, continuous cell death, demyelination, Wallerian degeneration, astrogliosis and glial scarring [235].

Despite the observation that spontaneous repair of neural environment may occur in patients affected by acute and/or chronic inflammatory and degenerative disorders of the nervous system, including SCI patients, this process is usually not sufficient to promote a functional and stable recovery of the highly compromised nervous system architecture [1]. Among a number of innovative therapeutics aiming at CNS repair and/or regeneration, cell-based therapies represent the most promising approaches. In particular, stem cell-based therapies have shown remarkable evidences in their capability to protect the CNS from chronic inflammation-driven degeneration, such as that occurring in EAE/MS, stroke and SCI. Interestingly, it has been demonstrated that non-hematopoietic somatic stem cells, such as NPCs, can promote the protection of the damaged nervous system through mechanisms other than cell replacement [228]. Evidences from transplanted NPCs in immune-mediated experimental demyelination and stroke showed the capability of transplanted cells to mediate efficient bystander myelin repair and axonal protection/rescue [22, 26, 297, 298]. A new concept has been therefore proposed to describe the capability of NPCs to adapt fate and functions to specific microenvironments, named *therapeutic plasticity* [310]. Several studies have shown that transplantation of NPCs in SCI rodent models resulted in a functional integration of transplanted cells into the host perilesional cord tissue, differentiation into oligodendrocytes, and improvement in locomotor recovery [7, 26, 291, 309]. Moreover, sub-acute transplantation with NPCs showed a reduced volume of the lesion site, decreased volume of macrophage/microglial infiltration at lesion site, and decreased volumes of demyelination, compared to controls, suggesting that delayed (sub acute) NPC transplantation may significantly interfere with the development of main secondary events after SCIs [26]. Additionally, the route of cell administration may impact on the therapeutic outcome. Direct intraparechymal injection represents is one of

the most used route of cellular transplantation in animal models of SCI. This invasive method allows, through direct access to the site of injury via laminectomy, multiple injections into the injury epicentre and/or into the parenchyma adjacent to the injury [7, 26]. Despite the invasiveness of this technique, augmenting the risk of causing further trauma to the injured tissue during surgery, some clinical trials showed promising outcomes with no remarkable complications [311, 312].

While NPCs have elicited promising results, the last few decades have seen the development of novel technologies for the generation of iPSCs, leading to the possibility of an easily accessible cell source, such as the skin, and the possibility of autologous transplantation [305]. In this regard, iNSCs represent an even more promising technology, with the direct reprogramming of skin fibroblasts into neural precursor cells being faster compared to iPSC technology and involving less manipulation and therefore less chance to develop teratomas [305]. The use of constitutively expressed Yamanaka factors (Sox2, Klf4, and c-Myc) [300] and a regulated expression of Oct4 that reduces the induction of pluripotency, has allowed for the possibility of generating a stably expandable (more than 50 passages) iNSCs which ultimately can be induced to efficiently differentiate into cells of each of the neural lineages [6].

Therefore, considering the remarkable therapeutic potential of iNSCs, we are aiming to characterize their capability of exerting beneficial roles upon transplantation compared to the well-described effects of NPCs. For this purpose, we employed a moderate contusive model of SCI; due to their similarity to the majority of human injuries, and the great incidence of this type of injury in humans, contusion and compression models are the most employed animal models of SCI [313].

Preliminary data showed no differences in the BMS scores between a PBS-injected control group and transplanted groups, either with NPCs or iNSCs. In explaining this apparent non-outcome, it is important to remember that evidence shows that motor and locomotor-like movements are observed in the hind limbs of even complete paraplegic mice without intervention, i.e. as spontaneous regeneration. Mice subject to complete

spinal cord transection showed signs of locomotor activity [314], as was previously observed in adult cat [315]. Cellular mechanisms responsible for the motor and locomotor-like recovery in complete spinal animals remain largely unknown. The progressive return of hind limb movements over time observed in complete spinal transection animals could be attributed to time-dependent plastic changes in networks of the lumbo-sacral spinal cord that can generate walking in the absence of supraspinal input (i.e. central pattern generators) [316].

CST organization represents another limit to rodent models. CST is characterized by a main common function conserved through species, the cortical modulation of spinal cord activity, although it performs also other functions, such as descending control of afferent inputs, selection, gating and gain control of spinal reflexes, direct and indirect excitation of motoneurons, inhibition of motoneurons, autonomic control and long-term plasticity of spinal cord circuits. It is deducible how evolutionary changes have lead to remarkable differences. In fact, in human and primate the CST has increased in the size of the neocortex and consequently in the amount of the neocortex giving rise to the CST [271]. Therefore, the CST location, as a result of evolution, differs between species: in rodents, the CST projects mainly in the dorsal horn neurons and premotor spinal circuits, whereas human and non-human primate CST projects mainly to ventral horn, with soma axons creating direct synapses into motor neurons, in particular axons innervating hand muscles [270]. Differences in location are also reflected in the responses to SCI, CST damage does not completely compromise stepping in rodents, underlying the importance of other nervous pathways, such as the rubrospinal tract [271]. Therefore, the considerable spontaneous recovery observed in control mice may mask some effects of treatments, even though these still represent preliminary data and number of employed mice has to be increased to be relevant.

Finally, BMS evaluation, as adaptation of the Basso Beattie Bresnahan (BBB) score for rats, represents a gross measurement of locomotor functions, lacking the specificity and sensitivity for the detection of smaller and finer changes in motor behaviour [317]. For this reason, a more detailed scale was introduced, called BMS subscore, that evaluates improvements in stepping frequency, coordination, paw position, trunk stability, and tail

position. A cumulative score can be calculated over time to discriminate differences in the fine details of locomotion that BMS score may not reveal. In addition, each attribute of the subscore, such as paw position, can be used to compare different groups as individual locomotor features [27]. We therefore applied BMS subscore on mice that reached a score of 5 on the BMS scale (i.e frequent or consistent plantar stepping, no coordination -OR- frequent or consistent plantar stepping, some coordination, paws *rotated* at initial contact and lift off (R/R)) and we observed a trend in the improvement of fine locomotor capabilities of transplanted groups compared to control group. Nevertheless, these are still preliminary data and the number of subjects for each group has to be increased in order to evaluate effects from transplantation and to attain statistically significant results. We are aiming to improve the assessment of accuracy, and therefore the evaluation of proper connections between functional sensory and motor systems, by using foot slip test through horizontal ladder walking test on which animal can walk along variable rung spacing [318].

Cell transplantation may lead to the development of allodynia, defined as hyperalgesic responses to normally innocuous stimuli, due to nociceptive fiber sprouting in the dorsal horn regions rostral to the injury site or associated to astrocytic differentiation of grafted NSPCs as observed in SCI rodents [319, 320]. Von Frey hair test was assessed weekly after injury and after transplantation by applying up and down approach as previously described [28]; animals transplanted with either NPCs or iNSCs did not show any signs of allodynia, confirming the safety of grafted cells in this sense. To further confirm these results, thermal nociception was assessed by Hargreaves' test, by measuring withdrawal latency following thermal stimulation to the paw, allowing the measuring of cutaneous pain thresholds [308, 321]. Transplantation of NPCs or iNSCs did not induce any hyperalgesia in the present study.

Another important result to be assessed upon transplantation are represented by the survival rate of cells upon transplantation. Subacute transplantations have been shown to be more effective rather than acute or chronic; in fact inflammatory responses immediately after injury create a cytotoxic environment, unfavourable for NPC transplantation. On the contrary, during the subacute phase (1 to 2 weeks post-injury) the inflammatory response is reduced and the glial scar is starting to form, therefore

NPC transplantation has the potential to modulate the development of secondary injury mechanisms [288, 322]. However, poor graft survival after NPC transplantation has been reported in SCI models, with usually less than 10% of grafted NPCs surviving [26, 323, 324]. Preliminary data upon local transplantation of iNSCs showed similar results as previously seen for NPCs: 4 weeks after transplantation 5.54 ± 0.94 % of transplanted cells survived in the host environment, while 7 weeks after transplantation only 1.94 ± 0.43 % survived, in line with evidence from the literature. Further quantifications are being assessed to characterize better comparisons between NPCs and iNSCs transplantation, as well as the differentiation of grafted cells.

Finally, the injured microenvironment could alter both the engraftment dynamics and the availability of differentiation cues since it is well-known that niches provide extrinsic cues that influence many aspects of stem cell biology [325, 326]. Therefore, the damaged environment may influence both the fate and migration of transplanted cells. Previous evidences showed a great migratory capability of NPCs upon transplantation, in particular grafted-cells migrate both in the rostral and caudal portion of the injured spinal cord [26], however they also migrate toward the lesion site surrounding it [326, 327]. In the present experiment we saw negligible iNSC migration from the injection site at 4 weeks post-transplantation, however we did observe a migration towards the lesion site at 7 weeks.

Although these represent preliminary data, transplantation of iNSCs retains the potential to ameliorate the hostile injured environment upon SCI. Improvement in fine locomotor capabilities may suggest a modulation of the secondary mechanism involved in the pathology that further investigations are aimed at elucidating, such as a reduction in lesion volume, promotion of remyelination or modulation of inflammatory response. Ultimately, iNSCs have a greater latent translational value compared to the most commonly used NPCs, since their employment may overcome the ethical and practical barrier to translation faced in using fetal NSCs or the teratogenic potential of autologous induced pluripotent stem cells (iPSCs).

6) CONCLUSIONS

Spinal cord injury (SCI) is a highly debilitating pathology characterized by different mechanisms that take part in the worsening of the pathology [1]. Of particular interest is the role of reactive astrocytes in SCI as, in recent decades, their dual role in the pathology has been unravelled: while they play a beneficial role in the acute stages by, for example, limiting the spreading of the inflammatory response, in the chronic phase they can exert inhibitory functions limiting axonal regeneration [256]. This dichotomous nature has led to controversial results in pre-clinical studies. Indeed, the ablation of canonical markers, i.e. the upregulation of GFAP and vimentin, in reactive astrocytes using transgenic mice has shown both a worsening of the pathology [9] and an increased axon regeneration [12] in different studies. Moreover, improvements in functional outcomes have been observed by the application of siRNA targeted against *Gfap* and *vimentin* in rodent models of SCI [14, 15]. siRNA technologies allow for the possibility of modulating the extent and timing of gene regulation, a subtler alternative to the knockout technique in which target mRNA/proteins, and thus the effects in which they play a role, are severely ablated [16]. Thus, the possibility of finely regulating the expression of target genes might be a promising approach for modulating reactive astrocytes in CNS disease since they have showed both beneficial and detrimental roles depending of the time window. For this reason, we envision that a time-specific modulation of this phenomenon may lead to remarkable beneficial outcomes: the presence of reactive astrocytes in the acute phase of the pathology might limit the spreading of secondary damages, such as the inflammatory response, preserving the spared tissue from further damage, while the modulation of astrocyte reactivity in the sub-acute phase might prevent the formation of the glial scar at later stages and consequently diminish the detrimental effects of astrogliosis. Nevertheless, astrogliosis is finely regulated by several mechanisms, and the identification of new therapeutic targets that modulate these different activities may lead to more efficacious treatments compared to the most classical markers, such as intermediate filament upregulation; hence the interest in targeting Lcn2. Lcn2 has been shown to play several functions in the CNS upon damage or infection, such as regulation of cell cycle and apoptosis in different cell types, it can also acts as cytokine in the promotion of the inflammatory

response, but more intriguingly it has been observed that Lcn2 is mainly secreted in reactive astrocytes in the CNS[82, 185]. Moreover, it has been shown that astrocyte-secreted Lcn2 is able to perpetuate this reactive state in an autocrine manner [185]. Therefore, silencing of Lcn2 in the sub-acute phase may lead to a modulation of the inflammatory response and secondary damage upon SCI.

Small interfering RNA (siRNA) holds great promise for targeted gene silencing in therapeutic applications and the advances in nanotechnology have allowed for the development of several nanomaterials, amongst which RNA nanotechnology is the highly promising [144, 145]. In fact, RNA-based technology possesses several advantages over other materials, such as structural and functional versatility and high stability *in vivo* [172]. In particular, 3WJ-pRNA showed a remarkable potential as a powerful therapeutic platform.

Nevertheless, due to the complexity of SCI pathology, a single approach is unlikely to be sufficient for promoting recovery, whereas a combination of approaches may augment the therapeutic potential. Stem cell transplantation, having the capability of both influencing bystander mechanisms to promote regeneration in the CNS and the possibility of cell replacement by cell differentiation upon transplantation, make it one of the most promising approaches in SCI research. Furthermore, the development of innovative techniques for reprogramming somatic cells into neuronal precursors, such as iNSCs, paved the way for the possibility of autologous transplants. For these reasons, our ultimate goal is to employ 3WJ-pRNA nanotherapeutics targeting Lcn2 in order to modulate astrogliosis and increase the potential of subsequent iNSC transplantation in a murine model of moderate SCI.

To screen the efficacy of our 3WJ-pRNA we first developed and optimised a differentiation protocol for *in vitro* differentiation of NPC-derived astrocytes. Thus, we showed the reproducibility of our protocol and homogeneity of our astrocyte cultures compared to the most commonly employed astrocyte-differentiation protocols or primary astrocyte cultures. Reproducibility and homogeneity are indeed essential aspects for studies that aim to assess the efficacy of compounds, since they avoid

variability between replicate that can finally lead to misleading interpretation of knockdown results. 3WJ-pRNA nanotherapeutics use, previously having shown great potential, primarily in cancer-therapeutic approaches [210], showed non-cytotoxicity and non-immunogenic effects in this first study employing the technology in a CNS environment [211]. Moreover, we showed the efficacious knockdown of different astrogliosis-associated genes (*Gfap*, *Vim* and *Lcn2*), by significant reductions in their mRNA and protein expression using relatively small doses of siRNA-3WJ (5 nM). Furthermore, knockdown was target-specific without off-target effects.

Gfap and *Vim* knockdown were employed herein *as a proof of concept*, while *Lcn2* knockdown has been investigated as a putative therapeutic target. Indeed, the knockdown of *Lcn2* resulted in a concomitant decrease in the secretion of this neuroinflammatogen and greatly reduced the induction of pro-inflammatory genes in astrocytes exposed to astrocyte-conditioned media from activated donor astrocytes with or without treatment with Lcn2-3WJ, suggesting the important role of secreted Lcn2 to induce a pro-inflammatory phenotype in recipient astrocytes. These results therefore suggest the possibility to modulate astrocytic phenotype toward a less pro-inflammatory phenotype through RNA nanotechnology-mediated regulation of Lcn2.

Before combining 3WJ-pRNA treatment and subacute transplantation of iNSCs we aimed to characterize engrafted iNSCs in a murine model of moderate SCI. Preliminary data showed the potential of transplanted cells to promote improvements in fine locomotor functions, without inducing any allodynia or nociceptive effects. Moreover, we observed the capability of cells to integrate into the host tissue, although only a limited percentage survived upon transplantation.

In conclusion, based on the availability of a reliable *in vitro* model of astrocytes that we developed, we were able to assess the efficiency of 3WJ-pRNA in downregulating the expression of markers *and* propagators of astrogliosis. Additionally, preliminary data on iNSC transplantation suggests a potential role of grafted-cells in promoting recovery, with greater latent translational value over NPCs since their employment may overcome the ethical and practical barrier to translation faced in using fetal NPCs or the

teratogenic potential of autologous induced pluripotent stem cells (iPSCs). We therefore envision that RNA nanotechnology-mediated modulation of secondary mechanisms, such as astrogliosis, upon SCI may enhance the survival of iNSCs by favouring a more amenable environment for transplantation and integration, promoting cellular survival and leading to enhanced anatomical and functional recovery after SCI.

6.1 FUTURE AIMS

The 3WJ constructs that we employed in thus study was functionalised with siRNA, however a key characteristic of 3WJ-pRNA nanotechnology if the possibility to incorporate multiple different functionalities. Thus, future goals aim to multifunctionalization such constructs to optimise them for *in vivo* application. Chemical modifications will be included to enhance *in vivo* stability and promote intracellular delivery. Ultimately, our aim is to incorporate an astrocyte-specific aptamer in order to maximize the uptake by target cells and minimize off-target loss.

Lcn2, a novel marker in CNS diseases, will be further investigated. The involvement of astrocyte-secreted Lcn2 in different mechanisms, such as in promotion of inflammatory response, will drive further investigations on its effect on microglia and macrophage polarization, influences that we attend to address by employing astrocyte-condition medium experiments. Astrocyte-conditioned medium transfer, as key experiment in revealing the capability of secreted Lcn2 to propagate detrimental effects, will be also employed to explore the effect of the secreted protein on neuronal fate, since Lcn2 may lead to neural death [199] and the capability of 3WJ-pRNA capability to revert this process will be then assessed.

Modulation of Lcn2 expression will be assessed *in vivo* prior to cells transplantation in order to evaluate the beneficial role of Lcn2 downregulation in promoting regeneration, with a particular attention to the chronic phase of injury. Indeed, modulation of Lcn2 as pro-inflammatory actor in the central nervous system may also lead to an extended

therapeutic window for treatments of chronic phase, still the most challenging situation in SCI research.

Transplanted iNSCs will be further characterized, by evaluation of fine locomotor movements by using different behavioural assessment, such as the use of horizontal ladder to discriminate the increased capability of controlling paw placement in transplanted mice compared to controls. Differentiation of grafted-iNSCs will be further evaluate as well as modulation of secondary mechanism upon SCI and transplantation, such as quantification of lesion volume, analysis of the peri-lesional inflammatory infiltrate and secondary tissue damage axons and myelin.
Finally, combinations of 3WJ-pRNA nanotherapeutics and iNSCs transplantation, in different therapeutic time windows (chronic phase modulation represent an intriguing although challenging scenario), will be applied to our murine model of SCI to evaluate the therapeutic potential of this combinatorial approach.

7) BIBLIOGRAPHY

1. Almad, A., F.R. Sahinkaya, and D.M. McTigue, *Oligodendrocyte fate after spinal cord injury.* Neurotherapeutics, 2011. **8**(2): p. 262-73.
2. Ramer, L.M., M.S. Ramer, and E.J. Bradbury, *Restoring function after spinal cord injury: towards clinical translation of experimental strategies.* Lancet Neurol, 2014. **13**(12): p. 1241-56.
3. Moon, L. and M.B. Bunge, *From animal models to humans: strategies for promoting CNS axon regeneration and recovery of limb function after spinal cord injury.* J Neurol Phys Ther, 2005. **29**(2): p. 55-69.
4. Okano, H., et al., *Regeneration-based therapies for spinal cord injuries.* Neurochem Int, 2007. **51**(2-4): p. 68-73.
5. Schwab, J.M., et al., *Experimental strategies to promote spinal cord regeneration--an integrative perspective.* Prog Neurobiol, 2006. **78**(2): p. 91-116.
6. Thier, M., et al., *Direct conversion of fibroblasts into stably expandable neural stem cells.* Cell Stem Cell, 2012. **10**(4): p. 473-9.
7. Karimi-Abdolrezaee, S., et al., *Delayed transplantation of adult neural precursor cells promotes remyelination and functional neurological recovery after spinal cord injury.* J Neurosci, 2006. **26**(13): p. 3377-89.
8. Thuret, S., L.D. Moon, and F.H. Gage, *Therapeutic interventions after spinal cord injury.* Nat Rev Neurosci, 2006. **7**(8): p. 628-43.
9. Faulkner, J.R., et al., *Reactive astrocytes protect tissue and preserve function after spinal cord injury.* J Neurosci, 2004. **24**(9): p. 2143-55.
10. Pekny, M., U. Wilhelmsson, and M. Pekna, *The dual role of astrocyte activation and reactive gliosis.* Neurosci Lett, 2014.
11. Bush, T.G., et al., *Leukocyte infiltration, neuronal degeneration, and neurite outgrowth after ablation of scar-forming, reactive astrocytes in adult transgenic mice.* Neuron, 1999. **23**(2): p. 297-308.
12. Menet, V., et al., *Axonal plasticity and functional recovery after spinal cord injury in mice deficient in both glial fibrillary acidic protein and vimentin genes.* Proc Natl Acad Sci U S A, 2003. **100**(15): p. 8999-9004.
13. Wilhelmsson, U., et al., *Absence of glial fibrillary acidic protein and vimentin prevents hypertrophy of astrocytic processes and improves post-traumatic regeneration.* J Neurosci, 2004. **24**(21): p. 5016-21.

14. Toyooka, T., et al., *Down-regulation of glial fibrillary acidic protein and vimentin by RNA interference improves acute urinary dysfunction associated with spinal cord injury in rats.* J Neurotrauma, 2011. **28**(4): p. 607-18.
15. Ando, T., et al., *Photomechanical wave-driven delivery of siRNAs targeting intermediate filament proteins promotes functional recovery after spinal cord injury in rats.* PLoS One, 2012. **7**(12): p. e51744.
16. Voorhoeve, P.M. and R. Agami, *Knockdown stands up.* Trends Biotechnol, 2003. **21**(1): p. 2-4.
17. Rathore, K.I., et al., *Lipocalin 2 plays an immunomodulatory role and has detrimental effects after spinal cord injury.* J Neurosci, 2011. **31**(38): p. 13412-9.
18. Pai, S.I., et al., *Prospects of RNA interference therapy for cancer.* Gene Ther, 2006. **13**(6): p. 464-77.
19. Singh, M.S. and D. Peer, *RNA nanomedicines: the next generation drugs?* Curr Opin Biotechnol, 2016. **39**: p. 28-34.
20. Butovsky, O., et al., *Microglia activated by IL-4 or IFN-gamma differentially induce neurogenesis and oligodendrogenesis from adult stem/progenitor cells.* Mol Cell Neurosci, 2006. **31**(1): p. 149-60.
21. Pluchino, S., *Typical and Atypical Neural Stem Cell Niches.* Electronic Journal of Biology, 2008. **4(2)**: p. 68-78.
22. Pluchino, S., et al., *Neurosphere-derived multipotent precursors promote neuroprotection by an immunomodulatory mechanism.* Nature, 2005. **436**(7048): p. 266-71.
23. Ando, T., et al., *Propagation characteristics of photomechanical waves and their application to gene delivery into deep tissue.* Ultrasound Med Biol, 2012. **38**(1): p. 75-84.
24. Schindelin, J., et al., *Fiji: an open-source platform for biological-image analysis.* Nat Methods, 2012. **9**(7): p. 676-82.
25. Livak, K.J. and T.D. Schmittgen, *Analysis of relative gene expression data using real-time quantitative PCR and the 2(-Delta Delta C(T)) Method.* Methods, 2001. **25**(4): p. 402-8.
26. Cusimano, M., et al., *Transplanted neural stem/precursor cells instruct phagocytes and reduce secondary tissue damage in the injured spinal cord.* Brain, 2012. **135**(Pt 2): p. 447-60.

27. Basso, D.M., et al., *Basso Mouse Scale for locomotion detects differences in recovery after spinal cord injury in five common mouse strains.* J Neurotrauma, 2006. **23**(5): p. 635-59.
28. Chaplan, S.R., et al., *Quantitative assessment of tactile allodynia in the rat paw.* J Neurosci Methods, 1994. **53**(1): p. 55-63.
29. Allen, N.J., et al., *Astrocyte glypicans 4 and 6 promote formation of excitatory synapses via GluA1 AMPA receptors.* Nature, 2012. **486**(7403): p. 410-4.
30. Pascual, O., et al., *Astrocytic purinergic signaling coordinates synaptic networks.* Science, 2005. **310**(5745): p. 113-6.
31. Perea, G., M. Navarrete, and A. Araque, *Tripartite synapses: astrocytes process and control synaptic information.* Trends Neurosci, 2009. **32**(8): p. 421-31.
32. Cabezas, R., et al., *Astrocytic modulation of blood brain barrier: perspectives on Parkinson's disease.* Front Cell Neurosci, 2014. **8**: p. 211.
33. Iadecola, C. and M. Nedergaard, *Glial regulation of the cerebral microvasculature.* Nat Neurosci, 2007. **10**(11): p. 1369-76.
34. Sofroniew, M.V., *Astrogliosis.* Cold Spring Harb Perspect Biol, 2014. **7**(2): p. a020420.
35. Pekny, M., et al., *Astrocytes: a central element in neurological diseases.* Acta Neuropathol, 2016. **131**(3): p. 323-45.
36. Sofroniew, M.V. and H.V. Vinters, *Astrocytes: biology and pathology.* Acta Neuropathol, 2010. **119**(1): p. 7-35.
37. Barres, B.A., *The mystery and magic of glia: a perspective on their roles in health and disease.* Neuron, 2008. **60**(3): p. 430-40.
38. R., V., *Cellular pathology: as based upon physiological and pathological histology.* . First edition ed. Berlin: August Hirschwald, 1858 Twenty lectures delivered in the pathological institute of Berlin during the months of February, March and April, 1858 [in German].
39. Kriegstein, A. and A. Alvarez-Buylla, *The glial nature of embryonic and adult neural stem cells.* Annu Rev Neurosci, 2009. **32**: p. 149-84.
40. Fishell, G. and A.R. Kriegstein, *Neurons from radial glia: the consequences of asymmetric inheritance.* Curr Opin Neurobiol, 2003. **13**(1): p. 34-41.
41. Miyata, T., et al., *Asymmetric inheritance of radial glial fibers by cortical neurons.* Neuron, 2001. **31**(5): p. 727-41.
42. Hartfuss, E., et al., *Characterization of CNS precursor subtypes and radial glia.* Dev Biol, 2001. **229**(1): p. 15-30.

43. Gotz, M. and Y.A. Barde, *Radial glial cells defined and major intermediates between embryonic stem cells and CNS neurons.* Neuron, 2005. **46**(3): p. 369-72.
44. Ndubaku, U. and M.E. de Bellard, *Glial cells: old cells with new twists.* Acta Histochem, 2008. **110**(3): p. 182-95.
45. Konno, D., et al., *Neuroepithelial progenitors undergo LGN-dependent planar divisions to maintain self-renewability during mammalian neurogenesis.* Nat Cell Biol, 2008. **10**(1): p. 93-101.
46. Rasin, M.R., et al., *Numb and Numbl are required for maintenance of cadherin-based adhesion and polarity of neural progenitors.* Nat Neurosci, 2007. **10**(7): p. 819-27.
47. Mori, T., A. Buffo, and M. Gotz, *The novel roles of glial cells revisited: the contribution of radial glia and astrocytes to neurogenesis.* Curr Top Dev Biol, 2005. **69**: p. 67-99.
48. Weiss, S., et al., *Multipotent CNS stem cells are present in the adult mammalian spinal cord and ventricular neuroaxis.* J Neurosci, 1996. **16**(23): p. 7599-609.
49. Palmer, T.D., J. Ray, and F.H. Gage, *FGF-2-responsive neuronal progenitors reside in proliferative and quiescent regions of the adult rodent brain.* Mol Cell Neurosci, 1995. **6**(5): p. 474-86.
50. Doetsch, F., *A niche for adult neural stem cells.* Curr Opin Genet Dev, 2003. **13**(5): p. 543-50.
51. Lois, C. and A. Alvarez-Buylla, *Proliferating subventricular zone cells in the adult mammalian forebrain can differentiate into neurons and glia.* Proc Natl Acad Sci U S A, 1993. **90**(5): p. 2074-7.
52. Doetsch, F., et al., *Subventricular zone astrocytes are neural stem cells in the adult mammalian brain.* Cell, 1999. **97**(6): p. 703-16.
53. Ponti, G., et al., *Cell cycle and lineage progression of neural progenitors in the ventricular-subventricular zones of adult mice.* Proc Natl Acad Sci U S A, 2013. **110**(11): p. E1045-54.
54. Holland, E.C. and H.E. Varmus, *Basic fibroblast growth factor induces cell migration and proliferation after glia-specific gene transfer in mice.* Proc Natl Acad Sci U S A, 1998. **95**(3): p. 1218-23.
55. Seri, B., et al., *Cell types, lineage, and architecture of the germinal zone in the adult dentate gyrus.* J Comp Neurol, 2004. **478**(4): p. 359-78.
56. Doetsch, F., *The glial identity of neural stem cells.* Nat Neurosci, 2003. **6**(11): p. 1127-34.

57. Bushong, E.A., et al., *Protoplasmic astrocytes in CA1 stratum radiatum occupy separate anatomical domains.* J Neurosci, 2002. **22**(1): p. 183-92.
58. Kimelberg, H.K. and M. Nedergaard, *Functions of astrocytes and their potential as therapeutic targets.* Neurotherapeutics, 2010. **7**(4): p. 338-53.
59. Oberheim, N.A., et al., *Uniquely hominid features of adult human astrocytes.* J Neurosci, 2009. **29**(10): p. 3276-87.
60. Zhang, Y. and B.A. Barres, *Astrocyte heterogeneity: an underappreciated topic in neurobiology.* Curr Opin Neurobiol, 2010. **20**(5): p. 588-94.
61. Goncalves, C.A., M.C. Leite, and P. Nardin, *Biological and methodological features of the measurement of S100B, a putative marker of brain injury.* Clin Biochem, 2008. **41**(10-11): p. 755-63.
62. Rickmann, M. and J.R. Wolff, *Modifications of S100-protein immunoreactivity in rat brain induced by tissue preparation.* Histochem Cell Biol, 1995. **103**(2): p. 135-45.
63. Anderson, C.M. and R.A. Swanson, *Astrocyte glutamate transport: review of properties, regulation, and physiological functions.* Glia, 2000. **32**(1): p. 1-14.
64. Rickmann, M. and J.R. Wolff, *S100 protein expression in subpopulations of neurons of rat brain.* Neuroscience, 1995. **67**(4): p. 977-91.
65. Cahoy, J.D., et al., *A transcriptome database for astrocytes, neurons, and oligodendrocytes: a new resource for understanding brain development and function.* J Neurosci, 2008. **28**(1): p. 264-78.
66. Zhang, Y., et al., *An RNA-sequencing transcriptome and splicing database of glia, neurons, and vascular cells of the cerebral cortex.* J Neurosci, 2014. **34**(36): p. 11929-47.
67. Yang, Y., et al., *Molecular comparison of GLT1+ and ALDH1L1+ astrocytes in vivo in astroglial reporter mice.* Glia, 2011. **59**(2): p. 200-7.
68. Chung, W.S., et al., *Astrocytes mediate synapse elimination through MEGF10 and MERTK pathways.* Nature, 2013. **504**(7480): p. 394-400.
69. Pekna, M., M. Pekny, and M. Nilsson, *Modulation of neural plasticity as a basis for stroke rehabilitation.* Stroke, 2012. **43**(10): p. 2819-28.
70. Araque, A., et al., *Tripartite synapses: glia, the unacknowledged partner.* Trends Neurosci, 1999. **22**(5): p. 208-15.
71. Agulhon, C., et al., *Calcium Signaling and Gliotransmission in Normal vs. Reactive Astrocytes.* Front Pharmacol, 2012. **3**: p. 139.
72. Halassa, M.M., T. Fellin, and P.G. Haydon, *The tripartite synapse: roles for gliotransmission in health and disease.* Trends Mol Med, 2007. **13**(2): p. 54-63.

73. Simard, M. and M. Nedergaard, *The neurobiology of glia in the context of water and ion homeostasis.* Neuroscience, 2004. **129**(4): p. 877-96.
74. Brown, A.M. and B.R. Ransom, *Astrocyte glycogen and brain energy metabolism.* Glia, 2007. **55**(12): p. 1263-71.
75. Rouach, N., et al., *Astroglial metabolic networks sustain hippocampal synaptic transmission.* Science, 2008. **322**(5907): p. 1551-5.
76. Sofroniew, M.V., *Astrogliosis.* Cold Spring Harb Perspect Biol, 2015. **7**(2): p. a020420.
77. Sofroniew, M.V., *Molecular dissection of reactive astrogliosis and glial scar formation.* Trends Neurosci, 2009. **32**(12): p. 638-47.
78. Filous, A.R. and J. Silver, *"Targeting astrocytes in CNS injury and disease: A translational research approach".* Prog Neurobiol, 2016.
79. Burda, J.E., A.M. Bernstein, and M.V. Sofroniew, *Astrocyte roles in traumatic brain injury.* Exp Neurol, 2016. **275 Pt 3**: p. 305-15.
80. Verkhratsky, A., et al., *Astroglial calcium signalling in Alzheimer's disease.* Biochem Biophys Res Commun, 2016.
81. Maragakis, N.J. and J.D. Rothstein, *Mechanisms of Disease: astrocytes in neurodegenerative disease.* Nat Clin Pract Neurol, 2006. **2**(12): p. 679-89.
82. Zamanian, J.L., et al., *Genomic analysis of reactive astrogliosis.* J Neurosci, 2012. **32**(18): p. 6391-410.
83. Silver, J. and J.H. Miller, *Regeneration beyond the glial scar.* Nat Rev Neurosci, 2004. **5**(2): p. 146-56.
84. Verkhratsky, A., et al., *Neurological diseases as primary gliopathies: a reassessment of neurocentrism.* ASN Neuro, 2012. **4**(3).
85. Rothstein, J.D., L.J. Martin, and R.W. Kuncl, *Decreased glutamate transport by the brain and spinal cord in amyotrophic lateral sclerosis.* N Engl J Med, 1992. **326**(22): p. 1464-8.
86. Guo, H., et al., *Increased expression of the glial glutamate transporter EAAT2 modulates excitotoxicity and delays the onset but not the outcome of ALS in mice.* Hum Mol Genet, 2003. **12**(19): p. 2519-32.
87. Nagele, R.G., et al., *Contribution of glial cells to the development of amyloid plaques in Alzheimer's disease.* Neurobiol Aging, 2004. **25**(5): p. 663-74.
88. Vis, J.C., et al., *Connexin expression in Huntington's diseased human brain.* Cell Biol Int, 1998. **22**(11-12): p. 837-47.
89. Noristani, H.N., et al., *Spinal cord injury induces astroglial conversion towards neuronal lineage.* Mol Neurodegener, 2016. **11**(1): p. 68.

90. O'Callaghan, J.P., et al., *Early activation of STAT3 regulates reactive astrogliosis induced by diverse forms of neurotoxicity.* PLoS One, 2014. **9**(7): p. e102003.
91. Herrmann, J.E., et al., *STAT3 is a critical regulator of astrogliosis and scar formation after spinal cord injury.* J Neurosci, 2008. **28**(28): p. 7231-43.
92. Okada, S., et al., *Conditional ablation of Stat3 or Socs3 discloses a dual role for reactive astrocytes after spinal cord injury.* Nat Med, 2006. **12**(7): p. 829-34.
93. Sofroniew, M.V., *Multiple roles for astrocytes as effectors of cytokines and inflammatory mediators.* Neuroscientist, 2014. **20**(2): p. 160-72.
94. Anderson, M.A., et al., *Astrocyte scar formation aids central nervous system axon regeneration.* Nature, 2016. **532**(7598): p. 195-200.
95. Fawcett, J.W., *Overcoming inhibition in the damaged spinal cord.* J Neurotrauma, 2006. **23**(3-4): p. 371-83.
96. Pekny, M. and M. Nilsson, *Astrocyte activation and reactive gliosis.* Glia, 2005. **50**(4): p. 427-34.
97. Swanson, R.A., W. Ying, and T.M. Kauppinen, *Astrocyte influences on ischemic neuronal death.* Curr Mol Med, 2004. **4**(2): p. 193-205.
98. Martinez, F.O. and S. Gordon, *The M1 and M2 paradigm of macrophage activation: time for reassessment.* F1000Prime Rep, 2014. **6**: p. 13.
99. Liddelow, S.A., et al., *Neurotoxic reactive astrocytes are induced by activated microglia.* Nature, 2017.
100. Anderson, M.A., Y. Ao, and M.V. Sofroniew, *Heterogeneity of reactive astrocytes.* Neurosci Lett, 2014. **565**: p. 23-9.
101. Brunet, J.F., et al., *Early acquisition of typical metabolic features upon differentiation of mouse neural stem cells into astrocytes.* Glia, 2004. **46**(1): p. 8-17.
102. Losciuto, S., et al., *An efficient method to limit microglia-dependent effects in astroglial cultures.* J Neurosci Methods, 2012. **207**(1): p. 59-71.
103. Raponi, E., et al., *S100B expression defines a state in which GFAP-expressing cells lose their neural stem cell potential and acquire a more mature developmental stage.* Glia, 2007. **55**(2): p. 165-77.
104. Morrison, R.S. and J. de Vellis, *Growth of purified astrocytes in a chemically defined medium.* Proc Natl Acad Sci U S A, 1981. **78**(11): p. 7205-9.
105. Roybon, L., et al., *Human stem cell-derived spinal cord astrocytes with defined mature or reactive phenotypes.* Cell Rep, 2013. **4**(5): p. 1035-48.

106. Zhang, P.W., et al., *Generation of GFAP::GFP astrocyte reporter lines from human adult fibroblast-derived iPS cells using zinc-finger nuclease technology.* Glia, 2016. **64**(1): p. 63-75.
107. Mor, E., et al., *Species-specific microRNA roles elucidated following astrocyte activation.* Nucleic Acids Res, 2011. **39**(9): p. 3710-23.
108. Brambilla, R., et al., *Inhibition of astroglial nuclear factor kappaB reduces inflammation and improves functional recovery after spinal cord injury.* J Exp Med, 2005. **202**(1): p. 145-56.
109. Chen, K., et al., *RNA-seq characterization of spinal cord injury transcriptome in acute/subacute phases: a resource for understanding the pathology at the systems level.* PLoS One, 2013. **8**(8): p. e72567.
110. Ceyzeriat, K., et al., *The complex STATEs of astrocyte reactivity: How are they controlled by the JAK-STAT3 pathway?* Neuroscience, 2016. **330**: p. 205-18.
111. Tyzack, G.E., et al., *Astrocyte response to motor neuron injury promotes structural synaptic plasticity via STAT3-regulated TSP-1 expression.* Nat Commun, 2014. **5**: p. 4294.
112. Oliva, A.A., Jr., et al., *STAT3 signaling after traumatic brain injury.* J Neurochem, 2012. **120**(5): p. 710-20.
113. LeComte, M.D., et al., *Notch1-STAT3-ETBR signaling axis controls reactive astrocyte proliferation after brain injury.* Proc Natl Acad Sci U S A, 2015. **112**(28): p. 8726-31.
114. Sarafian, T.A., et al., *Disruption of astrocyte STAT3 signaling decreases mitochondrial function and increases oxidative stress in vitro.* PLoS One, 2010. **5**(3): p. e9532.
115. Krencik, R. and S.C. Zhang, *Directed differentiation of functional astroglial subtypes from human pluripotent stem cells.* Nat Protoc, 2011. **6**(11): p. 1710-7.
116. Brahmachari, S., Y.K. Fung, and K. Pahan, *Induction of glial fibrillary acidic protein expression in astrocytes by nitric oxide.* J Neurosci, 2006. **26**(18): p. 4930-9.
117. Gorina, R., et al., *Astrocyte TLR4 activation induces a proinflammatory environment through the interplay between MyD88-dependent NFkappaB signaling, MAPK, and Jak1/Stat1 pathways.* Glia, 2011. **59**(2): p. 242-55.
118. Hamby, M.E., et al., *Inflammatory mediators alter the astrocyte transcriptome and calcium signaling elicited by multiple G-protein-coupled receptors.* J Neurosci, 2012. **32**(42): p. 14489-510.
119. Pang, Y., Z. Cai, and P.G. Rhodes, *Analysis of genes differentially expressed in astrocytes stimulated with lipopolysaccharide using cDNA arrays.* Brain Res, 2001. **914**(1-2): p. 15-22.

120. Tarassishin, L., H.S. Suh, and S.C. Lee, *LPS and IL-1 differentially activate mouse and human astrocytes: role of CD14.* Glia, 2014. **62**(6): p. 999-1013.
121. Yong, V.W., et al., *Gamma-interferon promotes proliferation of adult human astrocytes in vitro and reactive gliosis in the adult mouse brain in vivo.* Proc Natl Acad Sci U S A, 1991. **88**(16): p. 7016-20.
122. Lange, S.C., et al., *Primary cultures of astrocytes: their value in understanding astrocytes in health and disease.* Neurochem Res, 2012. **37**(11): p. 2569-88.
123. Chou, R.C. and T.J. Langan, *In vitro synchronization of mammalian astrocytic cultures by serum deprivation.* Brain Res Brain Res Protoc, 2003. **11**(3): p. 162-7.
124. Kim, S.U., et al., *Culture of purified rat astrocytes in serum-free medium supplemented with mitogen.* Brain Res, 1983. **274**(1): p. 79-86.
125. Shaltouki, A., et al., *Efficient generation of astrocytes from human pluripotent stem cells in defined conditions.* Stem Cells, 2013. **31**(5): p. 941-52.
126. Cragnolini, A.B., et al., *Nerve growth factor attenuates proliferation of astrocytes via the p75 neurotrophin receptor.* Glia, 2009. **57**(13): p. 1386-92.
127. Codeluppi, S., et al., *Influence of rat substrain and growth conditions on the characteristics of primary cultures of adult rat spinal cord astrocytes.* J Neurosci Methods, 2011. **197**(1): p. 118-27.
128. Pasca, A.M., et al., *Functional cortical neurons and astrocytes from human pluripotent stem cells in 3D culture.* Nat Methods, 2015. **12**(7): p. 671-8.
129. Placone, A.L., et al., *Human astrocytes develop physiological morphology and remain quiescent in a novel 3D matrix.* Biomaterials, 2015. **42**: p. 134-43.
130. Georges, P.C., et al., *Matrices with compliance comparable to that of brain tissue select neuronal over glial growth in mixed cortical cultures.* Biophys J, 2006. **90**(8): p. 3012-8.
131. Kang, W., et al., *Astrocyte activation is suppressed in both normal and injured brain by FGF signaling.* Proc Natl Acad Sci U S A, 2014. **111**(29): p. E2987-95.
132. Reilly, J.F., P.A. Maher, and V.G. Kumari, *Regulation of astrocyte GFAP expression by TGF-beta1 and FGF-2.* Glia, 1998. **22**(2): p. 202-10.
133. Ye, L., et al., *The Role of bFGF in the Excessive Activation of Astrocytes Is Related to the Inhibition of TLR4/NFkappaB Signals.* Int J Mol Sci, 2015. **17**(1).
134. Hashioka, S., A. Klegeris, and P.L. McGeer, *Proton pump inhibitors reduce interferon-gamma-induced neurotoxicity and STAT3 phosphorylation of human astrocytes.* Glia, 2011. **59**(5): p. 833-40.

135. Halonen, S.K., et al., *Microarray analysis of IFN-gamma response genes in astrocytes.* J Neuroimmunol, 2006. **175**(1-2): p. 19-30.
136. Dong, Y. and E.N. Benveniste, *Immune function of astrocytes.* Glia, 2001. **36**(2): p. 180-90.
137. Carpentier, P.A., et al., *Differential activation of astrocytes by innate and adaptive immune stimuli.* Glia, 2005. **49**(3): p. 360-74.
138. Saha, R.N. and K. Pahan, *Signals for the induction of nitric oxide synthase in astrocytes.* Neurochem Int, 2006. **49**(2): p. 154-63.
139. Van Wagoner, N.J. and E.N. Benveniste, *Interleukin-6 expression and regulation in astrocytes.* J Neuroimmunol, 1999. **100**(1-2): p. 124-39.
140. Hariri, R.J., et al., *Traumatic injury induces interleukin-6 production by human astrocytes.* Brain Res, 1994. **636**(1): p. 139-42.
141. Nakano, Y., et al., *Astrocytic TLR4 expression and LPS-induced nuclear translocation of STAT3 in the sensory circumventricular organs of adult mouse brain.* J Neuroimmunol, 2015. **278**: p. 144-58.
142. Kim, B.Y., J.T. Rutka, and W.C. Chan, *Nanomedicine.* N Engl J Med, 2010. **363**(25): p. 2434-43.
143. Dawidczyk, C.M., L.M. Russell, and P.C. Searson, *Nanomedicines for cancer therapy: state-of-the-art and limitations to pre-clinical studies that hinder future developments.* Front Chem, 2014. **2**: p. 69.
144. Chen, J. and J. Xie, *Progress on RNAi-based molecular medicines.* Int J Nanomedicine, 2012. **7**: p. 3971-80.
145. Guo, P., *The emerging field of RNA nanotechnology.* Nat Nanotechnol, 2010. **5**(12): p. 833-42.
146. Parveen, S., R. Misra, and S.K. Sahoo, *Nanoparticles: a boon to drug delivery, therapeutics, diagnostics and imaging.* Nanomedicine, 2012. **8**(2): p. 147-66.
147. Friberg, S. and A.M. Nystrom, *NANOMEDICINE: will it offer possibilities to overcome multiple drug resistance in cancer?* J Nanobiotechnology, 2016. **14**: p. 17.
148. Rizzo, L.Y., et al., *Recent progress in nanomedicine: therapeutic, diagnostic and theranostic applications.* Curr Opin Biotechnol, 2013. **24**(6): p. 1159-66.
149. Smith, J.E., et al., *Aptamer-conjugated nanoparticles for the collection and detection of multiple cancer cells.* Anal Chem, 2007. **79**(8): p. 3075-82.
150. Nune, S.K., et al., *Nanoparticles for biomedical imaging.* Expert Opin Drug Deliv, 2009. **6**(11): p. 1175-94.

151. Shu, D., et al., *Thermodynamically stable RNA three-way junction for constructing multifunctional nanoparticles for delivery of therapeutics.* Nat Nanotechnol, 2011. **6**(10): p. 658-67.
152. Miller, V.M., et al., *Targeting Alzheimer's disease genes with RNA interference: an efficient strategy for silencing mutant alleles.* Nucleic Acids Res, 2004. **32**(2): p. 661-8.
153. Boden, D., et al., *Human immunodeficiency virus type 1 escape from RNA interference.* J Virol, 2003. **77**(21): p. 11531-5.
154. Guo, P., et al., *Engineering RNA for targeted siRNA delivery and medical application.* Adv Drug Deliv Rev, 2010. **62**(6): p. 650-66.
155. Devi, G.R., *siRNA-based approaches in cancer therapy.* Cancer Gene Ther, 2006. **13**(9): p. 819-29.
156. Hamilton, A.J. and D.C. Baulcombe, *A species of small antisense RNA in posttranscriptional gene silencing in plants.* Science, 1999. **286**(5441): p. 950-2.
157. Aagaard, L. and J.J. Rossi, *RNAi therapeutics: principles, prospects and challenges.* Adv Drug Deliv Rev, 2007. **59**(2-3): p. 75-86.
158. Pratt, A.J. and I.J. MacRae, *The RNA-induced silencing complex: a versatile gene-silencing machine.* J Biol Chem, 2009. **284**(27): p. 17897-901.
159. Carthew, R.W. and E.J. Sontheimer, *Origins and Mechanisms of miRNAs and siRNAs.* Cell, 2009. **136**(4): p. 642-55.
160. Wilson, R.C. and J.A. Doudna, *Molecular mechanisms of RNA interference.* Annu Rev Biophys, 2013. **42**: p. 217-39.
161. Ui-Tei, K., et al., *Guidelines for the selection of highly effective siRNA sequences for mammalian and chick RNA interference.* Nucleic Acids Res, 2004. **32**(3): p. 936-48.
162. Taxman, D.J., et al., *Criteria for effective design, construction, and gene knockdown by shRNA vectors.* BMC Biotechnol, 2006. **6**: p. 7.
163. Moore, C.B., et al., *Short hairpin RNA (shRNA): design, delivery, and assessment of gene knockdown.* Methods Mol Biol, 2010. **629**: p. 141-58.
164. Chi, J.T., et al., *Genomewide view of gene silencing by small interfering RNAs.* Proc Natl Acad Sci U S A, 2003. **100**(11): p. 6343-6.
165. Semizarov, D., et al., *Specificity of short interfering RNA determined through gene expression signatures.* Proc Natl Acad Sci U S A, 2003. **100**(11): p. 6347-52.
166. Jackson, A.L., et al., *Expression profiling reveals off-target gene regulation by RNAi.* Nat Biotechnol, 2003. **21**(6): p. 635-7.
167. Reynolds, A., et al., *Induction of the interferon response by siRNA is cell type- and duplex length-dependent.* RNA, 2006. **12**(6): p. 988-93.

168. Jackson, A.L. and P.S. Linsley, *Recognizing and avoiding siRNA off-target effects for target identification and therapeutic application.* Nat Rev Drug Discov, 2010. **9**(1): p. 57-67.

169. Behlke, M.A., *Progress towards in vivo use of siRNAs.* Mol Ther, 2006. **13**(4): p. 644-70.

170. Gavrilov, K. and W.M. Saltzman, *Therapeutic siRNA: principles, challenges, and strategies.* Yale J Biol Med, 2012. **85**(2): p. 187-200.

171. Guo, P., et al., *Inter-RNA interaction of phage phi29 pRNA to form a hexameric complex for viral DNA transportation.* Mol Cell, 1998. **2**(1): p. 149-55.

172. Shu, Y., et al., *Stable RNA nanoparticles as potential new generation drugs for cancer therapy.* Adv Drug Deliv Rev, 2014. **66**: p. 74-89.

173. Shu, Y., et al., *Fabrication of 14 different RNA nanoparticles for specific tumor targeting without accumulation in normal organs.* RNA, 2013. **19**(6): p. 767-77.

174. Suk, K., *Lipocalin-2 as a therapeutic target for brain injury: An astrocentric perspective.* Prog Neurobiol, 2016. **144**: p. 158-72.

175. Jha, M.K., et al., *Diverse functional roles of lipocalin-2 in the central nervous system.* Neurosci Biobehav Rev, 2015. **49**: p. 135-56.

176. Flower, D.R., A.C. North, and C.E. Sansom, *The lipocalin protein family: structural and sequence overview.* Biochim Biophys Acta, 2000. **1482**(1-2): p. 9-24.

177. Flower, D.R., A.C. North, and T.K. Attwood, *Mouse oncogene protein 24p3 is a member of the lipocalin protein family.* Biochem Biophys Res Commun, 1991. **180**(1): p. 69-74.

178. Hraba-Renevey, S., et al., *SV40-induced expression of mouse gene 24p3 involves a post-transcriptional mechanism.* Oncogene, 1989. **4**(5): p. 601-8.

179. Cowland, J.B. and N. Borregaard, *Molecular characterization and pattern of tissue expression of the gene for neutrophil gelatinase-associated lipocalin from humans.* Genomics, 1997. **45**(1): p. 17-23.

180. Cowland, J.B., et al., *Neutrophil gelatinase-associated lipocalin is up-regulated in human epithelial cells by IL-1 beta, but not by TNF-alpha.* J Immunol, 2003. **171**(12): p. 6630-9.

181. Devireddy, L.R., et al., *A cell-surface receptor for lipocalin 24p3 selectively mediates apoptosis and iron uptake.* Cell, 2005. **123**(7): p. 1293-305.

182. Hvidberg, V., et al., *The endocytic receptor megalin binds the iron transporting neutrophil-gelatinase-associated lipocalin with high affinity and mediates its cellular uptake.* FEBS Lett, 2005. **579**(3): p. 773-7.

183. Jha, M.K., et al., *The pivotal role played by lipocalin-2 in chronic inflammatory pain.* Exp Neurol, 2014. **254**: p. 41-53.
184. Lee, S., et al., *A dual role of lipocalin 2 in the apoptosis and deramification of activated microglia.* J Immunol, 2007. **179**(5): p. 3231-41.
185. Lee, S., et al., *Lipocalin-2 is an autocrine mediator of reactive astrocytosis.* J Neurosci, 2009. **29**(1): p. 234-49.
186. Gajera, C.R., et al., *LRP2 in ependymal cells regulates BMP signaling in the adult neurogenic niche.* J Cell Sci, 2010. **123**(Pt 11): p. 1922-30.
187. Wicher, G., et al., *Low-density lipoprotein receptor-related protein (LRP)-2/megalin is transiently expressed in a subpopulation of neural progenitors in the embryonic mouse spinal cord.* J Comp Neurol, 2005. **492**(2): p. 123-31.
188. Wu, B., et al., *Network based analyses of gene expression profile of LCN2 overexpression in esophageal squamous cell carcinoma.* Sci Rep, 2014. **4**: p. 5403.
189. Goetz, D.H., et al., *The neutrophil lipocalin NGAL is a bacteriostatic agent that interferes with siderophore-mediated iron acquisition.* Mol Cell, 2002. **10**(5): p. 1033-43.
190. Cherayil, B.J., *The role of iron in the immune response to bacterial infection.* Immunol Res, 2011. **50**(1): p. 1-9.
191. Neilands, J.B., *Siderophores: structure and function of microbial iron transport compounds.* J Biol Chem, 1995. **270**(45): p. 26723-6.
192. Flo, T.H., et al., *Lipocalin 2 mediates an innate immune response to bacterial infection by sequestrating iron.* Nature, 2004. **432**(7019): p. 917-21.
193. Lee, S., et al., *Regulation by lipocalin-2 of neuronal cell death, migration, and morphology.* J Neurosci Res, 2012. **90**(3): p. 540-50.
194. Lee, S., et al., *Lipocalin-2 Is a chemokine inducer in the central nervous system: role of chemokine ligand 10 (CXCL10) in lipocalin-2-induced cell migration.* J Biol Chem, 2011. **286**(51): p. 43855-70.
195. Rubinstein, T., M. Pitashny, and C. Putterman, *The novel role of neutrophil gelatinase-B associated lipocalin (NGAL)/Lipocalin-2 as a biomarker for lupus nephritis.* Autoimmun Rev, 2008. **7**(3): p. 229-34.
196. Berard, J.L., et al., *Lipocalin 2 is a novel immune mediator of experimental autoimmune encephalomyelitis pathogenesis and is modulated in multiple sclerosis.* Glia, 2012. **60**(7): p. 1145-59.
197. Roth, G.A., et al., *Lipocalin-2 serum levels are increased in acute hepatic failure.* Transplant Proc, 2013. **45**(1): p. 241-4.

198. Jang, E., et al., *Secreted protein lipocalin-2 promotes microglial M1 polarization.* FASEB J, 2013. **27**(3): p. 1176-90.
199. Bi, F., et al., *Reactive astrocytes secrete lcn2 to promote neuron death.* Proc Natl Acad Sci U S A, 2013. **110**(10): p. 4069-74.
200. Jin, M., E. Jang, and K. Suk, *Lipocalin-2 Acts as a Neuroinflammatogen in Lipopolysaccharide-injected Mice.* Exp Neurobiol, 2014. **23**(2): p. 155-62.
201. Listwak, S.J., P. Rathore, and M. Herkenham, *Minimal NF-kappaB activity in neurons.* Neuroscience, 2013. **250**: p. 282-99.
202. Shiratori-Hayashi, M., et al., *STAT3-dependent reactive astrogliosis in the spinal dorsal horn underlies chronic itch.* Nat Med, 2015. **21**(8): p. 927-31.
203. Orihuela, R., C.A. McPherson, and G.J. Harry, *Microglial M1/M2 polarization and metabolic states.* Br J Pharmacol, 2016. **173**(4): p. 649-65.
204. Jang, E., et al., *Phenotypic polarization of activated astrocytes: the critical role of lipocalin-2 in the classical inflammatory activation of astrocytes.* J Immunol, 2013. **191**(10): p. 5204-19.
205. Schmittgen, T.D. and B.A. Zakrajsek, *Effect of experimental treatment on housekeeping gene expression: validation by real-time, quantitative RT-PCR.* J Biochem Biophys Methods, 2000. **46**(1-2): p. 69-81.
206. Kim, D.H., et al., *Interferon induction by siRNAs and ssRNAs synthesized by phage polymerase.* Nat Biotechnol, 2004. **22**(3): p. 321-5.
207. Hutvagner, G., et al., *Sequence-specific inhibition of small RNA function.* PLoS Biol, 2004. **2**(4): p. E98.
208. Shu, Y., et al., *Assembly of multifunctional phi29 pRNA nanoparticles for specific delivery of siRNA and other therapeutics to targeted cells.* Methods, 2011. **54**(2): p. 204-14.
209. Zhou, J., et al., *Dual functional RNA nanoparticles containing phi29 motor pRNA and anti-gp120 aptamer for cell-type specific delivery and HIV-1 inhibition.* Methods, 2011. **54**(2): p. 284-94.
210. Shu, D., et al., *Systemic Delivery of Anti-miRNA for Suppression of Triple Negative Breast Cancer Utilizing RNA Nanotechnology.* ACS Nano, 2015. **9**(10): p. 9731-40.
211. Lee, T.J., et al., *RNA Nanoparticle-Based Targeted Therapy for Glioblastoma through Inhibition of Oncogenic miR-21.* Mol Ther, 2017.
212. Kim, D.H., et al., *Synthetic dsRNA Dicer substrates enhance RNAi potency and efficacy.* Nat Biotechnol, 2005. **23**(2): p. 222-6.

213. Schlee, M. and G. Hartmann, *The chase for the RIG-I ligand--recent advances.* Mol Ther, 2010. **18**(7): p. 1254-62.
214. Goubau, D., et al., *Antiviral immunity via RIG-I-mediated recognition of RNA bearing 5'-diphosphates.* Nature, 2014. **514**(7522): p. 372-5.
215. Loo, Y.M. and M. Gale, Jr., *Immune signaling by RIG-I-like receptors.* Immunity, 2011. **34**(5): p. 680-92.
216. de Rivero Vaccari, J.P., et al., *Astrogliosis involves activation of retinoic acid-inducible gene-like signaling in the innate immune response after spinal cord injury.* Glia, 2012. **60**(3): p. 414-21.
217. Thorne, R.G. and C. Nicholson, *In vivo diffusion analysis with quantum dots and dextrans predicts the width of brain extracellular space.* Proc Natl Acad Sci U S A, 2006. **103**(14): p. 5567-72.
218. de Jonge, H.J., et al., *Evidence based selection of housekeeping genes.* PLoS One, 2007. **2**(9): p. e898.
219. Robbins, M., A. Judge, and I. MacLachlan, *siRNA and innate immunity.* Oligonucleotides, 2009. **19**(2): p. 89-102.
220. Thompson, A.J. and S.A. Locarnini, *Toll-like receptors, RIG-I-like RNA helicases and the antiviral innate immune response.* Immunol Cell Biol, 2007. **85**(6): p. 435-45.
221. Jensen, S. and A.R. Thomsen, *Sensing of RNA viruses: a review of innate immune receptors involved in recognizing RNA virus invasion.* J Virol, 2012. **86**(6): p. 2900-10.
222. Grimm, D., et al., *Fatality in mice due to oversaturation of cellular microRNA/short hairpin RNA pathways.* Nature, 2006. **441**(7092): p. 537-41.
223. Hong, S.W., et al., *Target gene abundance contributes to the efficiency of siRNA-mediated gene silencing.* Nucleic Acid Ther, 2014. **24**(3): p. 192-8.
224. Hu, X., et al., *Relative gene-silencing efficiencies of small interfering RNAs targeting sense and antisense transcripts from the same genetic locus.* Nucleic Acids Res, 2004. **32**(15): p. 4609-17.
225. Kim, S. and P.A. Coulombe, *Intermediate filament scaffolds fulfill mechanical, organizational, and signaling functions in the cytoplasm.* Genes Dev, 2007. **21**(13): p. 1581-97.
226. Chiu, F.C. and J.E. Goldman, *Synthesis and turnover of cytoskeletal proteins in cultured astrocytes.* J Neurochem, 1984. **42**(1): p. 166-74.
227. McDonald, J.W. and C. Sadowsky, *Spinal-cord injury.* Lancet, 2002. **359**(9304): p. 417-25.

228. Martino, G. and S. Pluchino, *The therapeutic potential of neural stem cells.* Nat Rev Neurosci, 2006. **7**(5): p. 395-406.
229. Bickenbach, J., et al., *A global picture of spinal cord injury.* International Perspectives on Spinal Cord Injury, 2013: p. 11-41.
230. Devivo, M.J., *Epidemiology of traumatic spinal cord injury: trends and future implications.* Spinal Cord, 2012. **50**(5): p. 365-72.
231. Lee, B.B., et al., *The global map for traumatic spinal cord injury epidemiology: update 2011, global incidence rate.* Spinal Cord, 2014. **52**(2): p. 110-6.
232. Bunge, R.P., et al., *Observations on the pathology of human spinal cord injury. A review and classification of 22 new cases with details from a case of chronic cord compression with extensive focal demyelination.* Adv Neurol, 1993. **59**: p. 75-89.
233. Norenberg, M.D., J. Smith, and A. Marcillo, *The pathology of human spinal cord injury: defining the problems.* J Neurotrauma, 2004. **21**(4): p. 429-40.
234. Kwon, B.K., et al., *Pathophysiology and pharmacologic treatment of acute spinal cord injury.* Spine J, 2004. **4**(4): p. 451-64.
235. Silva, N.A., et al., *From basics to clinical: a comprehensive review on spinal cord injury.* Prog Neurobiol, 2014. **114**: p. 25-57.
236. Bareyre, F.M. and M.E. Schwab, *Inflammation, degeneration and regeneration in the injured spinal cord: insights from DNA microarrays.* Trends Neurosci, 2003. **26**(10): p. 555-63.
237. Tator, C.H. and M.G. Fehlings, *Review of the secondary injury theory of acute spinal cord trauma with emphasis on vascular mechanisms.* J Neurosurg, 1991. **75**(1): p. 15-26.
238. Hall, E.D. and J.M. Braughler, *Free radicals in CNS injury.* Res Publ Assoc Res Nerv Ment Dis, 1993. **71**: p. 81-105.
239. Agrawal, S.K. and M.G. Fehlings, *Role of NMDA and non-NMDA ionotropic glutamate receptors in traumatic spinal cord axonal injury.* J Neurosci, 1997. **17**(3): p. 1055-63.
240. Park, E., A.A. Velumian, and M.G. Fehlings, *The role of excitotoxicity in secondary mechanisms of spinal cord injury: a review with an emphasis on the implications for white matter degeneration.* J Neurotrauma, 2004. **21**(6): p. 754-74.
241. Kwo, S., W. Young, and V. Decrescito, *Spinal cord sodium, potassium, calcium, and water concentration changes in rats after graded contusion injury.* J Neurotrauma, 1989. **6**(1): p. 13-24.
242. Beattie, M.S., A.A. Farooqui, and J.C. Bresnahan, *Review of current evidence for apoptosis after spinal cord injury.* J Neurotrauma, 2000. **17**(10): p. 915-25.

243. Zhang, N., et al., *Inflammation & apoptosis in spinal cord injury.* Indian J Med Res, 2012. **135**: p. 287-96.
244. Crowe, M.J., et al., *Apoptosis and delayed degeneration after spinal cord injury in rats and monkeys.* Nat Med, 1997. **3**(1): p. 73-6.
245. Emery, E., et al., *Apoptosis after traumatic human spinal cord injury.* J Neurosurg, 1998. **89**(6): p. 911-20.
246. Donnelly, D.J. and P.G. Popovich, *Inflammation and its role in neuroprotection, axonal regeneration and functional recovery after spinal cord injury.* Exp Neurol, 2008. **209**(2): p. 378-88.
247. Rowland, J.W., et al., *Current status of acute spinal cord injury pathophysiology and emerging therapies: promise on the horizon.* Neurosurg Focus, 2008. **25**(5): p. E2.
248. Schwab, J.M., et al., *The paradox of chronic neuroinflammation, systemic immune suppression, autoimmunity after traumatic chronic spinal cord injury.* Exp Neurol, 2014. **258**: p. 121-9.
249. Yan, P., et al., *Cellular localization of tumor necrosis factor-alpha following acute spinal cord injury in adult rats.* J Neurotrauma, 2001. **18**(5): p. 563-8.
250. Bethea, J.R., et al., *Systemically administered interleukin-10 reduces tumor necrosis factor-alpha production and significantly improves functional recovery following traumatic spinal cord injury in rats.* J Neurotrauma, 1999. **16**(10): p. 851-63.
251. Kim, G.M., et al., *Tumor necrosis factor receptor deletion reduces nuclear factor-kappaB activation, cellular inhibitor of apoptosis protein 2 expression, and functional recovery after traumatic spinal cord injury.* J Neurosci, 2001. **21**(17): p. 6617-25.
252. Wanner, I.B., et al., *Glial scar borders are formed by newly proliferated, elongated astrocytes that interact to corral inflammatory and fibrotic cells via STAT3-dependent mechanisms after spinal cord injury.* J Neurosci, 2013. **33**(31): p. 12870-86.
253. Busch, S.A. and J. Silver, *The role of extracellular matrix in CNS regeneration.* Curr Opin Neurobiol, 2007. **17**(1): p. 120-7.
254. McKeon, R.J., M.J. Jurynec, and C.R. Buck, *The chondroitin sulfate proteoglycans neurocan and phosphacan are expressed by reactive astrocytes in the chronic CNS glial scar.* J Neurosci, 1999. **19**(24): p. 10778-88.
255. McKeon, R.J., et al., *Reduction of neurite outgrowth in a model of glial scarring following CNS injury is correlated with the expression of inhibitory molecules on reactive astrocytes.* J Neurosci, 1991. **11**(11): p. 3398-411.
256. Fitch, M.T. and J. Silver, *CNS injury, glial scars, and inflammation: Inhibitory extracellular matrices and regeneration failure.* Exp Neurol, 2008. **209**(2): p. 294-301.

257. Pasterkamp, R.J., et al., *Evidence for a role of the chemorepellent semaphorin III and its receptor neuropilin-1 in the regeneration of primary olfactory axons.* J Neurosci, 1998. **18**(23): p. 9962-76.
258. Miranda, J.D., et al., *Induction of Eph B3 after spinal cord injury.* Exp Neurol, 1999. **156**(1): p. 218-22.
259. Borisoff, J.F., et al., *Suppression of Rho-kinase activity promotes axonal growth on inhibitory CNS substrates.* Mol Cell Neurosci, 2003. **22**(3): p. 405-16.
260. Smith-Thomas, L.C., et al., *Increased axon regeneration in astrocytes grown in the presence of proteoglycan synthesis inhibitors.* J Cell Sci, 1995. **108 (Pt 3)**: p. 1307-15.
261. Rolls, A., R. Shechter, and M. Schwartz, *The bright side of the glial scar in CNS repair.* Nat Rev Neurosci, 2009. **10**(3): p. 235-41.
262. Bradbury, E.J., et al., *Chondroitinase ABC promotes functional recovery after spinal cord injury.* Nature, 2002. **416**(6881): p. 636-40.
263. Bradbury, E.J. and L.M. Carter, *Manipulating the glial scar: chondroitinase ABC as a therapy for spinal cord injury.* Brain Res Bull, 2011. **84**(4-5): p. 306-16.
264. Zhang, N., et al., *Evaluation of spinal cord injury animal models.* Neural Regen Res, 2014. **9**(22): p. 2008-12.
265. Stokes, B.T. and L.B. Jakeman, *Experimental modelling of human spinal cord injury: a model that crosses the species barrier and mimics the spectrum of human cytopathology.* Spinal Cord, 2002. **40**(3): p. 101-9.
266. Basso, D.M., M.S. Beattie, and J.C. Bresnahan, *A sensitive and reliable locomotor rating scale for open field testing in rats.* J Neurotrauma, 1995. **12**(1): p. 1-21.
267. Akhtar, A.Z., J.J. Pippin, and C.B. Sandusky, *Animal models in spinal cord injury: a review.* Rev Neurosci, 2008. **19**(1): p. 47-60.
268. Wrathall, J.R., R.K. Pettegrew, and F. Harvey, *Spinal cord contusion in the rat: production of graded, reproducible, injury groups.* Exp Neurol, 1985. **88**(1): p. 108-22.
269. Jeffery, N.D., et al., *Clinical canine spinal cord injury provides an opportunity to examine the issues in translating laboratory techniques into practical therapy.* Spinal Cord, 2006. **44**(10): p. 584-93.
270. Courtine, G., et al., *Can experiments in nonhuman primates expedite the translation of treatments for spinal cord injury in humans?* Nat Med, 2007. **13**(5): p. 561-6.
271. Lemon, R.N. and J. Griffiths, *Comparing the function of the corticospinal system in different species: organizational differences for motor specialization?* Muscle Nerve, 2005. **32**(3): p. 261-79.

272. Kwon, B.K., et al., *Large animal and primate models of spinal cord injury for the testing of novel therapies.* Exp Neurol, 2015. **269**: p. 154-68.
273. Andrews, N.C., *Iron homeostasis: insights from genetics and animal models.* Nat Rev Genet, 2000. **1**(3): p. 208-17.
274. Scheff, S.W., et al., *Experimental modeling of spinal cord injury: characterization of a force-defined injury device.* J Neurotrauma, 2003. **20**(2): p. 179-93.
275. Poon, P.C., et al., *Clip compression model is useful for thoracic spinal cord injuries: histologic and functional correlates.* Spine (Phila Pa 1976), 2007. **32**(25): p. 2853-9.
276. Kwon, B.K., T.R. Oxland, and W. Tetzlaff, *Animal models used in spinal cord regeneration research.* Spine (Phila Pa 1976), 2002. **27**(14): p. 1504-10.
277. Talac, R., et al., *Animal models of spinal cord injury for evaluation of tissue engineering treatment strategies.* Biomaterials, 2004. **25**(9): p. 1505-10.
278. Kundi, S., R. Bicknell, and Z. Ahmed, *The role of angiogenic and wound-healing factors after spinal cord injury in mammals.* Neurosci Res, 2013. **76**(1-2): p. 1-9.
279. Fehlings, M.G., et al., *Early versus delayed decompression for traumatic cervical spinal cord injury: results of the Surgical Timing in Acute Spinal Cord Injury Study (STASCIS).* PLoS One, 2012. **7**(2): p. e32037.
280. Kabu, S., et al., *Drug delivery, cell-based therapies, and tissue engineering approaches for spinal cord injury.* J Control Release, 2015. **219**: p. 141-54.
281. Ulndreaj, A., et al., *Modulating the immune response in spinal cord injury.* Expert Rev Neurother, 2016. **16**(10): p. 1127-9.
282. Coleman, W.P., et al., *A critical appraisal of the reporting of the National Acute Spinal Cord Injury Studies (II and III) of methylprednisolone in acute spinal cord injury.* J Spinal Disord, 2000. **13**(3): p. 185-99.
283. Fehlings, M.G. and D.C. Baptiste, *Current status of clinical trials for acute spinal cord injury.* Injury, 2005. **36 Suppl 2**: p. B113-22.
284. Bracken, M.B., *Methylprednisolone and acute spinal cord injury: an update of the randomized evidence.* Spine (Phila Pa 1976), 2001. **26**(24 Suppl): p. S47-54.
285. Alilain, W.J., et al., *Functional regeneration of respiratory pathways after spinal cord injury.* Nature, 2011. **475**(7355): p. 196-200.
286. Bartus, K., et al., *Large-scale chondroitin sulfate proteoglycan digestion with chondroitinase gene therapy leads to reduced pathology and modulates macrophage phenotype following spinal cord contusion injury.* J Neurosci, 2014. **34**(14): p. 4822-36.

287. Laabs, T.L., et al., *Inhibiting glycosaminoglycan chain polymerization decreases the inhibitory activity of astrocyte-derived chondroitin sulfate proteoglycans.* J Neurosci, 2007. **27**(52): p. 14494-501.
288. Mothe, A.J. and C.H. Tator, *Review of transplantation of neural stem/progenitor cells for spinal cord injury.* Int J Dev Neurosci, 2013. **31**(7): p. 701-13.
289. Gage, F.H., *Mammalian neural stem cells.* Science, 2000. **287**(5457): p. 1433-8.
290. Reynolds, B.A. and S. Weiss, *Generation of neurons and astrocytes from isolated cells of the adult mammalian central nervous system.* Science, 1992. **255**(5052): p. 1707-10.
291. Tetzlaff, W., et al., *A systematic review of cellular transplantation therapies for spinal cord injury.* J Neurotrauma, 2011. **28**(8): p. 1611-82.
292. Lu, P., et al., *Long-distance growth and connectivity of neural stem cells after severe spinal cord injury.* Cell, 2012. **150**(6): p. 1264-73.
293. Jin, Y., et al., *Transplantation of neural progenitor cells in chronic spinal cord injury.* Neuroscience, 2016. **320**: p. 69-82.
294. Yokota, K., et al., *Engrafted Neural Stem/Progenitor Cells Promote Functional Recovery through Synapse Reorganization with Spared Host Neurons after Spinal Cord Injury.* Stem Cell Reports, 2015. **5**(2): p. 264-77.
295. Pluchino, S., et al., *Immune regulatory neural stem/precursor cells protect from central nervous system autoimmunity by restraining dendritic cell function.* PLoS One, 2009. **4**(6): p. e5959.
296. Bacigaluppi, M., et al., *Delayed post-ischaemic neuroprotection following systemic neural stem cell transplantation involves multiple mechanisms.* Brain, 2009. **132**(Pt 8): p. 2239-51.
297. Pluchino, S., et al., *Human neural stem cells ameliorate autoimmune encephalomyelitis in non-human primates.* Ann Neurol, 2009. **66**(3): p. 343-54.
298. Pluchino, S., et al., *Injection of adult neurospheres induces recovery in a chronic model of multiple sclerosis.* Nature, 2003. **422**(6933): p. 688-94.
299. Tropepe, V., et al., *Direct neural fate specification from embryonic stem cells: a primitive mammalian neural stem cell stage acquired through a default mechanism.* Neuron, 2001. **30**(1): p. 65-78.
300. Takahashi, K. and S. Yamanaka, *Induction of pluripotent stem cells from mouse embryonic and adult fibroblast cultures by defined factors.* Cell, 2006. **126**(4): p. 663-76.
301. Hockemeyer, D. and R. Jaenisch, *Induced Pluripotent Stem Cells Meet Genome Editing.* Cell Stem Cell, 2016. **18**(5): p. 573-86.

302. Lee, A.S., et al., *Tumorigenicity as a clinical hurdle for pluripotent stem cell therapies.* Nat Med, 2013. **19**(8): p. 998-1004.
303. Vierbuchen, T., et al., *Direct conversion of fibroblasts to functional neurons by defined factors.* Nature, 2010. **463**(7284): p. 1035-41.
304. Pfisterer, U., et al., *Direct conversion of human fibroblasts to dopaminergic neurons.* Proc Natl Acad Sci U S A, 2011. **108**(25): p. 10343-8.
305. Hermann, A. and A. Storch, *Induced neural stem cells (iNSCs) in neurodegenerative diseases.* J Neural Transm (Vienna), 2013. **120 Suppl 1**: p. S19-25.
306. Han, D.W., et al., *Direct reprogramming of fibroblasts into neural stem cells by defined factors.* Cell Stem Cell, 2012. **10**(4): p. 465-72.
307. Herrera, J.J., R.J. Haywood-Watson, 2nd, and R.J. Grill, *Acute and chronic deficits in the urinary bladder after spinal contusion injury in the adult rat.* J Neurotrauma, 2010. **27**(2): p. 423-31.
308. Hargreaves, K., et al., *A new and sensitive method for measuring thermal nociception in cutaneous hyperalgesia.* Pain, 1988. **32**(1): p. 77-88.
309. Cummings, B.J., et al., *Human neural stem cells differentiate and promote locomotor recovery in spinal cord-injured mice.* Proc Natl Acad Sci U S A, 2005. **102**(39): p. 14069-74.
310. Pluchino, S. and G. Martino, *The therapeutic plasticity of neural stem/precursor cells in multiple sclerosis.* J Neurol Sci, 2008. **265**(1-2): p. 105-10.
311. Park, J.H., et al., *Long-term results of spinal cord injury therapy using mesenchymal stem cells derived from bone marrow in humans.* Neurosurgery, 2012. **70**(5): p. 1238-47; discussion 1247.
312. Park, H.C., et al., *Treatment of complete spinal cord injury patients by autologous bone marrow cell transplantation and administration of granulocyte-macrophage colony stimulating factor.* Tissue Eng, 2005. **11**(5-6): p. 913-22.
313. Cheriyan, T., et al., *Spinal cord injury models: a review.* Spinal Cord, 2014. **52**(8): p. 588-95.
314. Guertin, P.A., *Semiquantitative assessment of hindlimb movement recovery without intervention in adult paraplegic mice.* Spinal Cord, 2005. **43**(3): p. 162-6.
315. de Leon, R.D., et al., *Locomotor capacity attributable to step training versus spontaneous recovery after spinalization in adult cats.* J Neurophysiol, 1998. **79**(3): p. 1329-40.
316. Bareyre, F.M., et al., *The injured spinal cord spontaneously forms a new intraspinal circuit in adult rats.* Nat Neurosci, 2004. **7**(3): p. 269-77.

317. Basso, D.M., *Behavioral testing after spinal cord injury: congruities, complexities, and controversies.* J Neurotrauma, 2004. **21**(4): p. 395-404.
318. Metz, G.A. and I.Q. Whishaw, *Cortical and subcortical lesions impair skilled walking in the ladder rung walking test: a new task to evaluate fore- and hindlimb stepping, placing, and co-ordination.* J Neurosci Methods, 2002. **115**(2): p. 169-79.
319. Macias, M.Y., et al., *Pain with no gain: allodynia following neural stem cell transplantation in spinal cord injury.* Exp Neurol, 2006. **201**(2): p. 335-48.
320. Hofstetter, C.P., et al., *Allodynia limits the usefulness of intraspinal neural stem cell grafts; directed differentiation improves outcome.* Nat Neurosci, 2005. **8**(3): p. 346-53.
321. Hama, A. and J. Sagen, *Behavioral characterization and effect of clinical drugs in a rat model of pain following spinal cord compression.* Brain Res, 2007. **1185**: p. 117-28.
322. Okada, S., et al., *In vivo imaging of engrafted neural stem cells: its application in evaluating the optimal timing of transplantation for spinal cord injury.* FASEB J, 2005. **19**(13): p. 1839-41.
323. Parr, A.M., et al., *Transplanted adult spinal cord-derived neural stem/progenitor cells promote early functional recovery after rat spinal cord injury.* Neuroscience, 2008. **155**(3): p. 760-70.
324. Teng, Y.D., et al., *Functional recovery following traumatic spinal cord injury mediated by a unique polymer scaffold seeded with neural stem cells.* Proc Natl Acad Sci U S A, 2002. **99**(5): p. 3024-9.
325. Decimo, I., et al., *Neural stem cell niches in health and diseases.* Curr Pharm Des, 2012. **18**(13): p. 1755-83.
326. Sontag, C.J., et al., *Injury to the spinal cord niche alters the engraftment dynamics of human neural stem cells.* Stem Cell Reports, 2014. **2**(5): p. 620-32.
327. Salazar, D.L., et al., *Human neural stem cells differentiate and promote locomotor recovery in an early chronic spinal cord injury NOD-scid mouse model.* PLoS One, 2010. **5**(8): p. e12272.

8) ACKNOWLEDGEMENTS

This dissertation is my own work, reporting on experiments carried out as part of a collaborative project with Jeroen Verheyen (PhD student) and Dr. Jayden Smith (postdoctoral researcher). Due to the nature of the collaboration some data was inevitably shared and in some instances biological replicates from different collaborators were pooled; however, I was integrally involved in the performance and interpretation of the bulk of the experiments described herein. Moreover, the text itself is an original synthesis of these results with my own analysis and conclusions.

I would like to express my gratitude to my supervisor Prof. Guido Fumagalli for letting me take part to this PhD program and his support and supervision during this three year-long PhD experience. I also wish my great thanks to all the people in the Sect. of Pharmacology, with which I shared the beginning of this path, in particular Dr. Valeria Berton for her help and supervision during my first year, and Dr. Ilaria Decimo and Dr. Fancesco Bifari.

I also would like to express my gratitude to Dr. Stefano Pluchino for the great and unique opportunity he offered me by joining his lab as a visiting PhD student during the last two years of PhD course, for his support, the critical and constructive supervision that taught me how to approach a scientific project.

A special thanks is for the two people with whom I had the great opportunity to collaborate: Jeroen Verheyen for all the help in our experiments and the crazy hours spent in the animal facility and in particular Dr. Jayden Smith who, with a great patience and enthusiasm, followed me step by step from the planning of the experiments to the analysis of the data and he taught the scientific critical approach to my work, although the warmest thanks is for all his support day by day especially in the most difficult periods.

I also would like to thanks all the people I had the pleasure to meet and know in Pluchino's lab, for all the support during these years by creating a stimulating environment and for all the funny moments shared together.

The greatest thanks are for my family, for my parents, as my inspiring models, that always supported and encouraged me, and my brother and his amazing family that always cheer me up.

Last but not the least a special thanks to Marco for the encouragement and the extreme patience in all these years, especially in the most difficult moments.